catalysts

MDPI

Review

Cobalt Oxides and Co-Al Mixed Oxides as Thermo-, Photo- and Electrocatalytic Materials: Properties and Perspectives of Industrial Applications

Guido Busca [1,2,*], Elena Spennati [1,2], Elisabetta Finocchio [1,2], Paola Riani [2,3] and Gabriella Garbarino [1,2]

[1] Dipartimento di Ingegneria Civile, Chimica e Ambientale, Università di Genova, Via Opera Pia 15, 16145 Genova, Italy; elena.spennati@edu.unige.it (E.S.); elisabetta.finocchio@unige.it (E.F.); gabriella.garbarino@unige.it (G.G.)
[2] Consorzio Interuniversitario Nazionale di Scienza e Tecnologia dei Materiali (INSTM), Unità di Ricerca di Genova, Via Dodecaneso 33, 16146 Genova, Italy; paola.riani@unige.it
[3] Dipartimento di Chimica e Chimica Industriale, Università di Genova, Via Dodecaneso 33, 16146 Genova, Italy
* Correspondence: guido.busca@unige.it; Tel.: +39-3292104505

Abstract

The literature data on the solid-state and surface chemistry of cobalt and cobalt–aluminum oxide and hydroxide systems are reviewed. The actual and potential applications of these materials in the fields of catalysis, electrocatalysis, photocatalysis, adsorption and sensor technologies are reviewed. A comprehensive analysis of the peculiar redox and acid–base properties of these cobalt-based systems, both at the solid–gas and at the solid–water solution interface, is conducted. Evidence is provided for the exceptional versatility of these systems and on their relevant potential for optimal applications, in particular, in several catalytic total oxidation reactions, in N_2O catalytic decomposition, in ammonia catalytic oxidation to NO, as electrocatalysts in water splitting reactions, as active elements in supercapacitors, and as precursors of cobalt metal-based systems. It is underlined that these systems could successfully substitute more critical and expensive noble metal-based systems in several technological fields.

Keywords: cobalt; aluminum; oxides; hydroxides; catalysts; electrocatalysts; photocatalysts; adsorbents; sensors

1. Introduction

Cobalt is considered as a quite critical element in occidental countries, mainly because most of its production occurs in the Democratic Republic of Congo and most of its processing is realized in China [1]. Additionally, some cobalt compounds have genotoxic and carcinogenic activity [2]. In spite of these limitations, cobalt and its oxides have many actual and potential applications. Their main application (>72%) in 2022 has been in the production of rechargeable lithium-ion batteries [1] such as the LCO batteries (based on $LiCoO_2$ electrodes) and NMC batteries (based on $Li(Mn,Ni,Co)O_2$ electrodes) [3]. Catalytic applications of cobalt are also relevant. It has a wide use as a homogeneous catalyst in liquid phase [4], such as cobalt acetate which is the homogenous catalyst of p-xylene oxidation to terephthalic acid (the monomer to produce polyesters such as PET, PolyEthyleneTerephthalate [5]). It is also used as a metallic Co/Al_2O_3 catalyst for Fischer Tropsch process [6,7], and as the dopant of molybdenum sulphide -based catalysts (CoMo), largely applied in hydrocarbon hydrodesulphurization processes in refineries [8]. The latter

Academic Editor: Hao Xu

Received: 30 December 2025
Revised: 3 February 2026
Accepted: 6 February 2026
Published: 1 April 2026

have also been recently applied for the catalytic hydrodeoxygenation of vegetable oils to produce Hydrogenated Vegetable Oil, the renewable Diesel fuel (HVO [9]). Cobalt also has relevant application in the production of alloys characterized by good corrosion and wear resistance, high-temperature strength, fatigue strength and biocompatibility, used in such applications as jet engine turbines and gas turbine generators, in nuclear power and chemical-processing industries as well as for orthopaedic implants [10]. Additionally, it has application in the biomedical field [11].

Metal oxide technologies also represent a very relevant industrial sector, such as in the fields of construction materials, electronic and electrocatalytic materials, insulators, electroceramics, pigments, glasses, refractories, abrasives, industrial catalysts, adsorbents, etc. [12]. In fact, pure and mixed cobalt oxides are extremely interesting materials for many of their bulk and surface properties. In addition to applications related to optical properties (i.e., for pigments used in glazes, glass, and enamels [13]), and to their electronic and chemical properties (such as in batteries [3]) they have practical or potential interest in many surface related applications, such as in the fields of adsorption, catalysis, electrocatalysis and supercapacitor technologies. Cobalt oxides also have interesting activities as catalysts used in environmental remediation [14]. Most of these applications are related to the electronic state of Co^{3+} and Co^{2+} ions and their redox properties. In several cases, to take advantage of these properties and improve stability, they are mixed with or supported on aluminas. In fact, aluminas are among the most applied supports in the field of heterogeneous catalysis and adsorption technologies [15]. Additionally, cobalt aluminates have many actual and potential applications. In this review, the preparation, the solid-state chemistry and the surface-related applications of cobalt oxides and cobalt-aluminium mixed oxides will be reviewed, together with their actual and potential industrial applications.

2. Solid-State Chemistry of Pure Cobalt Cobalt-Containing Phases

Several cobalt oxide and hydroxide phases exist in different conditions. For reference on the thermodynamic stability of different phases, in Figure 1 the cobalt-oxygen state diagram [16–18] is reported while in Figure 2 the Pourbaix diagram of the cobalt-water system [19,20] is reported. These diagrams allow us to interpret the metallurgy of cobalt [21] as well as the behavior of cobalt—based oxides and hydroxides towards several of their actual applications.

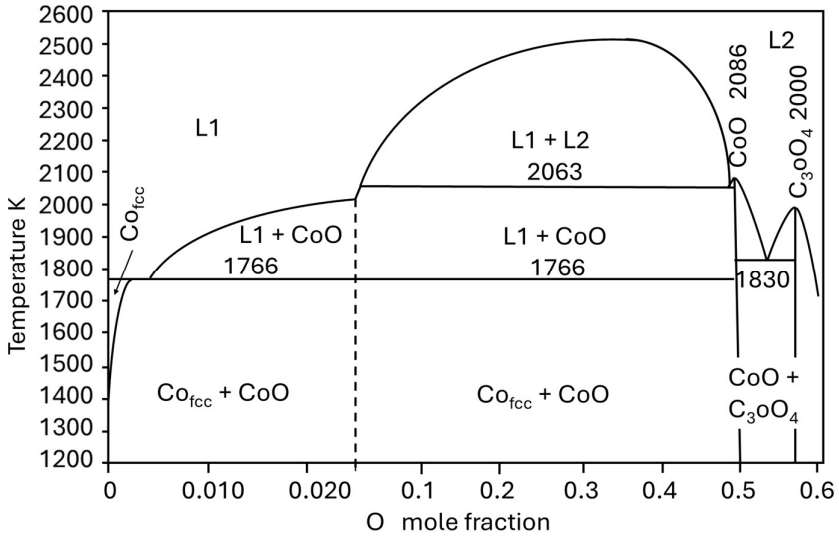

Figure 1. The Co-O phase diagram, data from ref. [16–18].

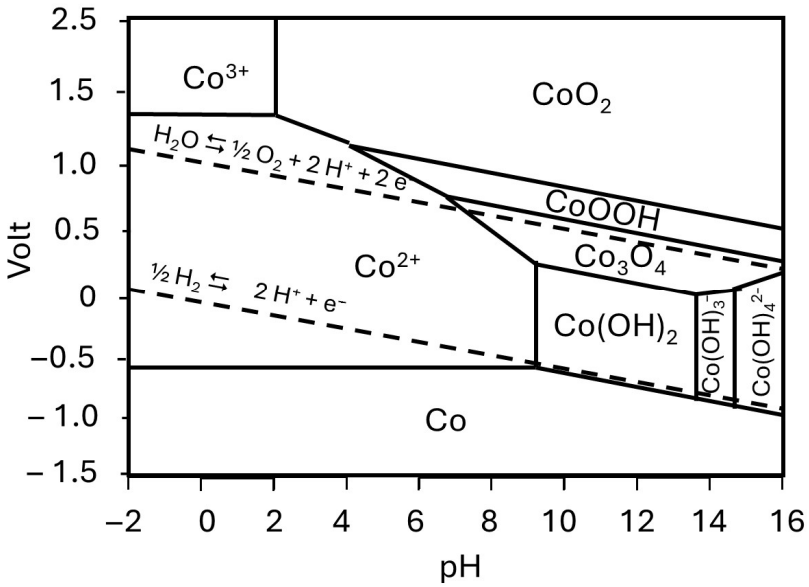

Figure 2. Pourbaix diagram of the cobalt-water system, with concentration of Co 10^{-6} mol kg−1. The potential is measured against normal hydrogen electrode (NHE) at standard conditions (T = 298.15 K, P = 1 bar, pH = 0). Combined from Refs. [19,20].

2.1. Cobalt Hydroxides

Co (II) hydroxide, usually denoted as β-$Co(OH)_2$, has a layered structure, isostructural to brucite $Mg(OH)_2$, with high spin (HS: $e^4t_2{}^3$) Co^{2+} ions occupying distorted octahedral sites in a cationic layer sandwiched in between two hydroxy-group layers [22,23] with a d-spacing of 4.6 Å. It shows typically a pink color [23]. The phase usually denoted as α-$Co(OH)_2$ is actually not a Co(II) hydroxide polymorph. In fact, it is a Co(II)-Co(III) layered hydroxycarbonate, hydroxynitrate or hydroxychloride [24–28] with a structure similar to that of hydrotalcite ($Mg_6Al_2(OH)_{16}{\cdot}CO_3{\cdot}4H_2O$) characterized by positively charged $[Co(OH)_2]^{x+}$ layers containing both divalent and trivalent cobalt ions intercalating balancing anions, that can be exchanged with each other such as carbonate, nitrate and chloride. These solids with different anions have a variable color, i.e., red [29] or green [23]. Both α- and β-$Co(OH)_2$ phases are intrinsic p-type semiconductors [30].

Heating β-$Co(OH)_2$ in N_2 atmosphere at 473–493 K [31] and in vacuum at 410 K [32] is reported to produce crystalline rock salt type CoO or an amorphous material that crystallizes to rock-salt-type CoO at 473–573 K [33], also in the presence of saturated water vapor [34]. The decomposition of the hydrotalcite-type α-phase is a more complex phenomenon and, in any case, calcination in air of both phases at 423–523 K produces Co_3O_4 [24].

According to Pankratov [35], two different phases of trivalent cobalt hydroxide $Co(OH)_3$ exist, a green phase and a brownish-black phase. Yang et al. reported the synthesis and the characterization, including XRD pattern, of $Co(OH)_3$ nanobelts [36]. However, the crystal structure of $Co(OH)_3$ phases does not seem to have been identified.

Trivalent cobalt oxy-hydroxide phases certainly exist, forming the mineral Heterogenite, an economically important source of cobalt, extracted mainly in the Democratic Republic of Congo (DRC). This mineral is composed of at least two polytypes of the CoOOH, which can also be precipitated individually. These polymorphs have the same layered structure, with different crystal stackings [37]. The polytype generally denoted as β-CoOOH has 3R crystal stacking (space group R $\bar{3}$m), and a brown color [29,38], while the γ-CoOOH polytype has 2H crystal stacking (space group $P6_3/mmc$) [39–41], a black color and high electrical conductivity [29,38]. In both polytypes Co^{3+} is bonded to six equivalent O^{2-} atoms to form edge-sharing CoO_6 octahedra, and takes the Low Spin (LS)

electronic configuration ($\tau^6{}_{2g}e^0{}_g$). All Co-O bond lengths are 2.02 Å. H^+ is bonded in a linear geometry to two equivalent O^{2-} atoms of two different layers with a strong H-bond 1.21 Å long. O^{2-} is bonded in a 4-coordinate geometry to three equivalent Co^{3+} ions and one H^+ ion. Both β-CoOOH [42] and γ-CoOOH [29] can be partially oxidized containing tetravalent cobalt. On the other hand, solids with H_xCoO_2 stoichiometry and x ~ 0.3, i.e., hydroxides of predominantly tetravalent cobalt, have also been prepared, obtained through cation exchange from M_xCoO_2 oxides (M = Li, Na) [43,44].

It can also be mentioned that a crystalline Co(III) hydroxycarbonate phase with stoichiometry $Co(OH)_2(CO_3)_{0.5}$ [45] or $Co(CO_3)_x(OH)_y$, is also reported to exist, and produces Co_3O_4 by decomposition [46].

As for the precipitation of cobalt hydroxides from water solutions, cobalt (II) hydroxide, whose pKs (logarithm of the solubility constant Ks) is reported to be 14.8 [47], can be prepared by precipitation [48–50] or hydrothermal synthesis [51] from Co^{2+}-containing water solutions at pH > 8.0 (Figure 2). $Co(OH)_2$ is actually an amphoteric hydroxide which is essentially insoluble at pH 10 ÷ 13, where it can act as the passivation layer for metallic cobalt (Figure 2), but dissolves in neutral and acidic solution, as well as in strongly basic conditions (pH > 13). Both α- and β-$Co(OH)_2$ can also be prepared through electrodeposition techniques [52–54]. Solid $Co(OH)_2$ can be electrochemically oxidized to CoOOH [55].

"Cobaltic hydroxide" $Co(OH)_3$, whose pKs of is reported to be 44.3 [47], can be precipitated from Co^{3+}-containing solutions, obtained oxidizing Co^{2+}-containing solutions, at a pH as low as -1 to 0 [48,56,57], and is consequently stable also in acidic solutions, as indeed reported for CoOOH [58]. CoOOH is considered to be insoluble at all pHs [59].

We have also to mention that tetravalent cobalt can be produced electrochemically at high voltages, but is essentially unstable in contact with water causing water oxidation [60,61].

2.2. Cobalt Oxides

As reported in the cobalt oxygen state diagram (Figure 1), two thermodynamically stable cobalt oxide phases exist: rock salt-type CoO and spinel Co_3O_4 [16–18,62]. CoO, which is stable at reduced oxygen pressures, and in air above near 1100 K [63,64], until its melting point which is reported at 2086 K [18] or at 2208 K [65], crystallizes in the cubic rock-salt or periclase (MgO) structure, with octahedrally coordinated High Spin ($e^4t_2{}^3$) Co^{2+} ions [66]. It has an antiferromagnetic behavior below the Néel temperature of 293 K [67]. When stoichiometric, CoO is a charge-transfer insulator, with energy gap of about 6 eV [68], which is strongly reduced in case of nanoparticles [69] and defective structures [70]. When treated in air or oxygen, it easily becomes non stoichiometric with formula CoO_{1+x} with $x \leq 0.0159$ and a p-type semiconducting behavior [71]. In oxygen-rich atmosphere the XPS features of CoO_{1+x} are similar to those of Co_3O_4 [72,73]. Kinetically limited conversion of rock salt type CoO to Co_3O_4 is commonly realized by calcination in air at temperatures > 523 K depending on CoO morphology [64,74,75]. Co_3O_4 grows on the surface of CoO in case of nanoparticles [74] and both at the surface and in the bulk for bulk particles [64].

On the other hand, in reducing conditions, or upon cobalt metal partial oxidation, CoO_{1-x} oxygen poor phases may also exist [76]. Depending on stoichiometry, particle size and morphology, the UV-vis-NIR spectrum of CoO is quite variable [77,78], and, accordingly, CoO can appear as olive-green or pink crystals, or as black powder [79]. Combination of cobalt monoxide with other oxides gives rise to a variety of colored pigments such as cobalt blue $CoAl_2O_4$ (see below), cobalt green (Co,Zn)O, cobalt violet $Co_3(PO_4)_2$, etc. The color of these materials is due to d-d transitions of the Co^{2+} ion.

With special preparation procedures, cobalt monoxide alternative polymorphs can be produced, with zinc blende and wurtzite structures [80,81], which are expected to have a complex frustrated antiferromagnetic ground state with no net magnetic moment in the bulk [82]. Atomistic simulation calculations predict the lattice energies of the three polymorphs to be relatively close, with the rock salt polymorph being most stable, followed by the wurtzite form and lastly zinc blende [62,80]. As evident from the Pourbaix diagram (Figure 2), CoO is thermodynamically unstable at room temperature and atmospheric pressure with respect to hydration producing $Co(OH)_2$ [83], which, as said, decomposes to CoO in inert atmosphere at 400–500 K.

As mentioned, Co_3O_4 is the thermodynamically stable form of cobalt oxide under ambient room temperature and oxygen partial pressure. Basically, it has the normal spinel structure with octahedrally coordinated low spin ($\tau^6{}_{2g}e^0{}_g$) Co^{3+} ions and tetrahedrally coordinated high spin ($e^4t_2{}^3$) Co^{2+} ions at relatively low temperatures. However, a certain degree of inversion is found, depending on particle size and on the preparation temperature [84] as well as on measurement temperature [17,85]. Co_3O_4 is antiferromagnetic at very low temperature, with a Néel temperature varying from around 15 to 40 K depending on particle size [86], while being paramagnetic at room and higher temperatures. However, weak ferromagnetism can be found in nanoparticles [87]. It is a semiconductor with a bandgap of 2.11 eV [88]. In oxidizing conditions an enrichment in Co^{3+} is found, in particular at the surface, according to XPS data [89,90]. In these conditions Co_3O_4 is a p-type semiconducting material [91]. According to its strong absorption in the entire visible region (Figure 3), Co_3O_4 usually has a dark blackish color, making it a black pigment [92] usually commercialized as "cobalt black pigment" or pigment black 13.

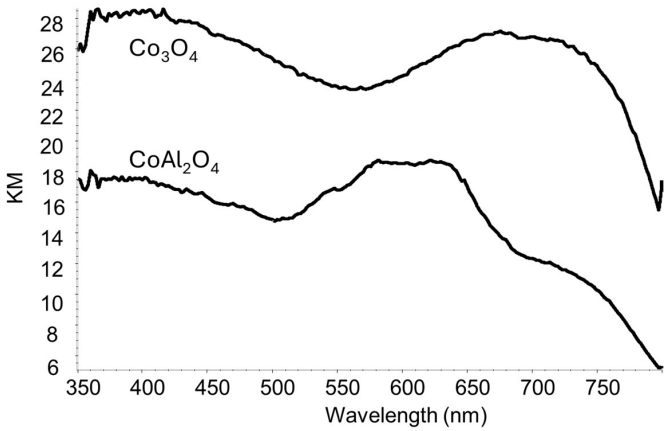

Figure 3. Visible spectra of Co_3O_4 and $CoAl_2O_4$ powders, from data of ref. [93].

As said, Co_3O_4 can be prepared by calcination of precipitated $Co(OH)_2$ and CoOOH at > 573 K [55,94,95], as well as by calcination of the cobalt nitrate and carbonate salts. It is also formed by calcining CoO in air at 523–873 K (depending on CoO morphology) [64,74,75]. Practically, Co_3O_4 preparation procedures are multiple, as summarized e.g., by Zhao and Ma [94], as reported in Table 1.

Table 1. Various synthesis methods of Co_3O_4 and advantages and disadvantages, according to [96].

Entry Name of the Synthetic Process	Advantages	Disadvantages
Hydrothermal reaction	The crystalline powder can be obtained directly without high-temperature sintering, the crystallinity is high, and the control the particle size of the produced crystal is easy	Strong dependence on production equipment

Table 1. *Cont.*

Entry Name of the Synthetic Process	Advantages	Disadvantages
Thermal decomposition	Thermal instability; pyrolysis products are different	The combustible gas is large and the residual carbon slag is small
Solution combustion	The process is simple, the operation is convenient, the purification efficiency is high, and the heat energy can be recovered	When the combustible component content is low, preheating energy consumption is required
Vapor deposition method	The film-forming device is simple and raw materials are easy to obtain	High reaction temperature
Coprecipitation	The process is simple, the cost is low, the preparation conditions are easy to control, and the synthesis cycle is short	Agglomeration or uneven composition
Sol–gel	Easy doping, uniform composition, low reaction temperature required	Poor film density; volume shrinkage
Template method	Easy synthesis and size control, especially for nanomaterials	High pH and ionic strength of the solution required
Chemical reduction method	Simple reagents and equipment; low cost	Reaction process not easy to control; impurities easily appear
Wet synthesis	Simple operation; can be a large number of syntheses	Hidden dangers in emissions and cooling methods
Ionic liquid-assisted method	Low melting point, good thermal stability	Complex process, high cost, conductivity low

As will become clear later on, one of the most relevant features of Co_3O_4 is the possibility to prepare it in a variety of different nanostructures, that can offer enhanced activity in different technologies. In fact, a number of approaches have been developed to produce different morphologies of Co_3O_4 nanoparticles [97–99] and in order to expose more reactive faces, e.g., for catalytic combustion [100] and CO oxidation [101]. In Figure 4, reproduced from ref. [102], methods for preparing cobalt-based nanoparticles are summarized. In Figure 5, reproduced from ref. [103], Field Emission Scanning Electron Microscopy (FE-SEM) images of cobalt oxide nanoparticles are reported, showing that morphology can significantly change even with small changes of synthesis temperature. On the other hand, looking at their industrial applications, economic aspects of such preparation procedures must also be taken into consideration [104], along with the stability of the resulting nanopowders (see below).

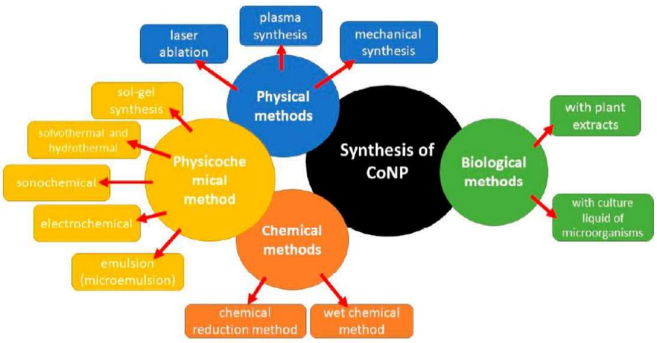

Figure 4. Main methods for the synthesis of cobalt nanoparticles, from ref. [102].

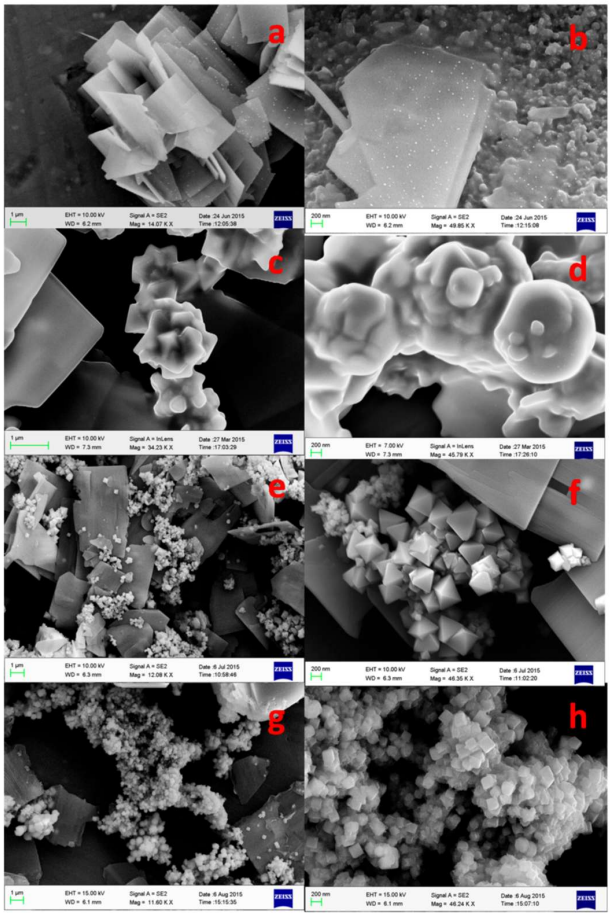

Figure 5. FE-SEM images of cobalt oxides prepared at (**a**,**b**) 100 °C, (**c**,**d**) 125 °C, (**e**,**f**) 150 °C, and (**g**,**h**) 180 °C at low (**left**) and high (**right**) magnifications [103].

Co_3O_4 decomposes to CoO at about 1110–1140 K in inert atmosphere [24,105] and at 1150–1230 K in air [24,106]. In Figure 6 the evolution of the XRD pattern of Co_3O_4 with the calcination temperature is shown, providing evidence of the appearance of the peaks of the CoO phase at 1173 K and the full disappearance of the peaks of the Co_3O_4 phase at 1373 K, when calcination is realized for 1 h [106].

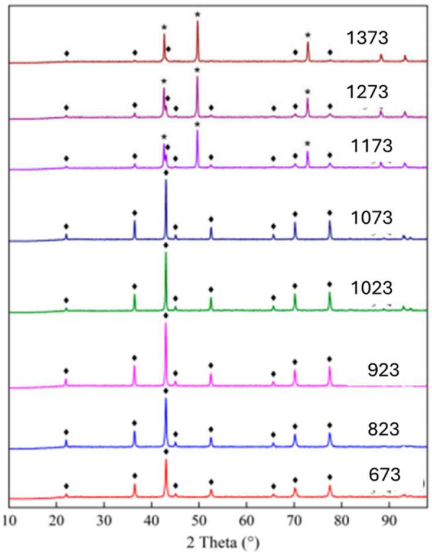

Figure 6. X-ray diffraction patterns of cobalt oxide, calcined at different temperatures (K): heating rate 10 K/min, followed by 1 h at the given temperature [106]. ♦ Co_3O_4; * CoO.

Taking into account the remarkable reaction enthalpy (844 kJ/kg) in the reversible $Co_3O_4 \leftrightarrows CoO + ½ O_2$ reaction this system is considered for thermochemical energy storage [107]. However, it has been found that sintering causes deterioration of the behavior upon thermochemical cycles.

Under vacuum, the decomposition of Co_3O_4 to CoO can be complete at a temperature as low as 673 K [108]. CoO-Co_3O_4 composite particles can also be produced [109]. Interestingly they appear to be ferromagnetic at r.t. [110]. Co_3O_4 is reported to convert into CoOOH when in contact with both acidic and basic solutions [58] without significant dissolution.

The possible existence of Co_2O_3 phases, either with corundum-type or bixbyite-type structure, is doubtful and a little bit controversial, based on theoretical calculations [111,112]. Apparently, corundum type Co_2O_3 has been synthesized under high pressure by Chenavas and Joubert [113] but is likely unstable at atmospheric pressure [62]. It can be remarked, however, that several trivalent-only cobalt mixed oxides exist, such as e.g., lanthanide cobaltites $LnCoO_3$ with bixbyite [112] and perovskite [114] structures, where Co^{3+} is in octahedral coordination.

CoO_2, with tetravalent cobalt, is the end term of the Li_xCoO_2 and Na_xCoO_2 series with x~0. It and can be obtained through an electrochemical method by deintercalation of Li^+ ions from Li_xCoO_2 [115–117]. Li_xCoO_2 [3] and Na_xCoO_2 [118] can be used as cathodes of Li- ion and Na- ion batteries, respectively, but, during the battery recharge, deintercalation is only partial. However, CoO_2 can be produced as an essentially stoichiometric material and is converted by hydrogen Temperature Programmed Reduction (TPR) to CoO at a little above 473 K [117]. More recently, CoO_2 has also been prepared by converting bulk $Ca_3Co_2O_6$ via a hydrothermal treatment [119]. CoO_2 is a layered structure with dark color and metallic paramagnetic behavior [120].

In Table 2 a summary on the structures of cobalt oxides and hydroxides is given.

Table 2. Reference data of cobalt oxides and hydroxides.

Formula or "Symbol"	Structure Type	Space Group	Color	References
$CoO_{1\pm x}$	rock salt	Fm $\bar{3}$m	variable with x	[16–18,62–71]
	wurtzite	$P6_3mc$	green	[62,79–82]
	zinc blende	F $\bar{4}$3m		[62,79,80,82]
Co_3O_4	spinel	Fd $\bar{3}$m	dark blackish	[16–18,62,84–91]
Co_2O_3	corundum	R3c	black	[62,111–113]
CoO_2	O1	P $\bar{3}$m1	dark	[115–117,119,120]
β-$Co(OH)_2$	brucite	P $\bar{3}$m1	pink	[22,23]
"α-$Co(OH)_2$"	hydrotalcite	P $\bar{3}$m1	variable	[24–28]
$Co(OH)_3$			brownish-black or green	[35,36,47,48]
β-CoOOH		R $\bar{3}$m	brownish	[28,38–42]
γ-CoOOH		$P6_3/mmc$	black	[28,38–42]
"H_xCoO_2"	O1	P $\bar{3}$m1		[43,44]

2.3. Metallic Cobalt

The thermodynamically stable phase of metallic cobalt at ambient temperatures is hexagonal close-packed (hcp), with ferromagnetic behavior and a Curie temperature of about 800 K. However, it usually converts, by heating, into the face-centered close packed phase (fcc), which is more stable above about 700 K [121–123]. This phase is ferromagnetic

too and becomes paramagnetic at the Curie temperature of about 1400 K, while it melts near 1700 K. The same phases can also appear in nanoparticles [124,125], that can sometimes appear as amorphous and superparamagnetic [126,127].

2.4. Redox Chemistry of Pure CoOx Phases

It has already been mentioned that Co_3O_4 decomposes to CoO by simple outgassing at ~673 K, but it has been reported that most of the CoO phase is reduced to metallic Co by simple vacuum annealing at temperatures above 633 K [128]. Both Co_3O_4 and, at slightly higher temperature, CoO are reduced to metallic cobalt at 473–673 K in hydrogen, although the position of the TPR peak strongly depends on experimental conditions [105,129–133].

Conversely, when a clean cobalt surface is exposed to air at room temperature, an 8–10~film of $Co(OH)_2$ forms in seconds or less. Exposure to air at 373–500 K results in the growth of a film of CoO. At 700 K in air the film appears to be a mixture of CoO and Co_3O_4 [134]. At high temperature (>1300 K) fcc cobalt can dissolve up to 0.25 at% of oxygen in its own structure (Figure 1). Oxidation of cobalt metal nanoparticles at 573 K in oxygen results in the formation of polycrystalline CoO followed by the formation of Co_3O_4 [135].

3. Solid-State Chemistry of Pure Aluminum-Containing Phases

The chemistry of aluminum oxides and hydroxides is a very complex one and has been the object of several reviews [136–138]. Although two oxyhydroxide phases and four different trihydroxide phases exist, the precipitation from an Al^{3+}-containing water solutions commonly produces, at low temperatures, either bayerite α-$Al(OH)_3$ or gibbsite γ-$Al(OH)_3$, depending mainly on pH, while boehmite (γ-AlOOH) and its poorly crystallized form pseudoboehmite are produced at higher temperatures (i.e., 350 K).

The thermal decomposition of hydroxides and oxyhydroxides gives rise to the many different alumina phases. The most common phases are more or less distorted defective spinel phases, i.e., cubic γ-Al_2O_3, which is usually prepared through the calcination of gelatinous pseudoboehmite or crystalline boehmite at around 723 K, or η-Al_2O_3, usually prepared through the decomposition of bayerite at 523–573 K. By further heating these phases, a distorted spinel phase forms, denoted as δ-Al_2O_3. At 970–1170 K, θ-Al_2O_3, which is isostructural with β-Ga_2O_3, also a spinel derived phase, forms.

Indeed, γ-Al_2O_3 is the most used material as a catalyst support due to its sufficiently high surface area (150–300 m^2/g), tunable porosity, stability up to 773 K and more, high dispersion ability for supported phases, and moderate cost and easy preparation.

All aluminum oxides and hydroxides finally produce, through calcination at 773–1273 K, the thermodynamically stable phase α-Al_2O_3 (corundum), a ceramic abrasive and refractory material (T_{melt} 2313 K), also used as an inert and thermally stable support of catalysts [139].

It can be taken into consideration that aluminas are unreducible by hydrogen, based on thermodynamics, until maybe very high temperatures [140,141], and that, accordingly, alumina reduction does not occur in H_2-Temperature Programmed Reduction experiments until 1273 K. Being also not further oxidable, alumina is a fully stable compound, in terms of its redox behavior, in normal conditions.

4. Solid-State Chemistry of Mixed Co-Al Phases

4.1. Co-Al Mixed Hydroxide Phases

The precipitation of Co^{2+}-Al^{3+} ion-containing solutions with a Co/Al ratio = 3 produces solids with a $Co_6Al_2(OH)_{16}X{\cdot}4H_2O$ composition, where X^- is most commonly the carbonate anion, with the structure of the mineral hydrotalcite [142–144], i.e., the isostructural Mg compound, best known among Layered Double Hydroxide (LDH) anionic

clays [145,146]. This phase is constituted by brucite ($Mg(OH)_2$)-like layers with water and anions in the interlayer region to compensate the positive charge of these layers when trivalent elements are present. Actually, hydrotalcite-like structures are obtained by precipitating a solution with a Co/Al ion molar ratio from 1 to 6 [147–149] with an expansion of the unit cell parameters by increasing the Co/Al ratio in the 1–4 range only. The constancy of the cell parameters in the samples with Co/Al 4–6 is consistent with the copresence of Co^{2+} and Co^{3+} in the samples with Co/Al ratio > 3, according to the size of the ions (Co^{2+} > Al^{3+}~Co^{3+}). On the other hand, samples with a Co/Al ratio < 3 represent solid solutions of the hydrotalcite-like double hydroxide phase and the so-called α-$Co(OH)_2$ phase (see above). The calcination in air of all these phases at 773 K for 5 h produces Co-Al mixed oxide spinel phases. However, if the calcination of the stoichiometric hydrotalcite-like compound $Co_6Al_2(OH)_{16}CO_3{\cdot}4H_2O$ is realized in nitrogen, the XRD analysis shows the production of a spectrum with relative broad peaks, due to the monophasic solid with a defective rock salt or periclase structure, i.e., Al^{3+}-containing CoO [150]. This phase is unstable and converts into $Co_{3-x}Al_xO_4$ spinel in an air atmosphere at 473 K.

The formation of Co-Al ammonium hydroxycarbonates with formula $NH_4CoAl_2(OH)_5(CO_3)_2{\cdot}2H_2O$ has also been reported, which can produce $CoAl_2O_4$ spinel by decomposition [151].

4.2. Bulk Co-Al Mixed Oxides

4.2.1. Rock Salt-Type Phases

The calcination in an inert atmosphere of Co-Al layered hydroxides with an Co/Al ratio > 1 can produce poorly crystallized rock salt-type solid solutions, i.e., CoO containing moderate amounts (Co/Al $\geq$ 3) of Al^{3+}, i.e., Al^{3+}-doped CoO [150]. However, these phases are thermodynamically unstable and crystallize in separate phases (CoO + $CoAl_2O_4$ spinel) by further heating. On the other hand, a small solubility of Al^{3+} in the CoO phase is also reported to occur at high temperatures in the CoO-Al_2O_3 phase diagram [152,153].

4.2.2. Co-Al Mixed Oxide Stoichiometric Spinel Phases

The CoO-Al_2O_3 phase diagram at high temperatures (>1273 K) has been reported by Mori [152]. It shows the spinel $CoAl_2O_4$ (melting point at 2253 K) as the only thermodynamically stable intermediate phase in between rock salt-type CoO and α-Al_2O_3, with a large solubility of Al_2O_3 into $CoAl_2O_4$ only above 1373 K, and no solubility with CoO.

Cobalt aluminate $CoAl_2O_4$ is a blue-colored normal spinel, with high-spin Co^{2+} in tetrahedral sites and Al^{3+} in octahedral sites, largely used for centuries as a pigment. The blue ceramic pigment $CoAl_2O_4$, denoted as Thénard's blue, cobalt blue, or Pigment Blue 28, is commonly prepared through a solid-state reaction between Co_3O_4 and Al_2O_3 at about 1573 K [154]. It is used for the coloration of different materials such as plastics, porcelain, enamel, paint, paper, rubber, glass, concrete, and glaze, and as a pigment in optical devices. When the calcination temperature is lower, the presence of Co^{3+} results in a darker color. As the temperature increases, a partial inversion of the spinel structure will occur [155].

Looking at what happens in an oxidizing environment, as said, Co_3O_4 spinel is the stable cobalt oxide phase. $CoAl_2O_4$ and Co_3O_4 are isostructural normal spinel solids, and a complete solubility in the compositional range Co/Al $\infty \div 0.5$, with an intermediate stoichiometry of Co_2AlO_4, is usually assumed. However, XRD data are interpreted by some authors to reveal a $CoAl_2O_4$-Co_3O_4 spinel phase separation occurring at high temperatures [156], although this might be an artifact due to the non-homogeneity of the samples.

In fact, the isostructural compounds Co_3O_4, Co_2AlO_4 and $CoAl_2O_4$ [157–161] have essentially the same XRD patterns with small peak shifts [162], while the increase in cobalt content in the spinel is reported to result in a slight decrease of the unit cell size or cubic lattice parameter [163]. Differentiation can be attempted using the intensity of the 111 peak at $2\theta = 19.0$, which is supposed to be most intense for Co_3O_4 [164], and the I(220)/I(311) intensity ratio, which is expected to be smallest for the $CoAl_2O_4$ phase [165,166]. Also, the skeletal IR spectra of the three stoichiometric Co-spinel phases Co_3O_4, Co_2AlO_4, and $CoAl_2O_4$ [127,164,167–171] were reported to differ very slightly for the peak position.

On the other hand, the end stoichiometric spinel phases Co_3O_4 and $CoAl_2O_4$, when crystalline and calcined at relatively high temperatures, have a different color and are consequently well distinguished through visible spectroscopy (Figure 3). Bulk Co_3O_4 is dark near to black, and accordingly has a strong absorption in the visible region with two broad and very strong absorption doublets centered near 400 and 700 nm [167,172] similar to that reported for $CoAl_2O_4$ if calcined at low temperature, which is black too [157,163,173]. Instead, as said, when calcined at a high temperature, $CoAl_2O_4$ is blue, and its visible spectrum shows a strong absorption triplet near 545, 582 and 627 nm, due to Co^{2+} d-d transitions [93,163,174,175] (Figure 3). Detailed spectroscopic studies indicate that $CoAl_2O_4$ may have a significant degree of spinel inversion when calcined at low temperatures (black), while it becomes a fully normal spinel (with high-spin Co^{2+} in tetrahedral sites, Al^{3+} and low-spin Co^{3+} in octahedral sites [162]) with a blue color when heated above 1073 K [174,176]. The XPS spectra show that stoichiometric $CoAl_2O_4$ may contain, at least at the surface, significant amounts of Co^{3+} [147], but samples treated at high temperatures do not show Co^{3+} [175,176].

Thus, the electronic spectrum indicates that $CoAl_2O_4$ calcined at low temperatures may contain Co_3O_4 species, or, in any case, a Co^{3+}-containing cobalt-rich spinel phase at least at the surface. To develop a blue color, cobalt ions must be entirely reduced to Co^{2+}, and this is realized through heat treatment even in air at $T > 1073$ K.

Co_2AlO_4 also presents similar visible spectra, depending on the calcination temperature, to $CoAl_2O_4$ [158]. The XPS spectra of Co_2AlO_4 calcined at 1023 K presents both features of Co^{2+} and Co^{3+} [159].

As already mentioned, Co-Al mixed oxide phases can be prepared at low temperatures through the decomposition of Co-Al mixed hydroxide phases or from sol–gel prepared solids [177]. Nanocrystalline cobalt aluminate was also successfully prepared using both the conventional and microwave combustion methods starting from nitrates and aloe vera plant extract [178], as well as through a number of soft chemistry techniques [179–181]. Solid state reaction of mixtures of separated cobalt oxide and alumina phases, which is, as said, the most common way to produce cobalt aluminate pigments, is a slow process, being predominant only above 1323 K [182] and normally realized above 1473 K [154].

4.2.3. Co-Doped Alumina Non-Stoichiometric Spinel Phases

Through the (co-)precipitation of Co-Al mixed solutions followed by calcination, Co_3O_4-Co_2AlO_4-$CoAl_2O_4$-γ-Al_2O_3 spinel-type solid solutions in the entire compositional range $Co/Al = \infty \div 0$ can be obtained. However, in the range $Co/Al = 0.5 \div 0$, these solid solutions are cation-deficient spinels, also denoted as Co-doped γ-aluminas. Such phases are (as with γ-Al_2O_3) metastable. Their thermal treatment reveals that Co^{2+} slightly inhibits the γ-Al_2O_3 to α-Al_2O_3 phase transition, and at 1273 K produces $CoAl_2O_4/\gamma$-Al_2O_3/α-Al_2O_3 composites [183,184]. Calcination at 1373 K results in blue colored biphasic $CoAl_2O_4/\alpha$-Al_2O_3 [185] in agreement with the data from the phase diagram [152].

The mixing of alumina and Co_3O_4 (0.40 mol concentration of Co_3O_4 or lower) followed by sintering at 1823 K or a higher temperature results in green cobalt sapphire powders, i.e., Co-doped corundum [186], characterized by visible main absorptions at 436 and 652 nm assigned to Co^{3+} ions [187,188]. After the reduction in hydrogen at 1623 K, the spectrum is modified, now showing a triplet at 540, 580, and 627 nm, assigned to Co^{2+} coming from Co^{3+} reduction [188,189], similar to that found on $CoAl_2O_4$, corresponding to a change in color from dark green to brownish blue. Similarly, the calcination of cobalt-doped boehmite gives rise to cobalt-doped corundum species, with nearly the same visible spectrum [190].

4.3. CoO_x/Al_2O_3 Materials Produced Through Impregnation Techniques

Supported cobalt oxide on alumina, used as an oxide catalyst or as a precursor of alumina-supported cobalt metal catalysts, is mostly prepared using γ-Al_2O_3 as the support and cobalt nitrate hexahydrate, $Co(NO_3)_2 \cdot 6H_2O$, as an impregnating salt, followed by calcination and/or reduction [191,192]. This is mostly due to the relatively easy and complete decomposition of this salt, as well as to the lack of any residue left on the surface when using this salt.

The impregnation of small amounts of Co^{2+} salts (i.e., nitrate) onto γ-Al_2O_3 followed by moderate temperature calcination results in the dispersion of Co ions, forming highly dispersed Co^{2+} ions on alumina, while the loading of larger amounts of cobalt species produces a surface layer with a spinel-like structure, whose XPS and UV-vis-NIR spectra are closely similar to those of $CoAl_2O_4$ [193], with the presence of Co^{2+} and the absence of Co^{3+} [194,195]. of these defective spinel materials results in a shift in the 440 XRD peak in the range 600–1100 K, providing evidence for the partial penetration of Co ions in the defective spinel structure of γ-Al_2O_3, and in the crystallization of $CoAl_2O_4$ and α-Al_2O_3 only at 1290 K [131], in agreement with the behavior of Co-doped γ-Al_2O_3 (see above). H_2-TPR experiments show that highly dispersed Co^{2+} species are almost non-reducible up to 1000 K, while the surface spinel layer is reduced in H_2-TPR conditions in the 700–900 K range [131,132,194] (Figure 7).

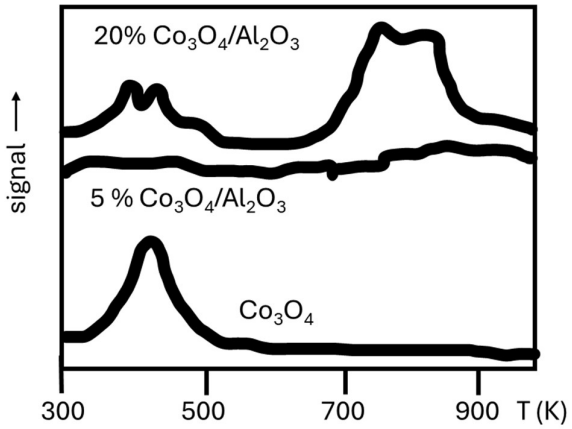

Figure 7. H_2-TPR curves of bulk Co_3O_4, low-loading and highly dispersed Co_3O_4/γ-Al_2O_3, and near-monolayer loaded Co_3O_4/γ-Al_2O_3 [195].

If the loaded amount exceeds a level that can be calculated to be sufficient for covering the entire support surface (monolayer amount), the features of the sample become those of a biphasic material. Taking into account that typical γ-Al_2O_3 supports have 150–250 m^2/g surface areas, the amount of cobalt on near-monolayer catalysts is 15–20 wt%. Over the theoretical monolayer loading, the visible and XPS spectra become analogous to those of Co_3O_4 (or $Co_{3-x}Al_xO_4$) stoichiometric spinel particles, which are also highly evident in the XRD pattern, present together with the features of the γ-Al_2O_3 support [193–196].

4.4. CoO_x/Al_2O_3 Materials Produced Through Other Techniques

According to a recent paper, low-Co-loading $CoO_x/\gamma Al_2O_3$ samples can be prepared using a dry solid-state technique, i.e., mixing and calcinating separated Co nitrate and dehydroxylated γAl_2O_3 [197]. These materials, in spite of their low cobalt loading, would show a high catalytic activity because of the presence of undispersed Co_3O_4 agglomerates. However, the real deposition of such particles on alumina, as well as the stability of these materials as catalysts, has not been ascertained. Zavyalova et al. [198] reported on a combustion synthesis method starting from impregnated cobalt nitrate on alumina for preparing CoO_x/Al_2O_3 total oxidation catalysts.

4.5. Reduction of CoOx-Al_2O_3 Materials as Precursors of Supported Cobalt Metal Catalysts and Their Industrial Application

As already mentioned, cobalt oxides are reduced by hydrogen to metallic cobalt at temperatures ranging from 473 to 673 K. In contrast, alumina is not reducible by hydrogen in normal conditions up to 1273 K. In parallel, the H_2 reduction at $T \leq 773$ K of biphasic CoO_x/Al_2O_3 samples, i.e., those presenting CoO- or Co_3O_4-phase particles within the material, results in the production of cobalt metal particles. This occurs, in particular, in the case of CoO_x/Al_2O_3 prepared by impregnation of γ-Al_2O_3 with an over-monolayer loading of cobalt oxide, and in the case of coprecipitated spinels with Co/Al ratio > 0.5. The H_2-reduction of these materials results in the formation of metallic cobalt particles interacting with or supported on alumina or Co^{2+}-containing alumina [131,132,194–196,199].

On the other hand, the presence of small amounts of Al^{3+} ions in cobalt oxides hinders cobalt reduction, thus increasing the stability of cobalt oxides in hydrogen reducing conditions [200]. Instead, samples based on bulk $CoAl_2O_4$, co-doped aluminas, and catalysts constituted by well-dispersed Co oxides in small amounts on alumina are much more resistant to reduction, starting to be reduced only above 1000 K in TPR conditions [131,132,194]. Nevertheless, the formation of small amounts of small-size dispersed cobalt metal particles or cobalt clusters supported by or interacting with alumina is possible already after a prolonged reduction also at 673–773 K [171,194,196]. The "surface spinel layer" predominant on Co_3O_4/Al_2O_3 samples, with a near-monolayer coverage, is mostly reduced in TPR experiments in the 700–900 K range (Figure 7).

CoO_x/Al_2O_3 materials have commercial applications as the precursors of metallic Co/Al_2O_3 catalysts, mainly used for hydrogenation reactions, such as the Fischer Tropsch synthesis of hydrocarbons from $CO/CO_2/H_2$ syngases [6,7]. In many cases, such precursors contain a cobalt oxide loading slightly exceeding the monolayer loading, thus producing small metal particles after pre-reduction, as occurs, e.g., with Co/γ-Al_2O_3 Fischer Tropsch catalysts [7,201] which usually contain nearly 20 wt% cobalt with alumina supports of 150–200 m^2/g [6,202]. Similar materials and procedures are also applied commercially in the manufacturing of Co/Al_2O_3 catalysts for other hydrogenation, dehydrogenation, amination and steam reforming catalysts [203,204].

It can be mentioned that the preparation of metallic alumina-supported cobalt catalysts can also be obtained using an impregnation of the support with cobalt carbonyls $Co_2(CO)_8$ or $Co_4(CO)_{12}$ in organic solutions [6]. In this case, the calcination step would not be needed; thus, oxidic precursors are not necessarily used.

5. Surface Chemistry of Catalytic Materials Based on Co and Al Oxides

5.1. Surface Chemistry of Cobalt Hydroxides

Very few data are reported on the surface chemistry of cobalt hydroxides. The surface of $Co(OH)_2$ polymorphs is reported to be covered by hydroxy groups that can be exchanged by carboxylate and anhydride groups, thus improving the electrocatalytic properties [205].

A point which recently raised much attention refers to the spin configuration of Co^{n+} surface sites on the surfaces of CoOOH. Authors have, in fact, concluded that surface Co^{3+} in the HS state (different from its LS state in the bulk) has a higher activity for the electrochemical Oxygen Evolution Reaction. According to Zhang et al., HS-surface coordinatively unsaturated Co^{3+} sites can be generated on CoOOH samples through the electrochemical oxidation of cobalt sulfides [206].

5.2. Surface Chemistry of CoO and Co_3O_4

Given the periclase structure of CoO and the only slightly larger lattice constant of CoO with respect to MgO (4.263 vs. 4.213 Å [207]), due to the slightly larger ionic radius of octahedrally coordinated Co^{2+} with respect to Mg^{2+} (0.745 Å vs. 0.72 Å [208], CoO is expected to have a highly ionic character and a predominant basic character at its surface [209,210], only slightly lower than that of MgO [211]. In fact, surface Co^{2+} ions are expected to act as weak Lewis acid sites, and, in parallel, surface oxide anions should be markedly basic. In contrast, the definitely higher polarizing power of Co^{3+} with respect to Co^{2+} due to a higher charge and smaller ionic radius (~0.6 Å) would result in a higher Lewis acidity of such sites when exposed at the surface.

On the other hand, it has been already said that CoO, CoO_{1+x} and Co_3O_4 easily transform each into the other, at least at the surface, through air, inert or vacuum pretreatments at moderate temperatures [212]. Most surface studies, in particular those realized through IR spectroscopy, are realized after outgassing at moderately high temperatures, such as at $T \geq 673$ K, in order to desorb water species, and this leads to the at least partial decomposition of Co_3O_4 to CoO [108,129,193]. Thus, the surface studies of cobalt oxides may give very different results depending on the pretreatments.

In fact, surface studies have been realized for Co_3O_4 with different pretreatments [129]. The slight reduction of a Co_3O_4 pure powder pressed disk even through simple outgassing, or, even more, in hydrogen (200 Torr, 523 K, 10 min) followed by outgassing at 373 K, strongly increases the transmittance to IR radiation and results in a hydroxylated surface. In fact, a main band at 3680 cm^{-1} is observed, similar to that previously observed and attributed to the surface OHs on CoO [213]. Over this pre-reduced sample, essentially transformed into CoO, methoxy species are formed from methanol at room temperature (C-O stretching at 1080 cm^{-1}), and Lewis-bonded ammonia (1611 cm^{-1} NH_3 asymmetric deformation, 1175 cm^{-1} NH_3 symmetric deformation) is formed from NH_3, confirming the ionic nature of the CoO surface, the moderate Lewis acidity of Co^{2+} surface sites, and their limited oxidation ability [129]. The IR spectra of NO adsorbed on Co_3O_4 outgassed at 773 K, mostly transformed into CoO according to XRD, have been reported by Topsøe and Topsøe [193], producing dinitrosyl species absorbing at 1865 and 1780 cm^{-1}, confirming the activity of surface cobalt sites, which are likely bivalent.

Studies of CO adsorption on outgassed Co_3O_4, essentially constituted by CoO, show the presence of a band at 2140 cm^{-1}, assigned to CO interacting with Co^{2+} centers, but also a number of other bands in the 2100–1700 cm^{-1} range that are attributed to different polycarbonyl species on reduced cobalt centers. This suggests that CO is able to reduce Co^{2+} to Co^{+} or even to Co metal centers at room temperature [129], or that a partial decomposition of CoO to Co metal already occurred under outgassing [135].

Over simply outgassed Co_3O_4 samples, likely still incompletely converted to CoO, methanol is oxidized on the surface at room temperature, producing carbonate ions and dioxymethylene species. Also, ammonia is oxidized on the simply outgassed Co_3O_4 surface, producing at room temperature amide, imide and NO^{+} species [129]. This confirms the strong oxidizing power of the Co_3O_4 surfaces. On the other hand, the adsorption of CO at 150 K over this simply outgassed Co_3O_4 surface gives rise to a single CO stretching

band whose frequency decreases slightly with increasing coverage (from near 2195 to near 2170 cm^{-1}) attributed to CO on Co^{3+} surface sites, while a C-O stretching at 2140 cm^{-1} was again assigned to CO interacting with Co^{2+} surface sites [129].

On the other hand, CO adsorption on unreduced Co_3O_4 produces CO_2 and surface carbonates at very low temperatures, such as T $\geq$ 323K [90,214] and CO adsorbed on reduced cobalt centers produces carbonyl species absorbing at 2120, 2070 and 2000 cm^{-1} (Figure 8). Structural and computational studies suggest that CO can adsorb and be oxidized even at 77 K over Co_3O_4 nanorods, and that the active sites for CO adsorption in an oxygen-containing atmosphere are Co^{3+} [215].

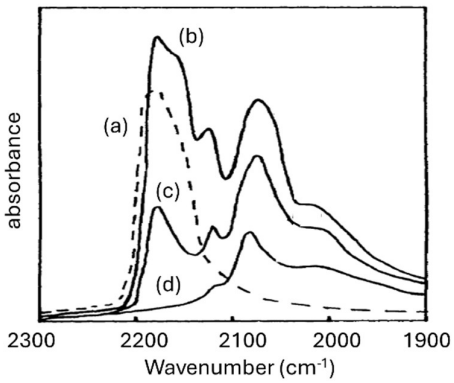

Figure 8. FTIR spectra of CO (100 Torr) adsorbed on Co_3O_4 (previously outgassed at 790 K) at 150 K (a) and at 300 K (b) and after evacuation at room temperature for 15 min (c) and 30 min (d) [129].

A more recent paper [216] reports an IRAS study of CO adsorption at 110 K on a Co_3O_4 (111) monocrystal face deposited on Ir(111). Similar bands were observed with a slightly different assignment, as reported in Figure 9. In any case, these data confirm the very strong oxidizing ability of the Co_3O_4 surface due to reduction of Co^{3+} to Co^{2+} with the release of surface oxygen species, while the surface of CoO retains an oxidation ability, together with a relevant acid–base behavior shifted towards basicity.

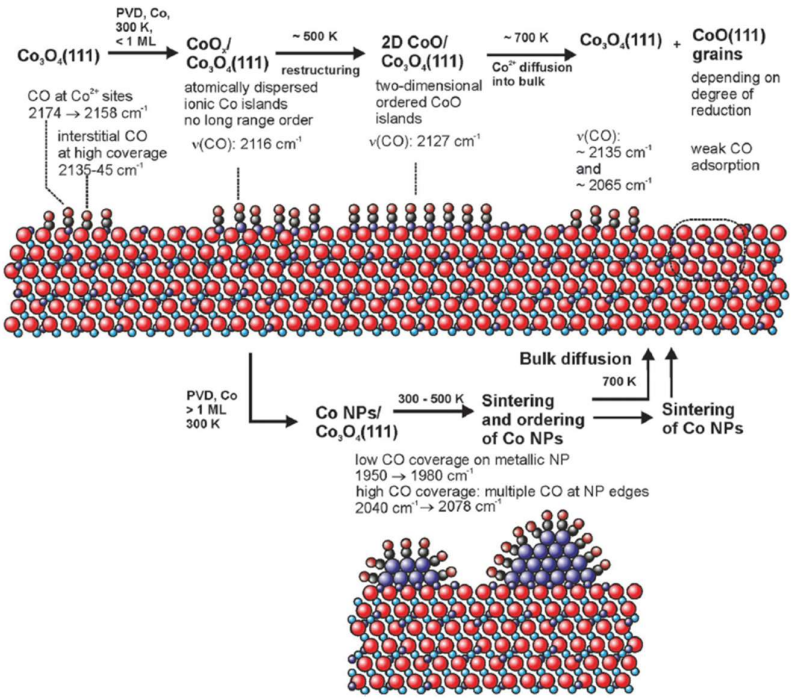

Figure 9. Schematic representation of the CO vibrational frequencies observed for adsorption on the different cobalt deposits on Co3O4(111)/Ir(100) investigated in Ref. [216].

Also, in the case of cobalt oxide, the spin configuration of Co^{n+} surface sites has relevance with respect to the activity in OER. The amount of surface octahedral HS Co^{3+} on Co_3O_4 can be increased by expanding the surface lattice constant through a complex preparation procedure [217]. Enhancing the concentration of surface HS Co^{3+} ions can be obtained in mixed oxide phases containing cobalt such as Zn-Co spinels [218] and $PrBaCo_2O_6$ (PBCO) double perovskite [219].

5.3. Surface Chemistry of $CoAl_2O_4$

Studies on the $CoAl_2O_4$ surface show that it is hydroxylated after outgassing at 773 K [160,220]. IR spectra of NO adsorbed on $CoAl_2O_4$ have been reported by Topsøe and Topsøe [193]. Also, in this case, like for Co_3O_4, the doublet at 1860, 1780 cm^{-1} is attributed to dinitrosyl species on Co^{2+}. However, a different intensity ratio between the two bands observed on $CoAl_2O_4$ and on Co_3O_4 suggests that the angle between the Co-nitrosyl species is different in the two cases.

CO adsorbed at 170 K and at room temperature on $CoAl_2O_4$ outgassed at 773 K is responsible for the main C-O stretching band at 2170 cm^{-1} and the shoulder near 2140 cm^{-1} [93,160,220]. They were assigned to CO coordinated on octahedral-like Al^{3+} and tetrahedral-like Co^{2+}, respectively, in agreement with the normal spinel nature of this solid. However, by increasing the contact time at r.t., the spectrum modifies, with the growth of bands in the region 2120–1950 cm^{-1} and also of absorptions in the carbonate region. This suggests that CO is oxidized by Co^{2+}, which is reduced to monovalent or zerovalent cobalt centers, as observed also for pure cobalt oxide (see above).

Pyridine adsorption on outgassed $CoAl_2O_4$ [93,160,220] confirms the location at the surface of both Al^{3+} and Co^{2+}, according to the splitting of the 8a vibrational mode of coordinated pyridine (1623 and 1608 cm^{-1}, respectively). Thus, $CoAl_2O_4$ surfaces retain a moderate oxidation ability after treatments in a vacuum due to the surface Co^{2+} ions and maybe residual Co^{3+} ions, as well as a marked acido-basic character due to the strong Al^{3+} Lewis acid centers and weaker Co^{2+} Lewis acid centers, the latter also showing a moderate oxidizing ability.

5.4. Surface Chemistry of Unreduced CoO_x/Al_2O_3 Materials

IR studies of CO adsorbed at a low temperature over outgassed CoO_x/Al_2O_3 [93,171] show two main components in the C-O stretching band, with a high frequency shoulder at 2190 cm^{-1} assigned to CO adsorbing on Al^{3+} and Co^{3+} ions and a main band near 2170 cm^{-1} assigned to CO adsorbing on Co^{2+} sites. However, the formation of CO_2 adsorbed species is also observed, confirming the strong oxidizing ability of part of surface cobalt oxide species over these samples.

The IR spectra of NO adsorbed on CoO_x/Al_2O_3 have been reported by Topsøe and Topsøe [193]. NO is reported to adsorb as a dinitrosyl species (doublet at 1860, 1780 cm^{-1}), similar to those found over $CoAl_2O_4$ and over cobalt cationic centers dispersed on the surface of low-loading samples. Instead, for the higher-loading sample, the spectrum becomes more similar to that found over Co oxide, confirming the coalescence of cobalt oxide particles [193].

The data indicate that the surface properties of largely dispersed sub-monolayer-loading CoO_x/Al_2O_3 have comparable properties to those of $CoAl_2O_4$ surfaces, in agreement with the formation of a cobalt aluminate spinel-like surface layer [193,194,196]. Higher-loaded samples, bypassing the monolayer coverage, contain Co_3O_4 or CoO particles, behaving in quite a similar way to unsupported oxides.

6. Catalytic Activity of Cobalt Oxides and CoO_x/Al_2O_3 Materials for Gas Phase Total Oxidations

6.1. CO Oxidation Catalysis

6.1.1. Co_3O_4 as a Low-Temperature CO Oxidation Catalyst

CO oxidation is a relevant process for removing the strongly poisonous CO molecule from breathing air [221]. Co_3O_4 is an active catalyst for CO oxidation even below room temperature [14] or at 300–400 K [97], but may suffer deactivation [222]. According to Cunningham et al. [223] Co_3O_4 is active in CO oxidation even at 217 K and retains a good stability even if the feed is wet. This was confirmed by Whang et al. [224]. As reviewed by Dei and Dhal [101], Co_3O_4-based nanomaterials are among the most active catalytic materials for very-low-temperature CO oxidation to CO_2. In fact, according to Xie et al. [215], Co_3O_4 nanorods not only catalyze CO oxidation at temperatures as low as −350 K but also remain stable in a moist stream of normal feed gas. The high activity in different cobalt oxide-based solids was attributed to electron-mobile Co^{2+}-O^{2-}-Co^{3+} linkages at the surface of the Co_3O_4 spinel [225] and depends on the concentration of surface Co^{3+} ions [215]. According to Tang et al. [72], bulk Co_3O_4 is covered by a CoO surface layer during low-temperature CO oxidation (353–413 K), while it is covered by a more active Co_3O_4 surface layer at higher temperatures. On the other hand, surface spectroscopic studies show a CO oxidation to surface carbonates at room temperature over Co_3O_4, due to a reaction with surface oxide species and Co^{3+} reducible cations [129]. In conclusion, Co_3O_4- and Co_3O_4-based materials are promising practical catalysts for low-temperature CO oxidation, competitive with noble metal-based catalysts and with copper and manganese oxide-based materials [226].

6.1.2. CoO_x/Al_2O_3 Catalysts for CO Oxidation

Mixed spinels with a Co^{2+}/Al^{3+} ratio of 1.5 and 3.0 show a higher activity and stability in CO oxidation at 300–373 K than unsupported Co_3O_4 [222]. Also, supported CoO_x/γ-Al_2O_3 catalysts find relevant activity in CO oxidation, which can be further improved through reduction + reoxidation pretreatments, leading to catalysts active at 423–523 K, in the case of 10–30 wt% $Co/\gamma Al_2O_3$ catalysts [227]. high activity is reported for catalysts prepared from cobalt acetate and precalcined in nitrogen [228], while the preparation method and properties of mesoporous alumina support have a considerable effect [229]. On the other hand, Thormählen et al. [230] produced a monolithic catalyst based on a Co_3O_4-$CoAl_2O_4$-Al_2O_3 system, with a 20% nominal Co_3O_4 content, and found that, after pre-oxidation, it was very active at low temperatures and with a light-off temperatures of 210 K, even lower than that of similarly prepared platinum-containing catalysts [231]. In summary, the addition of alumina to cobalt oxide may give rise to more stable and very active catalysts for low temperature CO oxidation, which can even compete with noble metal-based catalysts.

6.1.3. Cobalt Oxides in Preferential CO Oxidation (PROX) Catalysis

The preferential CO oxidation reaction allows the oxidation of CO in mixtures with hydrogen to CO_2, favoring the later purification of H_2 with washing or adsorption techniques. While noble metals such as platinum are mostly studied for this reaction, cobalt oxides are potentially very interesting too [232,233] The Co_3O_4 catalyst exhibits a very high activity, maintaining a 100% CO conversion and CO_2 yield without any hydrogen consumption between 423 and 448 K [234]. According to Lukashuk et al. [235], Co_3O_4 is reduced by H_2 to CoO and ultimately to metallic Co during CO-PROX, and this results in a loss of oxidation activity and in the coproduction of methane by CO hydrogenation on metallic cobalt. Catalysts based on Co_3O_4/γ-Al_2O_3 are also active in the PROX reaction at 323–473; the more

active, the lower the Co oxide particle size [236]. On the other hand, a full selectivity in CO oxidation is found below 498 K, while at higher temperatures hydrogen consumption is found and Co_3O_4 is reduced to CoO [236]. Studies on Co_3O_4/α-Al_2O_3 catalysts show that the catalytic activity implies a key role of Co^{3+} ions and that the 100 spinel face of Co_3O_4 is the most active one [237].

6.2. Hydrocarbon Total Oxidation Catalysis

6.2.1. Co Oxides as Methane Combustion Catalysts

Co_3O_4 was found as the most active bulk transition metal oxide catalyst for methane combustion in the early study of Anderson et al. [238], and this was confirmed more recently [239,240], although its stability is limited [241], lower than that of Mn_2O_3. On the other hand, mixed oxides, such as, e.g., cobalt–chromium spinels [239] and Co_3O_4-CeO_2 systems [97], may even have an increased methane combustion activity.

The catalytic combustion of methane and natural gas is used in combined cycle technologies to limit NOx emissions in electrical energy production [242,243]. In this case, a relatively high methane concentration is fed in air; thus, high temperatures are produced on the catalyst, such as 773–1273 K—in any case, sufficiently low to prevent the production of relevant amounts of NOx. To have a stable methane combustion activity at high temperatures, solid-state stabilization is needed. Low-surface-area (3 m^2/g) Co_3O_4 was found to be remarkably active in high-temperature methane combustion [244], although it was definitely less active than platinum-based catalysts. To increase stability, cobalt oxide must be mixed with refractory oxides, thus producing mixed phases as perovskites (e.g., $LaCoO_3$) and β-aluminas (e.g., $SrCo_xAl_{12-x}O_{19-\delta}$) [243–245].

Low-temperature methane combustion represents a technology for burning methane in low concentrations in air to reduce fugitive methane emissions [246] or to treat the flue gases of NG-fueled engines [247,248]. Thanks to the lower concentration of methane, heat evolution is limited, and the temperature in the catalyst bed is moderate, i.e., 500–873 K. In fact, Co_3O_4 is active in fully burning 1% methane in air at a gas hourly space velocity (GHSV) = 30,000 $mLg^{-1}h^{-1}$ at 723 K [249] and in 1% methane and 10% O_2 in nitrogen (e.g., oxygen-depleted air) at GHSV 36,000 $mLg^{-1}h^{-1}$ at 640 K [250]. Working at GHSV 60,000 $mLg^{-1}h^{-1}$ with a gas composed of 1000 ppm CH_4, 200 ppm NO, 3% CO_2, 5% H_2O, 20% O_2, and N_2 balance, the half-conversion temperatures of different mesoporous samples of Co_3O_4 were in the range 681–746 K [251].

6.2.2. Co Oxides as Higher Hydrocarbon Total Oxidation Catalysts

The potential use of cobalt oxides as catalysts for the total combustion of higher hydrocarbons and other Volatile Organic Compounds (VOCs) has been the subject of some reviews [14,97,252–254]. Co_3O_4 is reported to catalyze the total oxidation of aliphatic and aromatic hydrocarbons, as well as oxygenated compounds, in air or oxygen at very low temperatures. Co_3O_4 has the weakest metal–oxygen bond, and the easy reduction of Co^{3+} in Co_3O_4 to Co^{2+} could accelerate the formation of oxygen vacancies at low temperatures [255].

Cobalt oxides have also been tested in propane total oxidation, observed to occur, e.g., at 423–473 K (1000 ppm of C_3H_6 + 9% of O_2 in He at WHSV 36,000 mL g^{-1} h^{-1}) on Co_3O_4 (11 m^2/g) [97]. Propane combustion catalytic activity was found to be mainly dependent on the crystallite size, decreasing with an increase in the crystallite size, correspondingly depending on the surface area [256].

The light-off oxidation temperature of both propane and propene is similar for commercial Co_3O_4 in diluted O_2/He in flow conditions [257], but spectroscopic surface studies show that they are oxidized at the surface of Co_3O_{4+x} already at or just above room temper-

ature, respectively. Propene is oxidized "selectively" at the allylic methyl group, giving rise to acrylate species, while propane is probably attacked both at C(2) and at C(1), giving rise at 373 K to propanoates and acetates + formates. Acrylates are also formed from propane, probably arising from 2-propoxides via propylene. At higher temperatures, the adsorbed species are fully oxidized to CO_2 [258]. Surface spectroscopy data show that the full oxidation catalysis of transition metal oxides such as Co_3O_4 is the result of successive partial oxidation steps at the surfaces essentially involving oxide anions and reducible high-valency cations such as Co^{3+} [259].

Co_3O_4 also shows a high activity in the oxidation of aromatic hydrocarbons such as benzene and toluene at temperatures as low as 513–543 K [260,261]. It has been pointed out that pre-calcination conditions have a relevant effect on the activity of Co_3O_4 for the combustion of toluene [261,262]. Slow and weak deactivation is observed in both toluene and benzene's full oxidation on Co_3O_4 after 20–40 h.

6.2.3. CoOx/Al_2O_3 as Hydrocarbons Total Oxidation Catalysts

Supporting Co_3O_4 on alumina was found to decrease its activity in methane combustion [238,248,263]. Co_3O_4-γAl_2O_3 catalysts are reported to be less active than magnesia-, titania-, and, in particular, zirconia-supported Co_3O_4 [264] as well as $ZnAl_2O_4$-supported Co_3O_4 [263] and $MgAl_2O_4$-supported Co_3O_4 [265] in methane combustion. However, due to the stability and well-known properties of gamma alumina, the potential use of Co_3O_4/γ-Al_2O_3 as a methane combustion catalyst has been the subject of investigation [198,248,266]. According to Solsona et al. [256], Co_3O_4 supported on low-surface-area α-Al_2O_3 is more active as a propane combustion catalysts than Co_3O_4/γ-Al_2O_3, and this is due to the less dispersing properties of corundum surfaces with respect to surfaces, as well as to the low surface area, resulting in an agglomeration of bulk Co_3O_4 particles in the case of Co_3O_4/α-Al_2O_3. On the other hand, the activities in catalytic combustion of the supported cobalt catalysts depend obviously on the cobalt loading [241,256]. Indeed, the activities in propane combustion of 50% Co_3O_4/α-Al_2O_3 and of 50% Co_3O_4/γ-Al_2O_3 are only slightly lower than those of bulk Co_3O_4 at 423–523 K [256]. On the other hand, it was found that the activity of 10 wt% Co_3O_4/γ-Al_2O_3 in propane combustion can be greatly enhanced through structural modulation, i.e., through the reduction–passivation treatment of core shell materials, up to be capable of outperforming unsupported Co_3O_4 [267].

Supported $Co_3O_4/\gamma Al_2O_3$ [268] with an up to 21 wt% cobalt loading has also been tested in benzene oxidation. Benzene is completely burnt in the range of 473–573 K to CO_2, with a maximum activity for the sample with 21 wt% cobalt prepared using the equilibrium deposition filtration technique. Also, ex-hydrotalcite coprecipitated Co_3O_4-$CoAl_2O_4$ spinel samples are very active in benzene catalytic combustion, with a maximum activity for samples with a Co/Al atomic ratio = 5 [149] while details on the preparation also have some effect on catalytic activity [269]. Ex-hydrotalcite-type coprecipitated Co_3O_4-$CoAl_2O_4$ catalysts (Co/Al a.r. 2) also catalyzed full benzene oxidation at 373–573 K, but the activity of samples precalcined in nitrogen is better compared to that of samples pre-calcined in air, likely due to a higher surface area [150]. Similar catalysts also catalyze toluene combustion in similar conditions [147]. Also, cobalt-containing hierarchical laminated Al_2O_3 (3 and 5 wt% Co) catalyzes the total oxidation of toluene near 573 K [270].

6.3. Total Oxidation of Oxygenated Compounds and of Other VOC's

6.3.1. Co_3O_4 as a Catalyst for the Total Oxidation of Oxygenated Compounds

Co_3O_4 has high activity in catalyzing burning of formaldehyde, the most important gaseous pollutant in indoor environment primarily released from building materials, furniture, indoor combustion processes, such as cooking, incense burning, and smoking, already

at room or slightly higher temperature [271]. It is also able to catalyze full combustion of ethanol at 430 K [272], but the more toxic product acetaldehyde is produced at lower temperature when ethanol conversion is incomplete. Finocchio et al. reported on the isopropanol and acetone full oxidation on Co_3O_4 [258,260]. It was found that at moderate conversion, isopropanol is selectively oxy-dehydrogenated to acetone (80% selectivity at 500 K), but at higher temperature (i.e., 650 K) both isopropanol and acetone are fully converted to carbon oxides (Figure 10). The activity in isopropanol combustion was found to significantly depend on morphology of mesoporous Co_3O_4 catalyst powder [273].

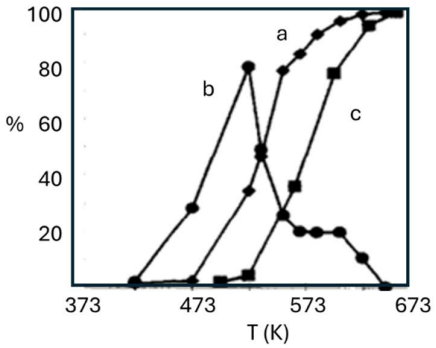

Figure 10. Isopropanol conversion (a) and acetone selectivity upon isopropanol conversion (b); acetone conversion (c) over Co_3O_4 [258].

6.3.2. Co_3O_4 as a Catalyst of Total Combustion of Chlorinated Hydrocarbons

The catalytic combustion of chlorinated VOCs represents a particular field [274] due to the effect of chlorine on catalyst stability, as well as on the fate of chlorine in the products. In fact, noble metal catalysts may suffer a deactivation by chlorine upon catalytic oxidation, while some transition metal can give rise to volatile chlorides. Also, zeolite structures can suffer instability in the presence of chlorine. Finally, while the evolution of HCl, which can be more easily washed down from combustion gas, is desirable, the oxidation of chlorine to Cl_2 should be avoided. DeRivas et al. [275] reported on the high activity of Co_3O_4 in the catalytic combustion of Ethylene Dichloride (EDC, 1.2-dichloroethane) with a 100% C-selectivity towards CO_2 and with a coproduction of HCl and Cl_2 at relatively low temperatures (623–673 K). Samples obtained via precipitation proved to be considerably more active than the supported noble (Pt, Pd) metals, protonic zeolites, and Ce/Zr and Mn/Zr mixed oxides, and were found to be highly stable despite the retention of chlorine on the catalyst surface. Yuan et al. [276] reported on the catalytic activity of Co_3O_4 in Vinyl Chloride Monomer (VCM, chloroethylene) catalytic combustion. Over catalysts produced through the template method and calcined at 673 K, working at 563 K with a space velocity of 30,000 $mL_{g_{cat}}{}^{-1}.h^{-1}$ and VCM concentration of 1000 ppm in air, the initial conversion is complete, while it exceeded 96% after 60 h of continuous reaction, with HCl as the main coproduct. At incomplete conversion, traces of chlorinated by-products ($CHCl_3$, CCl_4, C_2HCl_3, $C_2H_3Cl_3$) were formed. Depositing cobalt oxide over mesoporous silica was reported to improve catalytic performances in the combustion of chloride organics [277,278].

6.4. Cobalt Oxides as Catalysts for the Combustion of Hydrogen and of Fuel Cell Anode Tail Gas

The catalytic combustion of hydrogen may have relevant applications in the near future [279,280]. Cobalt oxide Co_3O_4 is reported to be the most active transition metal oxide as a catalyst for hydrogen combustion [281] and can be used as a component of non-noble metal catalysts [278,282]. A particular case can be represented by the anode tail gas of hydrogen fuel cells such as Solid Oxide Fuel Cells and Polymeric Electrolite

Membrane Fuel Cells. These gases contain hydrogen together with different amounts of CO and methane, and must be partially purged to avoid concentrations of such gases in the recycling of unconverted hydrogen. Such anode tail gas purge can be catalytically burnt to minimize the CH_4 and CO emissions and provide energy to the system. CoO_x/γ-Al_2O_3 catalysts were used for the combustion of anode tail gas produced in a proton-exchange membrane (PEM) fuel cell [283].

6.5. Diesel Soot Oxidation Catalysis

Co_3O_4 is the most active single-phase catalyst for the total oxidation of Diesel soot [284] at 623–723 K, which is further increased by doping with other elements such as silver, cerium, nickel, lanthanum, potassium, lead, and Pt as well, down to 523–623 K [285,286]. Also, $CoAl_2O_4$ spinels, in particular, after milling, show a high combustion activity similar to that of Pt/Al_2O_3 catalysts [287]. In fact, cobalt oxides are reported to be possible components of commercial Diesel catalyzed anti-particulate filters [288,289].

6.6. Stability and Deactivation of Cobalt Oxide-Based Catalysts for Gas-Phase Oxidation Reactions

As already remarked, the gas-phase oxidation catalytic activity of Co_3O_4 based catalysts strongly depends, in most cases, on morphology, being essentially the stronger the larger the surface area. In fact, an impressive number of papers have been recently published on the preparation of high-surface-area cobalt oxide- based nanoparticles with sophisticated soft chemistry methods [98–104]. On the other hand, even with classical methodologies Co_3O_4 with very high surface area can be obtained: as for example, 202 m^2/g from decomposition of $Co(OH)_2$ [290]. Indeed, quite few data are available on the thermal stability of such high surface area materials. Data indicate that Co_3O_4 samples heated above 773 K in oxidizing conditions tend to sinter rapidly, with increase of particle size and decrease of surface area [107,291]. As for example, in the case of cobalt oxide microflowers the surface area decreases from 77 to 12 m^2/g by increasing calcination temperature from 573 to 773 K [96]. In Figure 11, the TEM images of cobalt oxide nanoparticles are reported after heating in the TEM chamber, i.e., at a low pressure of $<10^{-5}$ Pa [108]. XRD analyses show that the starting sample is still Co_3O_4, while, already at 673 K it is fully converted into CoO, as at the final temperature of 1073 K. The TEM image shows that after heating at a temperature of 673 K, the surfaces of the nanocrystals became uneven and more faceted, due preferential exposition of particular crystallographic facets, but no significant particle size growth is observed. Instead, after heating at 1073 K particle coalescence clearly occurred [108]. Early data show that heat treatment of ex-oxalate Co_3O_4 for 24 h already causes a decreases of S_{BET} from 57 m^2/g to 33 m^2/g at 573 K, to 19 m^2/g at 673 K and to 5 m^2/g at 873 K [289]. Thus, sintering can be the cause of progressive loss in catalytic activity at moderate to high temperature depending also on time on stream [261,262]. On the other hand, high surface area can be not necessary for high temperature catalytic oxidation activity, such as e.g., for methane high temperature catalytic combustion at 773–1273 K [244,292], but also for CO oxidation at 333 K [289].

It is also well evident that catalytic activity is reduced when so high a temperature is raised when Co_3O_4 starts to decompose into CoO. On the other hand, in the presence of reductants, Co_3O_4 may be reduced at the surface at much lower temperature forming an epitaxial layer of CoO [237,293], loosing oxidation activity. Reversely, at low temperature in the presence of oxygen, CoO can become covered by a Co_3O_4 layer, thus acting as a very active oxidation catalyst [72]. Thus, catalytic activity in oxidation depends on the relative concentration of oxygen and reductants in the feed, even at low temperatures. The presence of water in the reaction medium, taking into account that water is also a coproduct of organic compound total oxidation, also negatively influences catalytic activity [263] due

to the basicity of water competing with oxygen and organic molecules for the adsorption of cobalt ions.

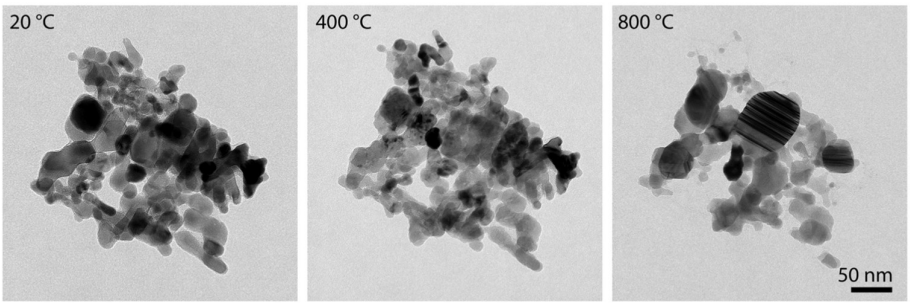

Figure 11. Bright-field TEM images of (initially) Co_3O_4 NPs at room temperature, at 673 and 1073 K [108].

Supporting cobalt oxides on alumina tend to reduce low temperature catalytic activity in oxidation, but may certainly increase solid state stability by limiting the sintering and surface area loss of the active cobalt oxide phase. This is the likely reason for the increased stability of catalytic activity finally producing even more performant catalysts at moderate temperatures [218].

7. Catalytic Activity of Cobalt Oxides in the Chemistry of Ammonia and Nitrogen Oxides

7.1. Ammonia Oxidation Catalysis

Ammonia oxidation to NO is the first step in the Ostwald process for nitric acid synthesis [294]. This reaction, where the co-production of the most stable products N_2 and N_2O must be limited, is realized at 1073–1173 K using Pt metal-based gauges. However, this commercial process suffers the serious drawback of losing platinum as volatile PtO. As an alternative, the development of monolithic honeycomb oxide catalysts has been considered. Among catalytic materials for such an application, cobalt oxide-based materials appear to have excellent properties [295] associated with minimal N_2O coproduction [296]. In fact, the pure oxide Co_3O_4 shows the maximum NO selectivity in ammonia oxidation at 923 K, but can be used only under atmospheric pressure and at a low ammonia concentration, otherwise it transforms to less selective CoO [294,295]. This effect is hindered by doping Co_3O_4 with ceria, thus increasing the high selectivity to NO at 993–1093 K [297]. Also supporting Co_3O_4 on $ZnAl_2O_4$ spinel improves Co_3O_4 stability in ammonia oxidation to NO [298]. In fact, several cobalt oxide based catalysts, including Co-Al mixed oxides, have been patented for such an application [299,300].

In contrast, supporting cobalt oxide on γ-Al_2O_3, at least at low and moderate coverages, results in catalysts with a low activity in oxidizing ammonia [297]. Ammonia conversion over CoO_x/γ-Al_2O_3 increases with cobalt loading [197,301] producing both NOx and N_2. However, 2% Co/γ-Al_2O_3 reduced in hydrogen at 873 K, which still predominantly contains Co^{2+}, gives rise to a stable, quite high selectivity (>80%) for N_2 [300], which can be useful for performing the so-called Selective Catalytic Oxidation (SCO) of ammonia to reduce ammonia slip, e.g., after DeNOxing devices for Diesel aftertreatment using Selective Catalytic Reduction with ammonia (SCR).

7.2. Catalysis for Oxidation of NO to NO_2

The NO-to-NO_2 oxidation reaction is a relevant process in Diesel car afterburner systems, previous to the so-called fast SCR reaction, i.e., the reduction of NO_2 to N_2 by ammonia [302]. It can also speed up the Ostwald process for nitric acid synthesis [303]. Co_3O_4 is a very effective catalyst for the high conversion of NO to NO_2 at 523–573 K

and a high space velocity of 238,000 h^{-1} [304]. The reaction raises the thermodynamic equilibrium near 550 K over Co_3O_4 [305]. However, the activity is significantly negatively affected by the presence of SO_2 in the stream [303]. This can limit its application in Diesel aftertreatment systems.

7.3. Catalysts for the Abatement of Nitrogen Oxides

7.3.1. N_2O Decomposition Catalysis

N_2O is a powerful Greenhouse Gas mainly produced through adipic acid and nitric acid synthesis processes, and, to a lesser extent, combustion processes. It could also be produced in ammonia-fueled internal combustion engines [306,307]. To abate it from waste gases, either its reduction by methane or its thermocatalytic decomposition may be accomplished [308]. Cobalt oxides [309], including Co_3O_4 and other cobalt-containing spinels [310] and perovskites [307,308], are among the most active catalysts for N_2O decomposition to $N_2 + O_2$ and are mentioned among commercially available catalysts. Alkali doping is reported to further enhance the catalytic activity of Co_3O_4 in N_2O decomposition [311–313]. Also Co-Al oxides produced through the calcination of hydrotalcite like hydroxycarbonates display a high N_2O decomposition activity [314–316]. The catalytic activity of Co_3O_4 in N_2O decomposition is inhibited in the presence of methane and of oxygen as well [317]. Doubly doped (K,Zn) α-Al_2O_3-supported Co_3O_4 [318] also has a high activity and a slight inhibition by oxygen, but is strongly inhibited by NO in the gas phase.

Co-Al spinels are able to catalyze the full decomposition of 5000 and 10,000 ppm of N_2O with and without the presence of oxygen in the feed gas near 673 K, the catalytic activity being slightly inhibited by oxygen [315]. Nevertheless, $Co_{3-x}Al_xO_4$ catalysts have been patented for N_2O decomposition [319], and seem to be commercially available too [320].

Actually, it seems that reduced cobalt oxide species are the most active in N_2O decomposition centers, as seen for a catalytic material Co/CoO_x@carbon catalyst obtained by pyrolyzing cobalt-containing zeolitic–imidazolate framework precursors (ZIF-67) at 923 K in a N_2 atmosphere [321]. This material allows the complete conversion of N_2O at 673 K. In fact, the samples obtained through pyrolysis in air contain Co_3O_4 and show an activity at much higher temperatures, as with pure Co_3O_4.

7.3.2. Cobalt Oxide Catalysts for the Selective Catalytic Reduction of NO_x by Ammonia (NH_3-SCR)

The Selective Catalytic Reduction of NO_x by ammonia (as a water solution or coming from the decomposition of urea water solution [322] is commercially used to abate NOx from waste gases of nitric acid plants, thermal power stations and Diesel engines. Commercial catalysts are based on V_2O_5-MoO_3(WO_3)-TiO_2 [323] or Fe- or Cu-containing zeolites [324,325]. Many transition metal oxides also have a high activity for this reaction [326,327], spinel-type oxides and mixed oxides [328]. Co_3O_4 is an active catalyst for the SCR of NOx by ammonia at low temperatures (e.g., 423 K), but its activity strongly depends on morphology factors and is reduced above 473 K [327,329]. However, SO_2 promotes the activity of Co_3O_4 at T > 473 K [328]. Co_3O_4 nanorods have a higher activity than other Co_3O_4 nanoparticles [330]. Pre-oxidized Co_3O_4 nanorods are more active than slightly reduced ones, suggesting that surface Co^{3+} ions act as the active sites for the reaction.

7.3.3. Cobalt Catalysts for the Selective Catalytic Reduction of NOx by Hydrocarbons (HC-SCR)

CoO_x/Al_2O_3 catalysts, both coprecipitated [331,332] and prepared through wet impregnation [333,334], find an interesting activity in NO_x SCR with propane at 623–723 K, which can be slightly further increased by doping with Sn [330], Zn, Ag, Ni [331], and Ba [333]. Interestingly, a small cobalt loading (e.g., 1% Co) is more effective in the SCR

reaction, while at a higher Co content (3% Co) the combustion by oxygen of propane limits SCR activity [333]. Dispersed surface Co^{2+} ions are supposed to be responsible for the SCR activity, while cobalt oxide particles are active in propane combustion [332,333].

7.3.4. Cobalt Oxide Catalysts for the Simultaneous NO_x and Soot Abatement in Diesel Engine Aftertreatment Systems

Bulk Co_3O_4-$CoAl_2O_4$ spinel phases were found to be very active for the simultaneous removal of NO_x and diesel soot particulates. In particular, the spinel with a Co/Al atomic ratio of 5 and calcination temperature of 1073 K is the best one, with a medium activity (T_i = 563 K) and high selectivity to N_2 formation, as well as a low selectivity to N_2O [335]. The presence of the Co_3O_4 spinel is likely a determinant. In fact, while low-defectivity $CoAl_2O_4$ has a low activity, the ball-milled $CoAl_2O_4$ spinel shows a high activity in soot oxidation in NO_x/O_2 [287]. In fact, the addition of cobalt oxide allows us to decrease the emissions of NO_2 in commercial catalyzed Diesel particulate filters [336].

8. Catalysts for Ozone Activation and Decomposition

Co_3O_4 shows a very high activity in decomposing 40 ppm of ozone in dry oxygen-enriched air at 298 K and WHSV 1,200,000 mL/gh, with a slight decline of activity with time [130]. However, the activity is almost lost in wet feed. A much higher stability was found for mixed MgO-CoO oxides. By comparing the activity of different Co-containing oxides, it was deduced that octahedral Co cations give rise to the most active sites. In contrast, according to the data of Liu et al. [337] tetrahedral Co^{2+} sites would give rise to the most active catalysts for this reaction. According to these authors, $CoAl_2O_4$ has a comparable activity with respect to Co_3O_4, but much lower if the reaction rate is normalized for surface area.

Also cobalt hydroxides have a high activity for ozone decomposition. β-$Co(OH)_2$ shows a ~90% ozone decomposition efficiency under a high space velocity (WHSV = 1,200,000 mLg^{-1} h^{-1}, 298 K, 40 ppm), which is far higher than that of α-$Co(OH)_2$ (~5%) [23].

CoO_x/Al_2O_3 shows a lower activity than Co_3O_4 [130], but is still of interest for both the reactions of ozone decomposition and oxidation with ozone, the catalyst remaining active with the time [338]. The catalytic activity with respect to the complete oxidation of iso-propanol and the oxidation of carbon monoxide in the presence of ozone is higher than in presence of oxygen. Co_3O_4 thin layers on oxidized aluminum honeycomb catalysts are also reported to be very active in ozonation in wastewater purification [339].

9. Cobalt Oxide/Alumina Catalysts for Liquid-Phase Oxidation Reactions

9.1. Catalysts for Aerobic Selective Oxidations in Liquid Phase

Pure Co_3O_4 was recognized as an excellent and reusable catalyst for the aerobic oxidation of vanillyl alcohol to vanillin, with an 80% conversion and 98% selectivity to vanillin [340] in a NaOH/isopropanol solution with 6.8 bar of O_2. A high surface area, small particle size and high exposition of Co^{3+} ions were considered as key factors for high efficiency in this reaction.

Co_3O_4 supported on alumina (9.6% Co) has been tested as a catalyst for the aerobic oxidation of complex alcohols to the corresponding carbonyl compounds in water solution in the presence of bases at total reflux conditions [341]: benzaldehyde yields from benzyl alcohol up to 93% were obtained.

The oxidation of styrene with oxygen in a dioxane solvent was tested using mesoporous cobalt/alumina catalysts, producing high selectivities to styrene oxide or benzaldehyde depending on the reaction conditions [342].

9.2. Co_3O_4 as an Active Catalyst in Advanced Oxidation Processes (AOP) for Water Contaminant Degradation with Peroxide Compounds

Co_3O_4 is reported to act as an outstanding catalyst for the activation of peracetic acid (PAA) in the degradation of water pollutants [343] such as orange G dye [344] and sulphonamides [345]. Similarly, Co_3O_4-based materials were found to effectively activate peroxymonosulfate (PMS: $KHSO_5$) for the degradation of organic pollutants such as paracetamol [346], 4-chlorophenol [347], several aromatic compounds [348], imidacloprid [349], tetracycline (TC) [350], enrofloxacin [351]. Nanoparticles and defect-engineered samples show a higher activity than commercial Co_3O_4 [346,347]. Electron paramagnetic resonance characterization, radical quenching, and probe oxidation experiments indicate that tetravalent cobalt ions are the dominant reactive species on the surface of Co_3O_4 in contact with PMS [348].

10. Cobalt Oxide Catalysts for the Hydrolysis of Hydride Compounds

Metal hydrides have a potential interest for hydrogen storage and transport. In particular, $NaBH_4$ is considered as a potential candidate for this application. In this context, the hydrogen generation obtained through hydrolysis represents a crucial step. This reaction is slow; thus, catalysis is needed to accelerate it [352]. Co_3O_4 [353], CoO-Co_3O_4 composites [354], carbon supported Co_3O_4 [355] and graphene supported Co_3O_4 [356] as well as a number of cobalt-containing metallic and oxide materials, are reported to act as among the most performant catalysts for the hydrolysis of $NaBH_4$ [356,357]. In fact, it seems that the best catalysts are based on Co-B alloys [358]. However, it has been concluded that the cobalt oxide phase serves as a key catalyst component that improves water activation in catalysts based on metallic Co-based alloys [359].

11. Cobalt Oxides as Photocatalysts

The semiconductor nature of Co_3O_4 with a bandgap of 1.8–2.2 eV also makes it suitable for photocatalysis applications under visible light [360]. However, these materials do not seem to be really competitive with other photocatalytic materials [361–363] mainly due to the fast electron hole recombination, which can only be partially improved by metal doping.

Co_3O_4-based materials have an interesting activity in the solar light photodegradation of water pollutants [364]. In particular, they are active in dye abatement technologies [365–369]. Also, Co hydroxides have a potentiality for this application [370].

CoO is reported to be an active solar photocatalyst for neutral water splitting [69]. Co_3O_4 shows hydrogen evolution activity with visible light in sulphuric acid [371] and in triethanolamine solution [372]. Lai et al. [373] developed superhydrophilic and superaerophobic Co_3O_4/Nickel-Molybdenum-Foam (NMF), efficient and stable as a bifunctional electrocatalyst for the overall water splitting reaction. Also, cobalt hydroxides have a water splitting photocatalytic activity [374]. In fact, even if cobalt-containing mixed oxides are considered as components of efficient water splitting photocatalysts [375,376] cobalt oxides do not seem to be competitive materials for this application with respect to other more active materials [375,377].

Cobalt oxides containing materials also have been reported as active for the Visible Light-Driven photocatalysis of CO_2 reduction, including ultrathin CoO atomic layers with varying concentrations of oxygen vacancies [378], Co_3O_4 with special morphology control [379], Co_3O_4 modified by nickel [380,381] and Co_3O_4 activated by N-bromosuccinimide [382].

12. Electrocatalytic Activity of Cobalt Oxide-Based Materials

Given the redox properties of cobalt in its oxides and hydroxides, their low solubility in neutral water and in moderately acid and basic solution [383,384] and their semiconducting behavior, they are active materials in several electrocatalytic systems [385], as for example, on both sides of the electrochemical water splitting reaction [386,387]. electrical conductivity is a main drawback for some of these applications, which can be overcome by depositing or combining cobalt oxides on/with carbon-based or metal-based conductive components [386]. The electrocatalytic semireactions involved are summarized in Table 3.

Table 3. Electrochemical semireactions catalyzed by cobalt-based materials.

Reaction Name	pH	Semireaction	Technologies
Oxygen Evolution Reaction (OER)	Alkaline	$4\ OH^-(aq) \rightarrow O_2(g) + 2\ H_2O(aq) + 4e^-$	AEL, MAB
	Acidic	$2\ H_2O(aq) \rightarrow O_2(g) + 4\ H^+\ (aq) + 4\ e^-$	PEMEC
Oxygen Reduction Reaction (ORR)	Alkaline	$O_2(g) + 2\ H_2O(aq) + 4e^- \rightarrow 4\ OH^-(aq)$	AFC, AEMFC, MAB
	Acidic	$O_2(g) + 4\ H^+\ (aq) + 4\ e^- \rightarrow 2\ H_2O(aq)$	PEMFC
	Gas	$½\ O_2 + 2e^- \rightarrow O^{2-}$	SOFC
Hydrogen Evolution Reaction (HER)	Alkaline	$2H_2O(aq) + 2e^- \rightarrow H_2(g) + 2OH^-(aq)$	AEL
	Acidic	$2H^+(aq) + 2e^- \rightarrow H_2(g)$	PEMFC

AEL: Alkaline Electrolysis; MAB: metal–air batteries; PEMEC: Polymeric Membrane Electrolysis Cells; AFC: Alkaline Fuel Cells; AEMFC: Alkaline Electrolite Membrane Fuel Cells; PEMFC: Polymeric Membrane Fuel Cells; SOFC: Solid Oxide Fuel Cells.

12.1. Activity of Cobalt Oxides and Hydroxides in the Oxygen Evolution Reaction (OER)

The Oxygen Evolution Reaction, OER, is the slow step in the electrochemical water splitting process [388]. Co_3O_4 has long been mentioned as a very active and stable electrocatalyst for OER. The stabilization of high valence cobalt is a key factor: in fact, high-valency oxides are reported to show a superior OER activity to their low-valence counterparts [389] According to a recent study [390], the presence of low-spin Co^{3+} on the surface of Co oxide-based particles is essential for high OER activity, because it promotes surface reconstruction, while the presence of high-spin Co^{2+} is detrimental. The spin state of surface Co^{3+} ions can be tuned in cobalt-containing mixed oxides such as perovkites [219]. The activity of Co_3O_4-based materials strongly depends on the surface area, particle size and morphology, with a high activity for a number of different nanoparticle shapes and sizes [391]. According to Liu et al. [386], the exposition of the 111 crystallographic plane enhances activity in the OER.

Cobalt oxides have been considered to replace more expensive RuO_2-IrO_2 based electrodes for PEM electrolyzers for water splitting, and have been patented for such an application [392,393]. In fact, Co_3O_4 demonstrates high stability in strongly acidic conditions for OER [394], which can be further increased by metal doping. On the other hand, Co_3O_4 is also of interest in basic solutions due to its high stability in these conditions. A number of cobalt-containing complex oxides or oxyhydroxides are of interest for OER [388].

It must be considered that cobalt oxide-based electrocatalyst may undergo reconstruction during OER e.g., producing high oxidation state hydroxides or oxyhydroxides [395]. In fact, it has been supposed that the surface active phase for OER implies the formation of CoOOH [58,396]. Indeed, CoOOH is a very active electrocatalyst for OER in basic solutions, with enhanced activity through defect engineering [397] and strain engineering to increase surface concentration of high spin Co^{3+} ions [398], as well as in acidic solutions [58]. Operando XAS measurements combined with DFT calculations suggest that a potential-dependent deprotonation reaction occurs during the OER, producing $Co^{3+}/^{4+}OOH_{1-x}$,

which acts as an active phase for the reaction [399]. However, CoOOH is not stable at high current densities due to Co dissolution [58].

The OER can also occur in nearly neutral conditions at the anodic side of CO_2 electrolysis cells. In this case the use of Co_3O_4 is considered promising in substitution of the most common iridium-based electrocatalysts [400].

The OER also occurs at solid/gas interfaces at the anodes of Solid Oxide Electrolysis Cells, where Co-based perovskite may act [401].

12.2. Cobalt Oxides for Hydrogen Evolution Reaction

Co_3O_4 is also studied as an electrocatalyst for the HER [386,391], the cathodic side of electrochemical water splitting, mostly tested in strongly basic conditions, such as 1 M KOH water solutions, but sometimes also in acidic conditions (e.g., 0.5 M H_2SO_4) [402]. Although its intrinsic activity is low due to limited electrical conduction, a combination with electrically conductive phases strongly increases its activity [402], such as in the case of three-dimensional crystalline/amorphous Co/Co_3O_4 core/shell nanosheets [403].

12.3. Cobalt Oxides for Oxygen Reduction Reaction ORR

The oxygen reduction reaction (ORR) occurs at the cathodic side of hydrogen fuel cells. Pure Co_3O_4 has some catalytic activity in ORR [402], whose mechanism involves two electron reductions of O_2 to HO_2^-, followed by disproportionation. The activity of Co_3O_4 increases when it is combined with active and conducting components producing very interesting devices for ORR [385,386,391,404]. example, for CoO combined with N-doped graphene, it is reported to exhibit a similar catalytic activity but superior stability to Pt in alkaline solutions [405].

The ORR occurs also at the cathodes of Solid Oxide Fuels Cells (SOFC), in this case in gas/solid phase, producing oxide anions O^{2-} from oxygen from air. It has been reported that the deposition of a layer of CoO_x grains onto the internal surface of a Lanthanum Strontium Manganite/Yttria-Stabilized Zirconia (LSM/YSZ) composite cathode enhances the reaction rate of ORR [406]. On the other hand, cobalt-containing perovskites appear to be even more efficient than the traditional LSM-based cathodes for the low-temperature operation of SOFC [407,408].

12.4. Cobalt Oxides as OER/ORR Bifunctional Electrocatalysts for Metal–Air Batteries

Bifunctional OER/ORR electrocatalysts are needed as electrode materials for metal–air batteries [409]. In fact, cobalt oxide- based materials represent an interesting option for metal-air batteries [410], and, in particular, for Zn-air batteries [411]. In particular, cobalt oxide nanoparticles combined with different types of supports have been tested for Mg-, Li- and Zn- air batteries [410,412,413]. The use of cobalt oxides for metal air batteries has been the object of recent patents [414].

12.5. Cobalt Oxides for Photoelectrocatalytic Reactions

Co_3O_4 has emerged as a candidate to serve as a photoelectrocatalyst specifically for the oxidation of water with oxygen in these materials to promote the production of intermediate reactive species (hydroxyl radicals and superoxide radicals), in particular for the abatement of water pollutants [94]. According to these authors, the preparation technology suitable for producing a high surface area and useful morphology for this practical application still needs to be investigated.

Cobalt oxide-containing materials, such as cobalt–phosphate amorphous oxyhydroxide [415], are also considered among promising photoelectrocatalysts for hydrogen evolution from water splitting reactions [416].

12.6. Cobalt Oxides for Lithium-Ion Battery (LIB) and Sodium-Ion Battery (NIB) Anodes

CoO and Co_3O_4 have recently generated great interest as the most attractive alternatives to commercial graphite as anode materials for LiBs [391,417,418]. The high theoretical capacity of 890 $mAhg^{-1}$ for Co_3O_4, which is almost three times higher than that of the commercially used graphite anode (less than 372 $mAhg^{-1}$), is particularly interesting. This value is due to the eight lithium ions reacting with one cobalt oxide unit in each formula unit. Depending on the cobalt oxide morphology, the following reactions

$$Co_3O_4 + 2\ Li^+ + 2e^- \leftrightarrows 3\ CoO + Li_2O$$

$$3CoO + 6\ Li^+ + 6\ e^- \leftrightarrows 3\ Co + 3\ Li_2O$$

occur stepwise, or the overall reaction

$$Co_3O_4 + 8\ Li^+ + 8e^- \leftrightarrows 3\ Co + 4\ Li_2O$$

occurs directly [419]. The corresponding reactions are observed using sodium ions [420,421]. Disadvantages of cobalt-based anodes for LIBs and SIBs include the fast loss of capacity due to low electronic conductivity and large volume expansion during charge/discharge [421].

12.7. Cobalt Oxides as Components of Cathodes of Lithium−Sulphur Batteries

Cobalt oxides are reported to act as a useful component of the cathodes of lithium–sulphur batteries. In fact, CoO. as such or formed over Co_3O_4, acts as a catalyst to facilitate the adsorption of polysulphides [422] and the conversion of lithium polysulphides (LiPSs) to Li_2S_2/Li_2S during the charge−discharge process, allowing for a high sulfur utilization in these batteries [423].

13. Cobalt Oxides as Adsorbents for H_2S Abatement

The high activity of cobalt oxide- and hydroxide-based systems in absorbing H_2S at a low temperature down to room temperature [424] has also been the object of interest. Mesoporous Co_3O_4 finds a much higher activity than commercial Co_3O_4 [424] for this application. Cobalt oxide-containing composite systems such as cobalt oxide–silica [425] or cobalt oxide–graphite oxide composites [426] also have an interesting activity. Co_3O_4-based solids absorb H_2S, producing Co_9S_8 + Co_3O_4 mixtures [427], or CoSOH and CoS, depending on the conditions [425]. Cobalt oxides can, however, be regenerated through oxidation only at quite high temperatures with the release of SO_2 [425,428].

14. Cobalt Oxide Materials as Sensor Materials

Taking into account the high catalytic combustion properties of Co_3O_4, as well as the redox and semiconducting behavior of both Co_3O_4 and CoO, cobalt oxide materials have potential applications as gas-phase sensors for molecules such as H_2, CO, NO, NO_2, NH_3, CH_4, toluene, xylene, formaldehyde, acetone, and ethanol [429,430]. These properties are strongly related to the surface area, porous nature and morphologies of the oxide, and can be increased by combining cobalt oxide with other components. In fact, a remarkable resistance response was found for Co_3O_4 films exposed to CH_4, H_2, CO, NO_2 and NH_3 at 513 K, such as in a CO gas sensor [431]. CoOOH has an even better response than Co_3O_4 at low temperatures and can detect CO concentrations of 1 ppm at 353 K [432]. It can also be applied to CH_4, H_2, NO_2, ethanol and water [432]. Also cobalt-doped alumina was found to act as an excellent gas sensor for benzene [433].

Cobalt oxides are also useful as optical gas sensors. In fact, the transmittance in visible light of stoichiometric CoO is far higher than that of oxidized Co_3O_4, which is a dark solid

(Figure 3). Therefore, cobalt oxides are active in sensing carbon monoxide in air, as seen using λ = 625 nm and 200 ppm of CO gas in dry air at 623 K, because the $Co_3O_4 \longrightarrow CoO$ phase transition occurs with a strong increase in light transmittance [434].

Co_3O_4 nanomaterials have been explored as effective electrode materials for enzyme-free glucose sensing in solutions, including Co_3O_4 spherical nanoparticles, porous nanorod and nanoflower shapes [435], Co_3O_4 nanoparticles on graphene [436], Co_3O_4 nanosheets [437] and straw-sheaf-like Co_3O_4 [438]. The mechanism of glucose detection is based on the oxidation of glucose to gluconolactone by electrochemically generated surface Co(IV) in basic solutions [435]. Despite the very interesting behavior, glucose detection is limited due to the poor electrical conductivity of cobalt oxide semiconductors and the associated sluggish reaction kinetics. To enhance performance, the photothermal effect-assisted electrochemical detection of glucose can be utilized. Co_3O_4 nanowire arrays supported on nickel foam were proposed for showing the good feasibility and reliability of this technique for glucose determination in human serum samples [439].

In similar ways, cobalt oxide-based sensors are investigated for the detection of other substances, e.g., hydrazine [440] and uric acid [441], and for the measure of chemical oxygen demand (COD) in polluted water [442].

15. Cobalt Oxides and Hydroxides in Supercapacitor Technologies

Supercapacitors are objects of much interest to be used as energy storage devices [443]. In fact, they exhibit a high power density and long-lasting lifespan with a high cyclic stability and reversibility, and they can be used in a wide temperature range (230–360 K).

Co_3O_4 is particularly attractive for supercapacitor applications [444,445], due to its low cost, remarkable redox activity, and the extremely high theoretical specific capacitance for Co_3O_4 of around 3560 Fg^{-1}. Co_3O_4-based materials have been patented for such an applications [446]. Its practical use is actually hindered by a poor electrical conductivity, low power density, and structural instability. Co_3O_4 supercapacitors use KOH solutions and work with a pseudocapacitor mechanism [444,445,447–451]. In fact, the electrochemical potential of Co_3O_4 in contact with KOH solutions is associated with the following reversible reactions:

$$Co_3O_4 + OH^- + H_2O \leftrightarrows 3\ CoOOH + e^-$$

$$CoOOH + OH^- \leftrightarrows CoO_2 + H_2O + e^-$$

The rate and extent of these reactions depend strongly on the morphology (size and shape [103]) of the nanoparticles used and in particular on the surface area. In practice, the real capacitance obtained is in the range 400–1820 Fg^{-1} [451]. The maximum value was obtained for Co_3O_4 nanoflakes with a 66 m^2/g surface area grown on Ni foam, produced through a hydrothermal method, with 2M KOH as the electrolyte [450]. This material retains 92% capacitance after 1000 cycles.

Also, cobalt hydroxides can be used for this application [370]. In particular, β-$Co(OH)_2$ has potential as a pseudocapacitor phase [451–453], due to its high capacitance, stability, and cyclability. According to a recent study [454] the oxidation reaction

$$Co(OH)_2 + OH^- \rightarrow CoOOH + H_2O + e^-$$

is almost irreversible, and is followed by the reversible redox couple

$$3\ CoOOH + e^- \leftrightarrows Co_3O_4 + H_2O + OH^-$$

while the reaction

$$CoOOH + OH^- \leftrightarrows CoO_2 + H_2O + e^-$$

only occurs at very high voltages. The reaction mechanism is summarized in Scheme 1.

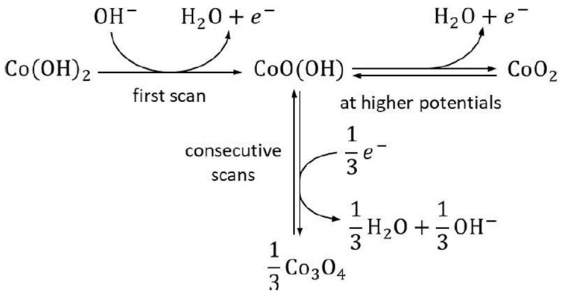

Scheme 1. Electrochemical processes occurring during the oxidation and re-reduction of $Co(OH)_2$ modified electrodes [453].

Also, Co-Al layered double hydroxides of the hydrotalcite type are reported to effectively act as supercapacitor materials [455]. An enhancement of the specific capacitance was observed for samples with Co:Al a.r. 2 (i.e., the richest in electrochemically inert Al and poorer in electrochemically active Co); thus, capacitance would be associated with an increased basal space, and with an increase in the electrochemical surface area and higher electrolyte diffusion.

Indeed, the combination of cobalt oxides together with other oxide materials, forming doped Co_3O_4, Co-containing spinels and other mixed oxides, results in a number of very active materials for supercapacitors [444,445].

16. Mechanistic Aspects of the Surface Activity of Cobalt Oxide-Based Systems

As said, Co_3O_4-containing materials show a very high activity in the catalytic combustion of hydrocarbons and VOCs. The catalytic oxidation activity of transition metal oxides is most commonly explained using the redox mechanism first described by Mars and Van Kreveken [456,457], implying the reduction of the oxide surface by the reactant as the rate determining step and the reoxidation of the oxide surface by O_2 from the gas phase. However, alternative mechanisms are possible, such as the so-called Langmuir−Hinshelwood (LH) route, where adsorbed oxygen species (such as O_2^-, O_2^{2-}, or O^-) react with an adsorbed form of the reducing reactant, and the Eley−Rideal (ER) route, where gas-phase oxygen reacts with the adsorbed reductant or vice versa.

The validity of the Mars–Van Krevelen or redox mechanism of CO oxidation on Co_3O_4 is supported by theoretical and experimental studies [90,221,458] as well as by spectroscopic studies [129], involving the Co^{3+}/Co^{2+} redox couple and oxygen vacancy formation. Bridging surface carbonate species should act as intermediates [129,459,460] The redox mechanism also occurs for CO oxidation on CoO_x/Al_2O_3 catalysts [231]. In the case of methane combustion over Co_3O_4, the redox mechanism was considered [461] but an interplay of redox and Langmuir−Hinshelwood mechanisms is likely occurring, depending on the reaction conditions (temperature and reactants to molar ratio [462]). In the VOC oxidation catalysis over Co_3O_4, the redox mechanism is considered to be predominant [254]. In fact, spectroscopic data show that VOC molecules, including hydrocarbons such as propane, propene, and toluene, but also alcohols, are progressively selectively converted to more oxidized surface species, up to full oxidation, with the reduction of the surface through a redox mechanism [257,258,463]. Also, the oxidation of ammonia to NO over Co_3O_4 is supposed to occur through a Mars–Van Krevelen mechanism involving Co^{3+} and Co^{2+} [464] as with other metal oxides [465].

A slightly different situation likely occurs in the case of the oxidation of NO to NO_2. The kinetics of this reaction over Co_3O_4 were interpreted as being limited by the rate-determining step constituted by the dissociation of adsorbed molecular oxygen, assisted

by gaseous NO to form NO_2 and surface-activated oxygen atoms in [305,466]. These species also react with NO to produce NO_2 and the surface where Co^{3+} is reduced to Co^{2+}. Also in this case, an interplay of redox and Langmuir−Hinshelwood mechanisms is likely occurring.

In order to have high catalytic combustion activity, morphological and structural stability at the reaction temperature are also needed. For this reason, supporting or combining cobalt oxides with quite refractory materials such as aluminas may increase performances in this field. This makes cobalt aluminate and Co_3O_4-Al_2O_3 composite materials stable and active catalytic materials for most gas-phase oxidation processes.

The ability of cobalt ions to change their redox state is the key feature of cobalt oxides and hydroxides for their electrocatalytic behavior. In this case, however, thanks to the anodic voltage that can be applied to cobalt oxide-containing electrodes, the oxidation of Co^{3+} to Co^{4+} also becomes possible, thus allowing the Co^{4+}/Co^{3+} couple to be active together with the Co^{3+}/Co^{2+} couple too. This makes Co_3O_4-based systems very active in the OER, thanks to the oxidation of water to oxygen by surface Co^{4+} ions. The mechanisms of catalytic oxidation and the electrocatalytic water splitting behavior of Co_3O_4 are schematized in Figure 12.

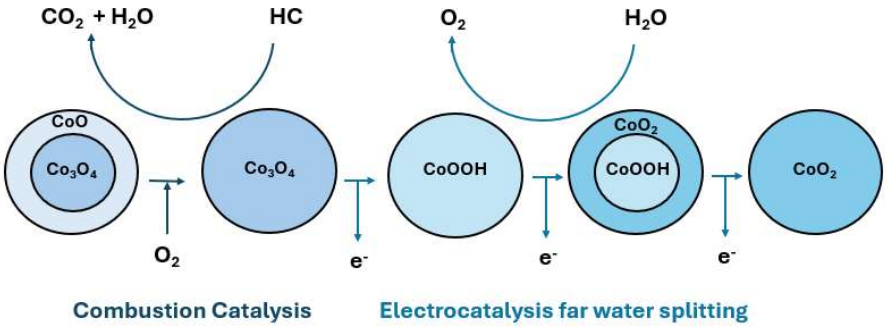

Figure 12. Schematics of the mechanism of catalytic and electrocatalytic behavior of Co_3O_4.

However, for electrochemical applications in contact with water solutions, other properties are needed. First of all, it is necessary to have an extremely low solubility in water in practical conditions. Indeed, the extremely low solubility of Co^{3+}-containing compounds (i.e., $Co(OH)_3$, CoOOH and Co_3O_4) at a low pH makes them very attractive for anodic applications at acidic pH. On the other hand, cobalt oxides and hydroxides also have a low solubility at neutral and medium basic pHs, allowing their use also in contact with moderately basic solutions.

Additionally, a sufficient electrical conductivity is needed for electrochemical applications. This is the main drawback of cobalt oxides for electrochemical applications. In fact, the most stable cobalt oxides and hydroxides are semiconducting solids with moderate conductivity. For this reason, to exploit the excellent redox and solubility properties of these materials in electrocatalysis, they may be combined with conducting solids, e.g., carbons or metallic foams. The same point is relevant for sensor applications of cobalt oxides. In most cases, combining cobalt oxide is detrimental due to further reduced conductivity.

The strong visible light absorbance by Co_3O_4, combined with its poor solubility and high redox activity, makes it interesting for visible photocatalytic applications, although, in this case, fast electron–hole recombination represents a strong drawback.

As seen, the ability of cobalt oxide and hydroxide phases to interconvert each other reversibly and quickly with redox behavior in contact with basic solutions, in particular, the CoOOH-Co_3O_4 and CoO_2-CoOOH systems, gives these systems an excellent behavior for supercapacitor applications with pseudocapacitor mechanisms.

A common additional property of these materials for all these applications is the possibility of producing them in a large variety of nanostructures. In fact, cobalt oxide and hydroxide nanomaterials provide an enhanced performance for most of these applications and also significant stability and reversibility.

17. Modification of Cobalt Oxides to Improve Performances

In several cases, as specified above, the production of modified cobalt oxides can improve performances in some of the mentioned applications. This can be obtained in different ways. One way is to combine it with alumina. In fact, as described above, the different types of alumina–cobalt oxide mixed phases can allow us to improve morphology and stability factors. The combination of cobalt oxide with alumina may allow the production of cobalt oxide-supported nanoparticles which retain a high redox activity with higher stability and better morphology. On the other hand, cobalt–alumina mixed oxide phases also allow the production of different cobalt oxide species, like more or less dispersed and even monoatomic cobalt ions on alumina surfaces, with peculiar redox properties for catalysis and adsorption. Cobalt alumina complex oxide phases frequently have a higher morphological and chemical stability than cobalt oxides. In Table 4, surface-related applications of cobalt–aluminum mixed oxide phases are reported.

Table 4. A summary of surface-related applications of CoO_x-Al_2O_3 materials.

Technology	Reference
Precursors of Co/Al_2O_3 Fischer Tropsch synthesis catalysts	[6,7,202,203]
Low-temperature CO oxidation	[222,227–231]
Preferential CO oxidation	[236,237]
Hydrocarbon combustion	[241,256]
Combustion of anode tail gas of PEMFC	[283]
Diesel soot combustion	[287,336]
N_2O decomposition	[308,310,314,315]
NOx SCR by propane	[331–335]
Simultaneous removal of NOx and Diesel soot particulates	[335,336]
O_3 activation and decomposition	[338]
Liquid-phase aerobic oxidations	[342]
Supercapacitor	[455]
Benzene sensor	[433]

Another way to increase or modify the catalytic activity of Co_3O_4 is doping. In Figure 13, the effect of doping Co_3O_4 with metallic elements on N2O's decomposition activity is summarized, also showing the structural effect of doping [313]. As shown, doping with alkali occurs at the surface and increases catalytic activity. The addition of Al^{3+} modifies the bulk and causes a partial deactivation, although, as said, it may increase stability.

However, to improve photo- and electrochemical behavior, an improvement of the electrical conduction properties may be needed. This can be done by supporting or mixing cobalt oxides on/with metal phases and foams, carbon materials and condicting ceramics. Alternatively or additionally, the combination of cobalt oxide phases with other metal elements can improve redox properties and electrical conduction and can also generate ionic conduction. In fact, mixed oxides generally have a higher conductivity and capacitive activity than single-metal oxides [467]. In fact, mixed cobalt oxides have a number of

potential applications [468]. Examples of applications of cobalt-containing mixed oxide phases are summarized in Table 5.

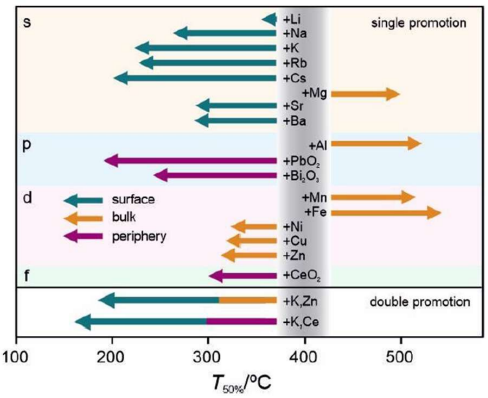

Figure 13. The deN_2O performance of doped Co_3O_4 phases compared by T50% parameter (catalytic test conditions: a mixture of gases 5% N_2O/He, GHSV = 7000 h^{-1}) [313].

Table 5. Examples of Co-containing mixed oxide phases and their application.

Structure Type	Element	Formula	Technology	Ref.
Composites	Lithium	Li_2O-Co_3O_4	LIBs anodes	[417–419]
	Sodium	Na_2O-Co_3O_4	SIBs anodes	[418,420]
	Cerium	CeO_2-Co_3O_4	catalytic combustion	[255]
			CO oxidation	[97]
Doping	Alkali	K-, Cs-doped Co_3O_4	N_2O decomposition	[311–313]
	Lithium	Li_xCoO_2	LIBs cathodes	[3]
	Sodium	Na_xCoO_2	SIBs cathodes	[118]
Amorphous	Phosphorus	Co_3O_4-$CoPO_4$	photoelectrocatalysis	[415]
Rock salt	Magnesium	$Mg_{1-x}Co_xO$	ozone decomposition	[130]
Spinel	Magnesium	$MgCo_2O_4$	N_2O decomposition	[310]
Spinel	Chromium	$Co_{1+x}Cr_{2-x}O_4$	catalytic combustion	[255]
Spinel	Iron	$(Co_{1-x}Fe_x)_3O_4$	supercapacitor	[444,445]
Spinel	Nickel	$Ni_{1x}Co_{3-x}O_4$	supercapacitor	[444,445]
Spinel	Manganese	$(Co_{1-x}Mn_x)_3O_4$	CO oxidation	[226]
			Catalytic combustion	[254]
			supercapacitor	[444,445]
Spinel	Copper	$Cu_xCo_{3-x}O_4$	CO oxidation	[226]
			catalytic combustion	[254]
Spinel	Zinc	$Zn_xCo_{3-x}O_4$	electrocatalysis OER	[218]
			N_2O decomposition	[313]
Perovskites	Lanthanum	$LaCoO_3$	catalytic combustion	[243–245]
			N_2O decomposition	[307,308]
			electrocatalysis OER	[400]
	Strontium	$SrCoO_3$	SOFC anodes	[406,407]
	Praseodimium, Barium	$PrBaCo_2O_6$	electrocatalysis OER	[400]
β-aluminas	Aluminum, Strontium	$SrCo_xAl_{12-x}O_{19-\delta}$	catalytic combustion	[243–245]

18. Industrial Applications and Perspectives

The data summarized above demonstrate the exceptional versatility of cobalt oxides and their combination with aluminas in a number of different applications. While most of the papers cited above report on academic studies, several of them are related to industrial research and patents, showing their enormous industrial interest at least in some fields.

In Table 6, the industrial applications of these materials and technologies with preindustrial studies and potential future applications are documented. It is evident that, while in some fields cobalt-based oxide materials already represent industrial-level products, in several fields they are promising candidates to substitute more expensive and more critical materials such as those based on noble metals and/or to introduce new more performant technologies.

Table 6. Actual and potential industrial applications of cobalt oxides and cobalt-aluminium mixed oxides.

Application		Materials	State	Ref.
pigments		$CoAl_2O_4$ "cobalt blue" Co_3O_4 "cobalt black"	commercial	[13,92,154]
catalysts	low/medium temperature CO oxidation	Co_3O_4 CoO_x/γ-Al_2O_3 Co_3O_4/α-Al_2O_3	might substitute noble metal-based systems	[14,96,221–231]
	chlorinated VOC combustion	Co_3O_4 Co_3O_4/SiO_2	more stable than noble metals, zeolites	[274–278]
	soot combustion	$CoAl_2O_4$ Co_3O_4	patented as components of Diesel active catalytic antiparticolate filters	[288]
	N_2O decomposition	$Co_{3-x}Al_xO_4$	patented, commercial	[319,320]
	ammonia oxidation to NO	Co_3O_4, $Co_{3-x}Al_xO_4$	patented for nitric acid synthesis process	[299,300]
	ozone activation and decomposition	Co_3O_4, $CoOx/\gamma$-Al_2O_3	under study	[23,337–339]
precursors of cobalt metal catalysts	precursor for Fischer Tropsch synthesis catalysts	$CoOx/\gamma$-Al_2O_3	commercial	[6,7,201–205]
	precursor for other metal catalysts	$CoOx/\gamma$-Al_2O_3	commercial	[203,204]
electrocatalysts and battery electrodes	anodes for water splitting	$Co_3O_4/CoOOH/CoO_2$	patented	[385–399]
	electrode for metal-air batteries	Co_3O_4	patented	[409–414]
	cathodes of lithium-ion batteries	Li_xCoO_2	commercial	[3]
	anodes of lithium-ion batteries	Co_3O_4	very high theoretical capacity	[33,159,417–421]
supercapacitors	active layer of supercapacitors	$CoO_2/CoOOH/Co_3O_4/Co(OH)_2$	patented	[103,370,443–455]

19. Conclusions

The data summarized here emphasize the enormous versatility of cobalt oxide-based materials for a number of at least potential technological applications. This is associated with the redox properties of Co^{n+} ions (n = 0,2,3,4), the related electrical conduction properties of their solid compounds, and also the magnetic and optical properties of these materials. It seems quite evident that cobalt oxide-based materials are in some way underutilized practically today but represent interesting alternatives to more expensive and critical materials, e.g., those based on platinum group metals and noble metals. It seems likely that the industrial application of cobalt oxide-based materials will strongly increase in the near future to sustain new technologies needed for the energy transition expected to occur shortly. To do this, the search and discovery of new cobalt resources would be beneficial, together with establishing processing technologies in more countries. On the other hand, recovering and reuse technologies should also be developed.

Author Contributions: G.B.: conceptualization, validation, writing—review and editing; E.S.: conceptualization, validation; E.F.: conceptualization, validation; P.R.: conceptualization, validation, writing—review and editing; G.G.: funding acquisition, conceptualization, validation, writing—review and editing. All authors have read and agreed to the published version of the manuscript.

Funding: E.S. and G.G. acknowledge National Recovery and Resilience Plan (NRRP), Mission 4 Component 2 Investment 1.3—Call for tender No. 1561 of 11 October 2022 of Ministero dell'Università e della Ricerca (MUR); funded by the European Union—NextGenerationEU Project title "Network 4 Energy Sustainable Transition—NEST" (Project code PE0000021).

Data Availability Statement: The data in this review paper come from the cited references.

Conflicts of Interest: The authors declare no conflicts of interest.

References

1. Cremona, A.; Colombo, C. Cobalt perspectives. *Chim. Ind. Online* **2024**, *8*, 44–49.
2. Lison, D.; van den Brule, S.; Van Maele-Fabry, G. Cobalt and its compounds: Update on genotoxic and carcinogenic activities. *Crit. Rev. Toxicol.* **2018**, *48*, 522–539. [CrossRef]
3. Li, M.; Lu, J. Cobalt in lithium-ion batteries. *Science* **2020**, *367*, 979–980. [CrossRef] [PubMed]
4. Tohidi, M.M.; Paymard, B.; Vasquez-García, S.R.; Fernández-Quiroz, D. Recent progress in applications of cobalt catalysts in organic reactions. *Tetrahedron* **2023**, *136*, 133352. [CrossRef]
5. Raghavendrachar, P.; Ramachandran, S. Liquid-Phase Catalytic Oxidation of p -Xylene. *Ind. Eng. Chem. Res.* **1992**, *31*, 453–462. [CrossRef]
6. Khodakov, A.Y.; Chu, W. Advances in the Development of Novel Cobalt Fischer−Tropsch Catalysts for Synthesis of Long-Chain Hydrocarbons and Clean Fuels. *Chem. Rev.* **2007**, *107*, 1692–1744. [CrossRef] [PubMed]
7. Busca, G.; Spennati, E.; Riani, P.; Garbarino, G. Mechanistic and Compositional Aspects of Industrial Catalysts for Selective CO_2 Hydrogenation Processes. *Catalysts* **2024**, *14*, 95. [CrossRef]
8. Shafiq, I.; Shafique, S.; Akhter, P.; Yang, W.; Hussain, M. Recent developments in alumina supported hydrodesulfurization catalysts for the production of sulfur-free refinery products: A technical review. *Catal. Rev.* **2022**, *64*, 1–86. [CrossRef]
9. Mussa, N.-S.; Toshtay, K.; Capron, M. Catalytic Applications in the Production of Hydrotreated Vegetable Oil (HVO) as a Renewable Fuel: A Review. *Catalysts* **2024**, *14*, 452. [CrossRef]
10. Affatato, S.; Grillini, L. Topography in bio-tribocorrosion. In *Bio-Tribocorrosion in Biomaterials and Medical Implants*; Yuan, Y., Ed.; Woodhead Publishing Series in Biomaterials; Elsevier: Cambridge, UK, 2013; pp. 1–21.
11. Waris, A.; Din, M.; Ali, A.; Afridi, S.; Baset, A.; Khan, A.U.; Ali, M. Green fabrication of Co and Co_3O_4 nanoparticles and their biomedical applications: A review. *Open Life Sci.* **2021**, *16*, 14–30. [CrossRef]
12. Fierro, J.L.G. (Ed.) *Metal Oxides Chemistry and Applications*; Taylor and Francis: New York, NY, USA, 2005.
13. Pfaff, G. Mixed metal oxide pigments. *Phys. Sci. Rev.* **2022**, *7*, 7–16. [CrossRef]
14. Ma, Z. Cobalt Oxide Catalysts for Environmental Remediation. *Curr. Catal.* **2014**, *3*, 15–26. [CrossRef]
15. Busca, G. Structural, surface and catalytic properties of aluminas. In *Advances in Catalysis*; Gates, B.C., Jentoft, F., Eds.; Elsevier: Amsterdam, The Netherlands, 2014; Volume 57, pp. 319–404.
16. Okamoto, H. Co-O (Cobalt-Oxygen). *J. Phase Equilibria Diffus.* **2008**, *29*, 548–549. [CrossRef]

17. Chen, M.; Hallstedt, B.; Gauckler, L.J. Thermodynamic assessment of the Co-O system. *J. Phase Equilibria* **2003**, *24*, 212–227. [CrossRef]
18. Zabdyr, L.A.; Fabrichnaya, O.B. Phase equilibria in the Co–Cu–O–Si system, Computer Coupling of Phase Diagrams and Thermochemistry. *Calphad* **2004**, *28*, 293–298. [CrossRef]
19. Chivot, J.; Mendoza, L.; Mansour, C.; Pauporte, T.; Cassir, M. New insight in the behaviour of Co–H_2O system at 25–150 °C, based on revised Pourbaix diagrams. *Corrosion Sci.* **2008**, *50*, 62–69. [CrossRef]
20. Bajdich, M.; García-Mota, M.; Vojvodic, A.; Nørskov, J.K.; Bell, A.T. Theoretical Investigation of the Activity of Cobalt Oxides for the Electrochemical Oxidation of Water. *J. Am. Chem. Soc.* **2013**, *135*, 13521−13530. [CrossRef]
21. Peek, E.; Åkre, T.; Asselin, E. Technical and business considerations of cobalt hydrometallurgy. *JOM* **2009**, *61*, 43–53. [CrossRef]
22. Mockenhaupt, C.; Zeiske, T.; Lutz, H.D. Crystal structure of brucite-type cobalt hydroxide β-Co{O(H,D)}$_2$—Neutron diffraction, IR and Raman spectroscopy. *J. Mol. Struct.* **1998**, *443*, 191–196. [CrossRef]
23. Zhang, L.; Zhou, X.; Chai, S.; Guan, J.; Fan, G.; Yang, W.; Ma, G.; Han, N.; Chen, Y. β-$Co(OH)_2$ Nanostructures with High Spin Co(II) in Distorted [CoO_6] for Catalytic Ozone Decomposition. *ACS Appl. Nano Mater.* **2022**, *5*, 18680−18690. [CrossRef]
24. Xu, Z.P.; Zeng, H.C. Thermal evolution of cobalt hydroxides: A comparative study of their various structural phases. *J. Mater. Chem.* **1998**, *8*, 2499–2506. [CrossRef]
25. Xu, Z.P.; Zeng, H.C. Interconversion of Brucite-like and Hydrotalcite-like Phases in Cobalt Hydroxide Compounds. *Chem. Mater.* **1999**, *11*, 67–74. [CrossRef]
26. Huang, Z.; Zhao, Y.; Song, Y.; Li, Y.; Wu, G.; Tang, H.; Zhao, J. Study on the oxidation process of cobalt hydroxide to cobalt oxides at low temperatures. *RSC Adv.* **2016**, *6*, 80059–80064. [CrossRef]
27. Wan, C.; Xie, G.; Zhang, M.; Huang, H.; Li, D.; Jiang, L. Efficient synthesis of Co^{2+}–Co^{3+} hydrotalcite-like compounds via NaOH precipitation in methanol–water under mild alkaline conditions. *Appl. Clay Sci.* **2023**, *232*, 106807. [CrossRef]
28. Park, J.Y.; Kim, H.Y.; Kim, Y.I.; Jo, S.Y.; Abbas, S.A.; Seo, D.; Ma, A.; Nam, K.M. Chemical and electrochemical synthesis of cobalt hydroxides: Selective phase transformation and application to distinct electrocatalytic reactions. *J. Mater. Chem. A* **2022**, *10*, 12047–12054. [CrossRef]
29. Butel, M.; Gautier, L.; Delmas, C. Cobalt oxyhydroxides obtained by 'chimie douce' reactions: Structure and electronic conductivity properties. *Solid State Ion.* **1999**, *122*, 271–284. [CrossRef]
30. Martinez, E.Y.; Zhu, K.; Li, C.W. Influence of the Defect Stability on n-Type Conductivity in Electron-Doped α- and β-$Co(OH)_2$ Nanosheets. *Inorg. Chem.* **2021**, *60*, 6950−6956. [CrossRef] [PubMed]
31. Hou, Y.; Kondoh, H.; Shimojo, M.; Kogure, T.; Ohta, T. High yield preparation of uniform cobalt hydroxide and oxide nanoplatelets and their characterization. *J. Phys. Chem. B* **2005**, *109*, 19094−19098. [CrossRef]
32. Mehandjiev, D.; Nikolova-Zhecheva, E. Mechanism of the decomposition of cobaltous compounds in vacuo. *Thermochim. Acta* **1980**, *37*, 145–154. [CrossRef]
33. Do, J.S.; Weng, C.H. Preparation and characterization of CoO used as anodic material of lithium battery. *J. Power Sources* **2005**, *146*, 482–486. [CrossRef]
34. Dwivedi, A.; Sharma, B.K.; Rajagopalan, N.; Sinha, S. Hydrothermal Decomposition of Cobalt Hydroxide in Saturated Water Vapor. *Ind. Eng. Chem. Res.* **2020**, *59*, 491−496. [CrossRef]
35. Pankratov, D.A.; Veligzhanin, A.A.; Zubavichus, Y.V. Structural Features of Green Cobalt(III) Hydroxide. *Russian J. Inorg. Chem.* **2013**, *58*, 67–73. [CrossRef]
36. Yang, Y.; Hyodo, H.; Kimura, K.; Sasaki, T. $Co(OH)_3$ nanobelts: Synthesis, characterization and shape-preserved transformation to pseudo-singlecrystalline Co_3O_4 nanobelts. *Nanotechnology* **2010**, *21*, 045605. [CrossRef] [PubMed]
37. Deliens, M.; Goethals, H. Polytypism of heterogenite. *Mineral. Mag.* **1973**, *39*, 152–157. [CrossRef]
38. Chang, Z.; Lia, H.; Tang, H.; Yuan, X.Z.; Wang, H. Synthesis of γ-CoOOH and its effects on the positive electrodes of nickel batteries. *Int. J. Hydrogen Energy* **2009**, *34*, 2435–2439. [CrossRef]
39. Burlet, C.; Goethals, H.; Vanbrabant, Y. Delafossite structure of heterogenite polytypes ($HCoO_2$) by Raman and infrared micro-spectroscopy. *Spectrochim. Acta Part A Mol. Biomol. Spectrosc.* **2016**, *159*, 90–97. [CrossRef]
40. Kudielka, A.; Bette, S.; Dinnebier, R.E.; Abeykoon, M.; Pietzonka, C.; Harbrecht, B. Variability of composition and structural disorder of nanocrystalline CoOOH materials. *J. Mater. Chem. C* **2017**, *5*, 2899–2909. [CrossRef]
41. Kusano, Y.; Kawasaki, S.; Takada, J.; Azuma, M. Synthesis and microstructure of single-crystalline cobalt oxyhydroxide and topotactic transformation to cobalt oxide. *J. Am. Ceram. Soc.* **2020**, *103*, 7240–7246. [CrossRef]
42. Pralong, V.; Delahaye-Vidal, A.; Beaudoin, B.; Leriche, J.B.; Tarascon, J.M. Electrochemical Behavior of Cobalt Hydroxide Used as Additive in the Nickel Hydroxide Electrode. *J. Electrochem. Soc.* **2000**, *147*, 1306–1313. [CrossRef]
43. Onoda, M.; Kikuchi, Y. Weakly correlated triangular lattice metal H_xCoO_2 with x≈0.3. *J. Phys. Condens. Matter* **2007**, *19*, 346206. [CrossRef]
44. Medina, E.A.; Aleksandrova, I.; Karppinen, M. Proton intercalation into different CoO_2 layer matrices. *J. Solid State Chem.* **2019**, *278*, 120899. [CrossRef]

45. Lin, X.; Li, H.; Musharavati, F.; Zalnezhad, E.; Bae, S.; Chod, B.Y.; Hui, O.K.S. Synthesis and characterization of cobalt hydroxide carbonate nanostructures. *RSC Adv.* **2017**, *7*, 46925. [CrossRef]
46. Schenk, A.S.; Goll, M.; Reith, L.; Roussel, M.; Blaschkowski, B.; Rosenfeldt, S.; Yin, X.; Schmahl, W.W.; Ludwigs, S. Hierarchically Structured Spherulitic Cobalt Hydroxide Carbonate as a Precursor to Ordered Nanostructures of Electrocatalytically Active Co_3O_4. *Cryst. Growth Des.* **2020**, *20*, 6407−6420. [CrossRef]
47. Blais, J.F.; Djedidi, Z.; Cheikh, R.; Tyagi, R.D.; Mercier, G. Metals Precipitation from Effluents: Review. In *Practice Periodical of Hazardous, Toxic, and Radioactive Waste Management, American Society of Civil Engineers*; ASCE Library: Reston, VA, USA, 2008; Volume 12, pp. 135–149.
48. Monhemius, J. Precipitation diagrams for metal hydroxides, sulphides, arsenates and phosphates. *Trans. Inst. Min. Metall.* **1977**, *86*, C202–C206.
49. Frolova, L.; Butyrina, T. Research of the Formation Cobalt (II) Hydroxide. In Proceedings of the IEEE 41st International Conference on Electronics and Nanotechnology (ELNANO), Kyiv, Ukraine, 10–14 October 2022; pp. 74–77.
50. Wang, X.; Wu, X.; Wang, X.; Xu, B.; Xia, H.; Gao, J.; Sun, H. A simple and industrially scalable approach to prepare $Co(OH)_2$ hexagonal nanoflake. *Mat. Lett.* **2016**, *164*, 432–435. [CrossRef]
51. Wang, B.; Lin, H.; Yin, Z. Hydrothermal synthesis of β-cobalt hydroxide with various morphologies in water/ethanol solutions. *Mater. Lett.* **2011**, *65*, 41–43. [CrossRef]
52. Kong, L.B.; Liu, M.C.; Lang, J.W.; Liu, M.; Luo, Y.C.; Kang, L. Porous cobalt hydroxide film electrodeposited on nickel foam with excellent electrochemical capacitive behavior. *J. Solid State Electrochem.* **2011**, *15*, 571–577. [CrossRef]
53. Aghazadeh, M.; Malek Barmi, A.A.; Gharailou, D.; Peyrovi, M.H.; Sabour, B.; Khosroshahi, F.N. Cobalt hydroxide ultra-fine nanoparticles with excellent energy storage ability. *Appl. Surf. Sci.* **2013**, *283*, 871–875. [CrossRef]
54. Wu, X.; Liu, M.; Jiang, Z.; Li, J.; Song, K.; Wei, A.; Meng, D.; Dong, T.; Gao, Z.; Zhang, W.; et al. Electrodeposition-Potential Tuning Rejuvenates the Concurrent Preparation from α-$Co(OH)_2$ with Larger Interlayer-Spacings to β-$Co(OH)_2$. *Batter. Supercaps* **2025**, *8*, e202400699. [CrossRef]
55. Liu, Y.C.; Koza, J.A.; Switzer, J.A. Conversion of electrodeposited $Co(OH)_2$ to CoOOH and Co_3O_4, and comparison of their catalytic activity for the oxygen evolution reaction. *Electrochim. Acta* **2014**, *140*, 359–365. [CrossRef]
56. Wallis, A.E.; West De Witt, H. Precipitation of Cobaltic Hydroxide. U.S. Patent US2377832A, 5 June 1945.
57. Vaughan, J.; Hawker, W.; White, D. Chemical aspects of mixed nickel-cobalt hydroxide precipitation and refining. In Proceedings of the ALTA Ni/Co/Cu Conference, Perth, Australia, 23–25 May 2011; pp. 23–25.
58. Huang, J.; Zhang, Z.; Spezzati, C.; Clark, A.H.; Hales, N.; Genz, N.S.; Daffé, N.; Skoupy, R.; Gubler, L.; Castelli, I.E.; et al. Directly synthesized cobalt oxyhydroxide as an oxygen evolution catalyst in proton exchange membrane water electrolyzers. *Nat. Commun.* **2025**, *16*, 7518. [CrossRef]
59. Alrehaily, L.M.; Joseph, J.M.; Biesinger, M.C.; Guzonas, D.A.; Wren, J.C. Gamma-radiolysis-assisted cobalt oxide nanoparticle formation. *Phys. Chem. Chem. Phys.* **2013**, *15*, 1014. [CrossRef] [PubMed]
60. Wasylenko, D.J.; Ganesamoorthy, C.; Borau-Garcia, J.; Berlinguette, C.P. Electrochemical evidence for catalytic water oxidation mediated by a high-valent cobalt complex. *Chem. Commun.* **2011**, *47*, 4249–4251. [CrossRef] [PubMed]
61. Gerken, J.B.; McAlpin, G.; Chen, J.Y.C.; Rigsby, M.L.; Casey, W.H.; Britt, R.D.; Stahl, S.S. Electrochemical Water Oxidation with Cobalt-Based Electrocatalysts from pH 0–14: The Thermodynamic Basis for Catalyst Structure, Stability, and Activity. *J. Am. Chem. Soc.* **2011**, *133*, 14431–14442. [CrossRef]
62. Kong, F.C.; Li, Y.F.; Shang, C.; Liu, Z.P. Stability and Phase Transition of Cobalt Oxide Phases by Machine Learning Global Potential Energy Surface. *J. Phys. Chem. C* **2019**, *123*, 17539−17547. [CrossRef]
63. Małecki, A.; Tareen, J.A.K.; Doumerc, J.P.; Rabardel, L.; Launay, J.C. Kinetics of thermal decomposition of Co_3O_4 powder and single crystals. *J. Solid State Chem.* **1985**, *56*, 49–57. [CrossRef]
64. Zyła, M.; Smoła, G.; Knapik, A.; Rysz, J.; Sitarz, M.; Grzesik, Z. The formation of the Co_3O_4 cobalt oxide within CoO substrate. *Corros. Sci.* **2016**, *112*, 536–541. [CrossRef]
65. O'Neil, M.J. (Ed.) *The Merck Index—An Encyclopedia of Chemicals, Drugs, and Biologicals*; Royal Society of Chemistry: Cambridge, UK, 2013; p. 436.
66. Sarte, P.M.; Songvilay, M.; Pachoud, E.; Ewings, R.A.; Frost, C.D.; Prabhakaran, D.; Hong, K.H.; Browne, A.J.; Yamani, Z.; Attfield, J.P.; et al. Spin-orbit excitons in CoO. *Phys. Rev. B* **2019**, *100*, 075143. [CrossRef]
67. Mandziak, A.; Soria, G.D.; Prieto, J.E.; Prieto, P.; Granados-Miralles, C.; Quesada, A.; Foerster, M.; Aballe, L.; de la Figuera, J. Tuning the Néel temperature in an antiferromagnet: The case of $Ni_xCo_{1-x}O$ microstructures. *Sci. Rep.* **2019**, *9*, 13584. [CrossRef]
68. Shen, Z.-X.; Allen, J.W.; Lindberg, P.A.P.; Dessau, D.S.; Wells, B.O.; Borg, A.; Ellis, W.; Kang, J.S.; Oh, S.-J.; Lindau, I.; et al. Photoemission study of CoO. *Phys. Rev. B* **1990**, *42*, 1817–1828. [CrossRef]
69. Liao, L.; Zhang, Q.; Su, Z.; Zhao, Z.; Wang, Y.; Li, Y.; Lu, X.; Wei, D.; Feng, G.; Yu, Q.; et al. Efficient solar water-splitting using a nanocrystalline CoO photocatalyst. *Nat. Nanotechnol.* **2014**, *9*, 69–73. [CrossRef]

70. Yin, M.Y.; Wang, X.C.; Mi, W.B.; Chen, G.F.; Yang, B.H. A first-principles prediction on the magnetism in CoO with Co and O Vacancies. *J. Alloys Compd.* **2014**, *610*, 422–427. [CrossRef]
71. Choi, J.S.; Chul, Y. Study of the nonstoichiometric compositions of cobaltous oxide. *Inorg. Chem.* **1974**, *13*, 1720–1724. [CrossRef]
72. Tang, Y.; Ma, L.; Dou, J.; Andolina, C.M.; Li, Y.; Ma, H.; House, S.D.; Zhang, X.; Yang, J.; Tao, F. Transition of surface phase of cobalt oxide during CO oxidation. *Phys. Chem. Chem. Phys.* **2018**, *20*, 6440–6449. [CrossRef]
73. Lukashuk, L.; Yigit, N.; Li, H.; Bernardi, J.; Föttinger, K.; Rupprechter, G. Operando XAS and NAP-XPS investigation of CO oxidation on meso- and nanoscale CoO catalysts. *Catal. Today* **2019**, *336*, 139–147. [CrossRef]
74. Tomlinson, W.J.; Easterlow, A. Kinetics and microstructure of oxidation of CoO to Co_3O_4 at 700–800 °C. *J. Phys. Chem. Solids* **1985**, *46*, 151–153. [CrossRef]
75. Saddeler, S.; Ulrich Hagemann, U.; Bendt, G.; Schulz, S. Core-shell Co_3O_4@CoO Nanoparticles for Enhanced OER Activity. *ChemCatChem* **2024**, *16*, e202301327. [CrossRef]
76. Chen, H.; Falling, L.J.; Kersell, H.; Yan, G.; Zhao, X.; Oliver-Meseguer, J.; Jaugstetter, M.; Nemsak, S.; Hunt, A.; Waluyo, I.; et al. Elucidating the active phases of CoO_x films on Au(111) in the CO oxidation reaction. *Nat. Commun.* **2023**, *14*, 6889. [CrossRef] [PubMed]
77. Barreca, D.; Massignan, C.; Daolio, S.; Fabrizio, M.; Piccirillo, C.; Armelao, L.; Tondello, E. Composition and Microstructure of Cobalt Oxide Thin Films Obtained from a Novel Cobalt(II) Precursor by Chemical Vapor Deposition. *Chem. Mater.* **2001**, *13*, 588–593. [CrossRef]
78. Deori, K.; Sasanka Deka, S. Morphology oriented surfactant dependent CoO and reaction time dependent Co_3O_4 nanocrystals from single synthesis method and their optical and magnetic properties. *CrystEngComm* **2013**, *15*, 8465–8474. [CrossRef]
79. Greenwood, N.N.; Earnshaw, A. *Chemistry of the Elements*, 2nd ed.; Elsevier: Oxford, UK, 1997; p. 1341.
80. Grimes, R.W.; Peter, D.; Lagerlöf, K.P.D. Polymorphs of Cobalt Oxide. *J. Am. Ceram. Soc.* **1991**, *74*, 270–273. [CrossRef]
81. Nam, K.M.; Shim, J.H.; Han, D.-W.; Kwon, H.S.; Kang, Y.-M.; Li, Y.; Song, H.; Seo, W.S.; Park, J.T. Syntheses and Characterization of Wurtzite CoO, Rocksalt CoO,and Spinel Co_3O_4 Nanocrystals: Their Interconversion and Tuning of Phase and Morphology. *Chem. Mater.* **2010**, *22*, 4446–4454. [CrossRef]
82. Archer, T.; Hanafin, R.; Sanvito, S. Magnetism of CoO polymorphs: Density functional theory and Monte Carlo simulations. *Phys. Rev. B* **2008**, *78*, 014431. [CrossRef]
83. Basavalingu, B.; Tareen, J.A.K.; Bhandage, G.T. Thermodynamic properties of $Co(OH)_2$ from hydrothermal equilibria in cobalt oxide systems. *J. Mat. Sci. Lett.* **1986**, *5*, 1227–1229. [CrossRef]
84. Sahoo, P.; Djieutedjeu, H.; Poudeu, P.F.P. Co_3O_4 nanostructures: The effect of synthesis conditions on particles size, magnetism and transport properties. *J. Mater. Chem. A* **2013**, *1*, 15022. [CrossRef]
85. Sparks, T.; Gurlo, A.; Bekheet, M.; Gaultois, M.; Cherkashinin, G.; Laversenne, L.; Clarke, D. High-temperature structure of Co_3O_4: Understanding spinel inversion using in situ and ex situ measurements. *Phys. Rev. B* **2019**, *99*, 104104. [CrossRef]
86. He, L.; Chen, C. Finite size effect on Néel temperature with Co_3O_4 nanoparticles. *J. Appl. Phys.* **2007**, *102*, 103911. [CrossRef]
87. Valan, M.F.; Manikandan, A.; Antony, S.A. A Novel Synthesis and Characterization Studies of Magnetic Co_3O_4 Nanoparticles. *J. Nanosci. Nanotechn.* **2015**, *15*, 4580–4586. [CrossRef] [PubMed]
88. Dittmer, A.; da Costa Gouveia, T.L.; Sivalingam, K.; DeBeer, S.; Neese, F.; Maganas, D. Revisiting the band gap problem in bulk Co_3O_4 and its isostructural Zn and Al derivatives through the lens of theoretical spectroscopy. *Phys. Chem. Chem. Phys.* **2025**, *27*, 17225–17244. [CrossRef]
89. Iablokov, V.; Barbosa, R.; Pollefeyt, G.; Van Driessche, I.; Chenakin, S.; Kruse, N. Catalytic CO Oxidation over Well-DefinedCobalt Oxide Nanoparticles: Size-Reactivity Correlation. *ACS Catal.* **2015**, *5*, 5714−5718. [CrossRef]
90. Lukashuk, L.; Yigit, N.; Rameshan, R.; Kolar, E.; Teschner, D.; Hävecker, M.; Knop-Gericke, A.; Schlögl, R.; Föttinger, K.; Rupprechter, G. Operando Insights into CO Oxidation on Cobalt Oxide Catalysts by NAP-XPS, FTIR, and XRD. *ACS Catal.* **2018**, *8*, 8630–8641. [CrossRef]
91. Miquelot, A.; Despotopoulou, M.; Vahlas, C.; Villeneuve, C.; Dragoe, N.; Prud'homme, N.; Debieu, O. Morphological, structural, optical, and electrical study of nanostructured thin films: Charge transport mechanism of p-type Co_3O_4. *Mater. Chem. Phys.* **2020**, *240*, 122059. [CrossRef]
92. Eliziário, S.A.; de Andrade, J.M.; Lima, S.J.G.; Paskocimas, C.A.; Soledade, L.E.B.; Hammer, P.; Longo, E.; Souza, A.G.; Santos, I.M.G. Black and green pigments based on chromium–cobalt spinels. *Mat. Chem. Phys.* **2011**, *129*, 619–624. [CrossRef]
93. Finocchio, E.; Montanari, T.; Resini, C.; Busca, G. Spectroscopic characterization of cobalt-containing solid catalysts. *J. Mol. Catal. A Chem.* **2003**, *204–205*, 535–544. [CrossRef]
94. Zhao, F.; Ma, H. Application of Co_3O_4 in Photoelectrocatalytic Treatment of Wastewater Polluted with Organic Compounds: A Review. *Crystals* **2023**, *13*, 634. [CrossRef]
95. Yang, J.; Liu, H.; Martens, W.N.; Frost, R.L. Synthesis and Characterization of Cobalt Hydroxide, Cobalt Oxyhydroxide, and Cobalt Oxide Nanodiscs. *J. Phys. Chem. C* **2010**, *114*, 111–119. [CrossRef]

96. Chen, X.; Cheng, J.P.; Shou, Q.L.; Liu, F.; Zhang, X.B. Effect of calcination temperature on the porous structure of cobalt oxide micro-flowers. *CrystEngComm* **2012**, *14*, 1271. [CrossRef]
97. Liotta, L.F.; Ousmane, M.; Di Carlo, G.; Pantaleo, G.; Deganello, G.; Marcì, G.; Retailleau, L.; Giroir-Fendler, A. Total oxidation of propene at low temperature over Co_3O_4 –CeO_2 mixed oxides: Role of surface oxygen vacancies and bulk oxygen mobility in the catalytic activity. *Appl. Catal. A Gen.* **2008**, *347*, 81–88. [CrossRef]
98. Han, W.; Tang, Z.; Lin, Q. Morphology-controlled synthesis of the metal–organic framework-derived nanorod interweaved lamellose structure Co_3O_4 for outstanding catalytic combustion performance. *Cryst. Growth Des.* **2019**, *19*, 4546–4556. [CrossRef]
99. Zhu, W.; Chen, X.; Li, C.; Liu, Z.; Liang, C. Manipulating morphology and surface engineering of spinel cobalt oxides to attain high catalytic performance for propane oxidation. *J. Catal.* **2021**, *396*, 179–191. [CrossRef]
100. Zhao, S.; Li, T.; Lin, J.; Wu, P.; Li, Y.; Li, A.; Chen, T.; Zhao, Y.; Chen, G.; Yang, L.; et al. Engineering Co^{3+} -rich crystal planes on Co_3O_4 hexagonal nanosheets for CO and hydrocarbons oxidation with enhanced catalytic activity and water resistance. *Chem. Eng. J.* **2021**, *420*, 130448. [CrossRef]
101. Dey, S.; Dhal, G.C. The catalytic activity of cobalt nanoparticles for low-temperature oxidation of carbon monoxide. *Mater. Today Chem.* **2019**, *14*, 100198. [CrossRef]
102. Vodyashkin, A.A.; Kezimana, P.; Prokonov, F.Y.; Vasilenko, I.A.; Stanishevskiy, Y.M. Current Methods for Synthesis and Potential Applications of Cobalt Nanoparticles: A Review. *Crystals* **2022**, *12*, 272. [CrossRef]
103. Samal, R.; Dash, B.; Sarangi, C.K.; Sanjay, K.; Subbaiah, T.; Senanayake, G.; Minakshi, M. Influence of Synthesis Temperature on the Growth and Surface Morphology of Co3O4 Nanocubes for Supercapacitor Applications. *Nanomaterials* **2017**, *7*, 356. [CrossRef]
104. Cahyadi, A.; Nandiyanto, A.B.D. Economic evaluation in industrial scale Co3O4 nanoparticle synthesis. *Arab. J. Chem. Environ. Res.* **2019**, *6*, 84–93.
105. Tang, C.W.; Wang, C.B.; Chienc, S.H. Characterization of cobalt oxides studied by FT-IR, Raman, TPR and TG-MS. *Thermochim. Acta* **2008**, *473*, 68–73. [CrossRef]
106. Khussain, B.; Sass, A.; Brodskiy, A.; Rakhmetova, K.; Torlopov, I.; Zhylkybek, M.; Baizhumanova, T.; Tungatarova, S.; Khussain, A.; Zhurinov, M.; et al. Patterns of Formation of Binary Cobalt–Magnesium Oxide Combustion Catalysts of Various Composition. *Catalysts* **2024**, *14*, 425. [CrossRef]
107. Van Winkle, M.; House, S.D.; Peng, Y.; Chen-Wiegart, Y.K.; Jungjohann, K.; Mangum, J.S. Revealing Progressive Degradation of Cobalt Oxide Nanoparticles During Thermochemical Redox Cycling via Operando STEM-EELS. *Nano Lett.* **2025**, *25*, 18075−18082. [CrossRef]
108. Chen, X.; Gog, H.; van Huism, M.A. Transformation of Co_3O_4 nanoparticles to CoO monitored by in situ TEM and predicted ferromagnetism at the Co_3O_4 /CoO interface from first principles. *J. Mater. Chem. C* **2021**, *9*, 5662. [CrossRef]
109. Raimundo, R.A.; Silva, J.N.; Silva, T.R.; Araújo, A.J.M.; Oliveira, J.F.G.A.; de Lima, L.C.; Morales, M.A.; Soares, M.M.; Macedo, D.A. Green chemistry synthesis of Co_3O_4-CoO nanocomposite and electrochemical assessment for oxygen evolution reaction. *Mater. Lett.* **2023**, *341*, 134196. [CrossRef]
110. Al-Senani, G.M.; Deraz, N.M.; Abd-Elkader, O.H. Magnetic and Characterization Studies of CoO/Co3O4 Nanocomposite. *Processes* **2020**, *8*, 844. [CrossRef]
111. Catti, M.; Sandrone, G. Ab initio Study of Corundum-Like Me_2O_3 Oxides (Me Ti, V, Cr, Fe, Co, Ni). *Faraday Discuss.* **1997**, *106*, 189–203. [CrossRef]
112. Shanbhag, P.N.; Biswas, R.K.; Pati, S.K.; Sundaresan, A.; Rao, C.N.R. Elusive Co_2O_3: A Combined Experimental and Theoretical Study. *ACS Omega* **2020**, *5*, 29009–29016. [CrossRef] [PubMed]
113. Chenavas, J.; Joubert, J.C. Low-spin → High-Spin State Transition in High Pressure Cobalt Sesquioxide. *Solid State Commun.* **1971**, *9*, 1057–1060. [CrossRef]
114. Raveau, B.; Seikh, M.M. Magnetic and Physical Properties of Cobalt Perovskites. In *Handbook of Magnetic Materials*; Elsevier: Amsterdam, The Netherlands, 2015; Volume 23, pp. 161–289.
115. Amatucci, G.G.; Tarascon, J.M.; Klein, L.C. CoO_2, The End Member of the Li_xCoO_2 Solid Solution. *J. Electrochem. Soc.* **1996**, *143*, 1114–1122. [CrossRef]
116. Tarascon, J.M.; Vaughan, G.; Chabre, Y.; Seguin, L.; Anne, M.; Strobel, P.; Amatucci, G. In Situ Structural and Electrochemical Study of $Ni_{1-x}Co_xO_2$ Metastable Oxides Prepared by Soft Chemistry. *J. Solid State Chem.* **1999**, *147*, 410–420. [CrossRef]
117. Motohashi, T.; Katsumata, Y.; Ono, T.; Kanno, R.; Karppinen, M.; Yamauchi, H. Synthesis and properties of CoO_2, the x = 0 end member of the Li_xCoO_2 and Na_xCoO_2 systems. *Chem. Mater.* **2007**, *19*, 5063–5066. [CrossRef]
118. Boddu, V.R.R.; Puthusseri, D.; Shirage, P.M.; Mathur, P.; Pol, V.G. Layered Na_xCoO_2-based cathodes for advanced Na-ion batteries: Review on challenges and advancements. *Ionics* **2021**, *27*, 4549–4572. [CrossRef]
119. Hettler, S.; Roy, K.S.; Arenal, R.; Panchakarla, L.S. Stable CoO_2 Nanoscrolls with Outstanding Electrical Properties. *Adv. Mater. Interfaces* **2024**, *11*, 2400317. [CrossRef]
120. Motohashi, T.; Ono, T.; Sugimoto, Y.; Masubuchi, Y.; Kikkawa, S.; Kanno, R.; Karppinen, M.; Yamauchi, H. Electronic phase diagram of the layered cobalt oxide system Li_xCoO_2 ($0.0 \leq x \leq 1.0$). *Phys. Rev.* **2009**, *80*, 165114. [CrossRef]

121. Houska, C.R.; Averbach, B.L.; Cohen, M. The Cobalt Transformation. *Acta Metall.* **1960**, *8*, 81−87. [CrossRef]
122. Erbudak, M.; Wetli, E.; Hochstrasser, M.; Pescia, D.; Vvedensky, D. Surface phase transitions during martensitic transformations of single-crystal Co. *Phys. Rev. Lett.* **1997**, *79*, 1893–1896. [CrossRef]
123. Yoo, C.S.; Söderlind, P.; Cynn, H. The phase diagram of cobalt at high pressure and temperature: The stability of γ(fcc)-cobalt and new ε'(dhcp)-cobalt. *J. Phys. Condens. Matter* **1998**, *10*, L311. [CrossRef]
124. Manjunatha, M.; Reddy, G.S.; Mallikarjunaiah, K.J.; Damle, R.; Ramesh, K.P. Determination of Phase Composition of Cobalt Nanoparticles Using ^{59}Co Internal Field Nuclear Magnetic Resonance. *J. Supercond. Novel Magn.* **2019**, *32*, 3201–3209. [CrossRef]
125. Khusnuriyalova, A.F.; Caporali, M.; Hey-Hawkins, J.E.; Sinyashin, O.G.; Yakhvarov, D.G. Preparation of Cobalt Nanoparticles. *Eur. J. Inorg. Chem.* **2021**, 3023–3047. [CrossRef]
126. Garbarino, G.; Riani, P.; Lucchini, M.A.; Canepa, F.; Kawale, S.; Busca, G. Cobalt-based nanoparticles as catalysts for low temperature hydrogen production by ethanol steam reforming. *Int. J. Hydrogen Energy* **2013**, *38*, 82–91. [CrossRef]
127. Riani, P.; Garbarino, G.; Cavattoni, T.; Canepa, F.; Busca, G. Unsupported cobalt nanoparticles as catalysts: Effect of preparation method on catalytic activity in CO_2 methanation and ethanol steam reforming. *Int. J. Hydrogen Energy* **2019**, *44*, 27319–27328. [CrossRef]
128. López Antón, R.; González, J.A.; Andrés, J.P.; Canales-Vázquez, J.; De Toro, J.A.; Riveiro, J.M. High-vacuum annealing reduction of Co/CoO nanoparticles. *Nanotechnology* **2014**, *25*, 105702. [CrossRef]
129. Busca, G.; Guidetti, R.; Lorenzelli, V. Fourier-transform infrared study of the surface properties of cobalt oxides. *J. Chem. Soc. Faraday Trans.* **1990**, *86*, 989–994. [CrossRef]
130. Zhang, L.; Huo, F.; Wang, A.; Chai, S.; Guan, J.; Fan, G.; Yang, W.; Ma, G.; Han, N.; Chen, Y. Coordination-Controlled Catalytic Activity of Cobalt Oxides for Ozone Decomposition. *Inorg. Chem.* **2023**, *62*, 9178−9189. [CrossRef]
131. Moulijn, J.A.; Arnoldy, P. Temperature-programmed reduction of CoO/Al_2O_3 catalysts. *J. Catal.* **1985**, *93*, 38–54.
132. Wang, W.-J.; Chen, Y.-W. Influence of metal loading on the reducibility and hydrogenation activity of cobalt/alumina catalysts. *Appl. Catal.* **1991**, *77*, 223–233. [CrossRef]
133. de la Peña O'Shea, V.A.; Homs, N.; Pereira, E.B.; Nafria, R.; Ramírez de la Piscina, P. X-ray diffraction study of Co_3O_4 activation under ethanol steam-reforming. *Catal. Today* **2007**, *126*, 148–152. [CrossRef]
134. Tompkins, H.G.; Augis, J.A. The Oxidation of Cobalt in Air from Room Temperature to 467 °C. *Oxid. Met.* **1981**, *16*, 355–369. [CrossRef]
135. Zhanga, D.; Jina, C.; Li, Z.Y.; Zhang, Z.; Li, J. Oxidation behavior of cobalt nanoparticles studied by in situ environmental transmission electron microscopy. *Sci. Bull.* **2017**, *62*, 775–778. [CrossRef] [PubMed]
136. Busca, G. The surface of transition aluminas. A critical Review. *Catal. Today* **2014**, *226*, 2–13. [CrossRef]
137. Busca, G. Structural, surface and catalytic properties of aluminas. *Adv. Catal.* **2014**, *57*, 319–404.
138. Yang, Y.; Miao, C.; Wang, R.; Zhang, R.; Li, X.; Wang, J.; Wang, X.; Yao, J. Advances in morphology-controlled alumina and its supported Pd catalysts: Synthesis and applications. *Chem. Soc. Rev.* **2024**, *53*, 5014–5053. [CrossRef]
139. Marturano, M.; Aglietti, E.F.; Ferretti, O. α-Al_2O_3 catalyst supports for synthesis gas production: Influence of different alumina bonding agents on support and catalyst properties. *Mater. Chem. Phys.* **1997**, *47*, 252–256. [CrossRef]
140. Braaten, O.; Kjekshus, A.; Kvande, H. The Possible Reduction of Alumina to Aluminum Using Hydrogen. *JOM* **2000**, *52*, 47–53. [CrossRef]
141. Helali, Z.; Jedidi, A.; Syzgantseva, O.A.; Calatayud, M.; Minot, C. Scaling reducibility of metal oxides. *Theor. Chem. Acc.* **2017**, *136*, 100. [CrossRef]
142. Reichle, W.T. Synthesis of anionic clay minerals (mixed metal hydroxides, hydrotalcite). *Solid State Ion.* **1986**, *22*, 135–141. [CrossRef]
143. Ulibarri, M.A.; Fernandez, J.M.; Labajos, F.M.; Rives, V. Anionic clays with variable valence cations: Synthesis and characterization of $[Co_{1-x}Al_{x(}OH)_2](CO_3)x/2\ nH_2O$. *Chem. Mater.* **1991**, *3*, 626–630. [CrossRef]
144. Thompson, H.A.; Parks, G.A.; Brown, G.E. Ambient-temperature synthesis, evolution, and characterization of cobalt-aluminum hydrotalcite-like solids. *Clays Clay Min.* **1999**, *47*, 425–438. [CrossRef]
145. Cavani, F.; Trifirò, F.; Vaccari, A. Hydrotalcite-type anionic clays: Preparation, properties and applications. *Catal. Today* **1991**, *11*, 173–301. [CrossRef]
146. Debecker, D.P.; Gaigneaux, E.M.; Busca, G. Exploring, tuning and exploiting the basicity of hydrotalcites for applications in heterogeneous catalysis. *Chem. Europ. J.* **2009**, *15*, 3920–3935. [CrossRef]
147. Białas, A.; Mazur, M.; Natkanski, P.; Dudek, B.; Kozak, M.; Wach, A.; Kustrowski, P. Hydrotalcite-derived cobalt–aluminum mixed oxide catalysts for toluene combustion. *Appl. Surf. Sci.* **2016**, *362*, 297–303. [CrossRef]
148. Leroux, F.; Moujahid, E.M.; Taviot-Gueho, C.; Besse, J.-P. Effect of layer charge modification for CoAl layered double hydroxides: Study by X-ray absorption spectroscopy. *Solid State Sci.* **2001**, *3*, 81–92. [CrossRef]
149. Li, D.; Ding, Y.; Wei, X.; Xiao, Y.; Jiang, L. Cobalt-aluminum mixed oxides prepared from layered double hydroxides for the total oxidation of benzene. *Appl. Catal. A Gen.* **2015**, *507*, 130–138. [CrossRef]

150. Wan, C.; Wei, X.; Cai, G.; Li, D.; Zhan, Y.; Xiao, Y.; Jiang, L. Hydrotalcite-derived aluminum-doped cobalt oxides for catalytic benzene combustion: Effect of calcination atmosphere. *Mol. Catal.* **2022**, *520*, 112160. [CrossRef]
151. Koroleva, L.F. Synthesis of Spinel-Based Ceramic Pigments from Hydroxycarbonates. *Glass Ceram.* **2004**, *61*, 299–302. [CrossRef]
152. Mori, T. Phase diagram of the system CoO-Al_2O_3. *Nippon. Seram. Kyokai. Gakkaishi* **1982**, *90*, 100–101.
153. Azurdia, J.; Marchal, J.; Laine, R.M. Synthesis and Characterization of Mixed-Metal Oxide Nanopowders Along the CoO_x–Al_2O_3 Tie Line Using Liquid-Feed Flame Spray Pyrolysis. *J. Am. Ceram. Soc.* **2006**, *89*, 2749–2756. [CrossRef]
154. Alarcón, J.; Escribano, P.; Marin, R.M. Co(II) based ceramic pigments. *Br. Ceram. Trans. J.* **1985**, *84*, 170–172.
155. Tielens, F.; Calatayud, M.; Franco, R.; M Recio, J.M.; Pérez-Ramírez, J.; Minot, C. Periodic DFT Study of the Structural and Electronic Properties of Bulk $CoAl_2O_4$ Spinel. *J. Phys. Chem. B* **2006**, *110*, 988–995. [CrossRef]
156. Zayat, M.; Levy, D. Blue $CoAl_2O_4$ Particles Prepared by the Sol-Gel and Citrate-Gel Methods. *Chem. Mater.* **2000**, *12*, 2763–2769. [CrossRef]
157. Garcia Casado, P.; Rasines, I. The series of spinels Co3−sAlsO4 (0 < s < 2): Study of Co_2AlO_4. *J. Solid State Chem.* **1984**, *52*, 187–190. [CrossRef]
158. Xi, X.; Nie, Z.; Ma, L.; Li, L.; Xu, X.; Zuo, T. Synthesis and characterization of ultrafine Co_2AlO_4 pigment by freeze–drying. *Powder Technol.* **2012**, *226*, 114–116. [CrossRef]
159. Zeng, K.; Tan, L.; Li, X.; Wang, Z.; Guo, H.; Wang, J.; Yan, G. Mono-Active Bimetallic Oxide Co_2AlO_4 with Yolk-Shell Structure as a Superior Lithium-Storage Material. *ChemElectroChem* **2019**, *6*, 3298–3302. [CrossRef]
160. Busca, G.; Lorenzelli, V.; Bolis, V. Preparation, bulk characterization and surface chemistry of high-surface-area cobalt aluminate. *Mater. Chem. Phys.* **1992**, *31*, 221–228. [CrossRef]
161. Serment, B.; Brochon, C.; Hadziioannou, G.; Buffière, S.; Demourgues, A.; Gaudon, M. The versatile Co^{2+}/Co^{3+} oxidation states in cobalt alumina spinel: How to design strong blue nanometric pigments for color electrophoretic display. *RSC Adv.* **2019**, *9*, 34125–34135. [CrossRef]
162. Tristan, N.; Zestrea, V.; Behr, G.; Klingeler, R.; Büchner, B.; Krug von Nidda, H.A.; Loidl, A.; Tsurkan, V. Spin frustration and magnetic exchange in cobalt aluminum oxide spinels. *Phys. Rev. B* **2008**, *77*, 094412. [CrossRef]
163. Zhang, W.; Li, Z.; Wu, G.; Wu, W.; Zeng, H.; Jiang, H.; Zhang, W.; Wu, R.; Xue, Q. Effects of Coloration of Spinel $CoAl_2O_4$ Cobalt Blue Pigments: Composition, Structure, and Cation Distribution. *Inorganics* **2023**, *11*, 368. [CrossRef]
164. Masoud, E.M.; El-Bellihi, A.A.; Bayoumy, W.A.; Abdelazeem, E.S. Structural, optical, magnetic, and electrical properties of nanospinels containing different molar ratios of cobalt and aluminum ions. *Ionics* **2017**, *23*, 2417–2427. [CrossRef]
165. Ouahdi, N.; Guillemet, S.; Demai, J.J.; Durand, B.; Er Rakho, L.; Moussa, R.; Samdi, A. Investigation of the reactivity of $AlCl_3$ and $CoCl_2$ toward molten alkali-metal nitrates in order to synthesize $CoAl_2O_4$. *Mater. Lett.* **2005**, *59*, 334–340. [CrossRef]
166. Yu, F.; Yang, J.; Ma, J.; Du, J.; Zhou, Y. Preparation of nanosized $CoAl_2O_4$ powders by sol–gel and sol–gel-hydrothermal methods. *J. Alloys Compd.* **2009**, *468*, 443–446. [CrossRef]
167. Garbarino, G.; Cavattoni, T.; Riani, P.; Busca, G. Support effects in metal catalysis: A study of the behavior of unsupported and silica-supported cobalt catalysts in the hydrogenation of CO_2 at atmospheric pressure. *Catal. Today* **2020**, *345*, 213–219. [CrossRef]
168. Lenglet, M.; Lefez, B. Infrared optical properties of cobalt (II) spinels. *Solid State Commun.* **1996**, *98*, 689–694. [CrossRef]
169. Li, Y.; Qiu, W.; Qin, F.; Fang, H.; Hadjiev, V.G.; Litvinov, D.; Bao, J. Identification of Cobalt Oxides with Raman Scattering and Fourier Transform Infrared Spectroscopy. *J. Phys. Chem. C* **2016**, *120*, 4511–4516. [CrossRef]
170. Mindru, I.; Marinescu, G.; Gingasu, D.; Patron, L.; Ghica, C.; Giurginca, M. Blue $CoAl_2O_4$ spinel via complexation method. *Mater. Chem. Phys.* **2010**, *122*, 491–497. [CrossRef]
171. Cornaro, U.; Rossini, S.; Montanari, T.; Finocchio, E.; Busca, G. K-doping of Co/Al_2O_3 low temperature Fischer–Tropsch catalysts. *Catal. Today* **2012**, *197*, 101–108. [CrossRef]
172. Chen, X.; Cai, S.; Yu, E.; Li, J.; Chen, J.; Jia, H. Photothermocatalytic performance of ACo_2O_4 type spinel with light-enhanced mobilizable active oxygen species for toluene oxidation. *Appl. Surf. Sci.* **2019**, *484*, 479–488. [CrossRef]
173. Yaemphutchong, S.; Wattanathana, W.; Chansaenpak, K.; Singkammo, S.; Kanjanaboos, P.; Siri-apai, P.; Janejobsakonkit, S.; Pipattanaporn, P.; Suetrong, N.; Wannapaiboon, S.; et al. Structural investigation and optical properties of cobalt aluminate pigments derived from thermal decomposition of mixed-metal nitrate co-crystals. *Ceram. Int.* **2022**, *48*, 18490–18501. [CrossRef]
174. Kurajic, S.; Popovic, J.; Tkalce, E.; Grzet, B.; Mandi, V. The effect of annealing temperature on the structure and optical properties of solegel derived nanocrystalline cobalt aluminate spinel. *Mater. Chem. Phys.* **2012**, *135*, 587–593. [CrossRef]
175. Duan, X.; Pan, M.; Yu, F.; Yuan, D. Synthesis, structure and optical properties of $CoAl_2O_4$ spinel nanocrystals. *J. Alloys Compd.* **2011**, *509*, 1079–1083. [CrossRef]
176. Li, Y.; Zhao, Z.; Zhao, M.; Zhu, H.; Ma, X.; Li, Z.; Lua, W.; Chen, X.; Ying, L.; Lind, R.; et al. Oxygen-vacancy induced structural changes of Co species in $CoAl_2O_4$ spinels for CO_2 hydrogenation. *Appl. Catal. B Environ. Energy* **2024**, *347*, 123824. [CrossRef]
177. El Jabbar, Y.; Lakhlifi, H.; El Ouatib, R.; Er-Rakho, L.; Guillemet-Fritsch, S.; Durand, B. Synthesis of cobalt aluminate spinel by sol-gel process: Investigation of starting reagents and precursors obtained after pyrolysis. *Chem. Data Collect.* **2021**, *35*, 100766. [CrossRef]

178. Ragupathi, C.; Vijaya, J.J.; Kennedy, L.J.; Bououdina, M. Combustion synthesis, structure, magnetic and optical properties of cobalt aluminate spinel nanocrystals. *Ceram. Int.* **2014**, *40*, 13067–13074. [CrossRef]
179. Lv, W.; Qiu, Q.; Wang, F.; Wei, S.; Liu, B.; Luo, Z. Sonochemical synthesis of cobalt aluminate nanoparticles under various preparation parameters. *Ultrason. Sonochem.* **2010**, *17*, 793–801. [CrossRef]
180. Karmaoui, M.; Silva, N.J.O.; Amaral, V.S.; Ibarra, A.; Millán, Á.; Palacio, F. Synthesis of cobalt aluminate nanopigments by a non-aqueous sol–gel route. *Nanoscale* **2013**, *5*, 4277–4283. [CrossRef]
181. Mindru, I.; Gingasu, D.; Patron, L.; Ianculescu, A.; Surdu, V.A.; Culita, D.C.; Preda, S.; Negut, C.D.; Oprea, O. A new approach: Synthesis of cobalt aluminate nanoparticles using tamarind fruit extract. *Mater. Sci. Eng. B* **2019**, *246*, 42–48. [CrossRef]
182. Nishina, T.; Yonemura, M.; Sekine, T.; Kotera, Y. Solid-State Reaction between Alumina and Cobalt Oxide. *J. Soc. Mat. Sci. Jpn.* **1972**, *21*, 544–547. [CrossRef]
183. Cava, S.; Tebcherani, S.M.; Pianaro, S.A.; Paskocimas, C.A.; Longo, E.; Varela, J.A. Structural and spectroscopic analysis of γ-Al_2O_3 to α-Al_2O_3-$CoAl_2O_4$ phase transition. *Mat. Chem. Phys.* **2006**, *97*, 102–108. [CrossRef]
184. Marinović, S.; Mudrinić, T.; Dojčinović, B.; Barudžija, T.; Banković, P.; Novaković, T. Cobalt-doped alumina catalysts in catalytic oxidation of tartrazine induced by Oxone®. *J. Environ. Chem. Eng.* **2021**, *9*, 106348. [CrossRef]
185. He, X.; Lei, Z. Synthesis and color properties of the CoAl2O4/Al2O3 hybrid blue pigments with low cobalt contents. *J. Mater. Sci.* **2020**, *55*, 13569–13577. [CrossRef]
186. Dutt, B.V.; Hurrell, J.P.; Kröger, F.A. High-Temperature Defect Structure of Cobalt-Doped α-Alumina. *J. Am. Ceram. Soc.* **1975**, *58*, 420–427. [CrossRef]
187. Donald, S. McClure, Optical Spectra of Transition-Metal Ions in Corundum. *J. Chem. Phys.* **1962**, *36*, 2757–2779.
188. Zhu, Z.; Zhang, H.; Wang, Y.; Wu, W.; Wu, L.; Zeng, N.; Ren, H.; Xu, S.; Goodman, B.A.; Deng, W. Preparation and optical properties of high-quality green cobalt sapphires. *J. Lumin.* **2024**, *267*, 120354. [CrossRef]
189. Müller, R.; Günthard, H.H. Spectroscopic study of the reduction of nickel and cobalt ions in sapphire. *J. Chem. Phys.* **2004**, *44*, 365–373. [CrossRef]
190. Danchevskaya, M.N.; Ivakin, Y.D.; Muravieva, G.P.; Luchkov, I.V. Synthesis and doping of fine-crystalline corundum in sub- and supercritical conditions. *J. Phys. Conf. Ser.* **2008**, *121*, 082001. [CrossRef]
191. Seham, A.; Mansour, A. Spectrothermal studies on the decomposition course of cobalt oxysalts Part II. Cobalt nitrate hexahydrate. *Mater. Chem. Phys.* **1994**, *36*, 317–323. [CrossRef]
192. Wigzell, F.A.; Jackson, S.D. The genesis of supported cobalt catalysts. *Appl. Petrochem. Res.* **2017**, *7*, 9–21. [CrossRef]
193. Topsøe, N.Y.; Topsøe, H. Adsorption Studies on Hydrodesulfurization Catalysts I. Infrared and Volumetric Study of NO Adsorption on Alumina-Supported Co, Mo, and Co-Mo Catalysts in Their Calcined State. *J. Catal.* **1982**, *75*, 354–374. [CrossRef]
194. Spennati, E.; Garbarino, G.; Savio, L.; Vattuone, L.; Riani, P.; Busca, G. CO_2 methanation vs reverse WGS activity on Co/γ-Al_2O_3 catalysts at atmospheric pressure: Effect of cobalt loading and silica addition on selectivity and stability. *Catal. Today* **2023**, *420*, 114164. [CrossRef]
195. Horlyck, J.; Sara, M.; Lovell, E.C.; Amal, R.; Scott, J. Effect of Metal-Support Interactions in Mixed Co/Al Catalysts for Dry Reforming of Methane. *ChemCatChem* **2019**, *11*, 3339–3551. [CrossRef]
196. Spennati, E.; Garbarino, G.; Riani, P.; Busca, G. Alumina-supported cobalt catalysts in the hydrogenation of CO_2 at atmospheric pressure. *Int. J. Hydrogen Energy* **2023**, *48*, 25006–25015. [CrossRef]
197. Byun, S.W.; Shin, H.; Bae, W.B.; Hazlett, M.J.; Kim, Y.J.; Lee, S.J.; Kim, M.; Kang, S.B. Dry synthesis of alumina-supported cobalt catalyst for highly enhanced catalytic oxidation. *Chem. Eng. J.* **2024**, *481*, 148316. [CrossRef]
198. Zavyalova, U.; Scholz, P.; Ondruschka, B. Influence of cobalt precursor and fuels on the performance of combustion synthesized Co_3O_4/γ-Al_2O_3 catalysts for total oxidation of methane. *Appl. Catal. A Gen.* **2007**, *323*, 226–233. [CrossRef]
199. Cherepanova, S.V.; Koemets, E.G.; Gerasimov, E.Y.; Simentsova, I.I.; Bulavchenko, O.A. Reducibility of Al^{3+}-Modified Co_3O_4: Influence of Aluminum Distribution. *Materials* **2023**, *16*, 6216. [CrossRef]
200. Lendzion-Bieluń, Z.; Jędrzejewski, R.; Arabczyk, W. The effect of aluminium oxide on the reduction of cobalt oxide and thermostabillity of cobalt and cobalt oxide. *Cent. Eur. J. Chem.* **2011**, *9*, 834–839. [CrossRef]
201. Jacobs, G.; Ma, W.; Davis, B.H. Influence of Reduction Promoters on Stability of Cobalt/γ-Alumina Fischer-Tropsch Synthesis Catalysts. *Catalysts* **2014**, *4*, 49–76. [CrossRef]
202. Diehl, F.; Hugues, F.; Marion, M.C.; Uzio, D. Cobalt-Based Catalyst for Fischer-Tropsch Synthesis. WIPO WO 2006067285 A1, 29 June 2006.
203. Bonne, R.L.; Lok, C.M. Cobalt on Alumina Catalysts. U.S. Patent US5874381A, 23 February 1999.
204. Osbourne, T.; O'Brien, R.; Kirchner, J.; Hu, X.D. Fluid/Slurry Bed Cobalt-Alumina Catalyst Made by Compounding and Spray Drying. U.S. Patent US7560412B2, 17 July 2009.
205. Qiao, C.; Rafai, S.; Cao, T.; Wang, Z.; Wang, H.; Zhu, Y.; Ma, X.; Xu, P.; Cao, C. Tuning Surface Electronic Structure of Two-Dimensional Cobalt-Based Hydroxide Nanosheets for Highly Efficient Water Oxidation. *ChemCatChem* **2020**, *12*, 2823–2832. [CrossRef]

206. Zhang, X.; Zhong, H.; Zhang, Q.; Zhang, Q.; Wu, C.; Yu, J.; Ma, Y.; An, H.; Wang, H.; Zou, Y.; et al. High-spin Co^{3+} in cobalt oxyhydroxide for efficient water oxidation. *Nat. Commun.* **2024**, *15*, 1383. [CrossRef]
207. Kannan, R.; Seehra, M.S. Percolation effects and magnetic properties of the randomly diluted fcc system $Co_pMg_{1-p}O$. *Phys. Rev. B* **1987**, *35*, 6847–6853. [CrossRef]
208. Shannon, R.D. Revised effective ionic radii and systematic studies of interatomic distances in halides and chalcogenides. *Acta Cryst.* **1976**, *A32*, 751–767. [CrossRef]
209. Busca, G. The surface acidity of solid oxides and its characterization by IR spectroscopic methods. An attempt at systematization. *Phys. Chem. Chem. Phys.* **1999**, *1*, 723–736. [CrossRef]
210. Busca, G. Bases and basic materials in industrial and environmental chemistry. Liquid versus solid basicity. *Chem. Rev.* **2010**, *110*, 2217–2249. [CrossRef]
211. Lenglet, M. Iono-Covalent Character of the Metal-Oxygen Bonds in Oxides: A Comparison of Experimental and Theoretical Data. *Act. Passiv. Electron. Compon.* **2004**, *27*, 1–60. [CrossRef]
212. Petitto, S.C.; Marsh, E.M.; Carson, G.A.; Langell, M.A. Cobalt oxide surface chemistry: The interaction of CoO(100), Co_3O_4 (110) and Co_3O_4 (111) with oxygen and water. *J. Mol. Catal. A Chem.* **2008**, *281*, 49–58. [CrossRef]
213. Tsyganenko, A.A.; Filimonov, V.N. I nfrared Spectra of Surface Hydroxyl Groups and Crystalline Structure of Oxides. *Spectrosc. Lett.* **1972**, *5*, 477–487. [CrossRef]
214. Grillo, F.; Natile, M.M.; Glisenti, A. Low temperature oxidation of carbon monoxide: The influence of water and oxygen on the reactivity of a Co_3O_4 powder surface. *Appl. Catal. B Environ.* **2004**, *48*, 267–274. [CrossRef]
215. Xie, X.; Li, Y.; Liu, Z.Q.; Haruta, M.; Shen, W. Low-temperature oxidation of CO catalysed by Co_3O_4 nanorods. *Nature* **2009**, *458*, 746–749. [CrossRef] [PubMed]
216. Mehl, S.; Ferstl, P.; Schuler, M.; Toghan, A.; Brummel, O.; Hammer, L.; Schneider, M.A.; Libuda, J. Thermal evolution of cobalt deposits on Co_3O_4(111): Atomically dispersed cobalt, two-dimensional CoO islands, and metallic Co nanoparticles. *Phys. Chem. Chem. Phys.* **2015**, *17*, 23538–23546. [CrossRef]
217. Hsu, S.H.; Hung, S.F.; Wang, H.Y.; Xiao, F.X.; Zhang, L.; Yang, H.; Chen, H.M.; Lee, J.M.; Liu, B. Tuning the Electronic Spin State of Catalysts by StrainControl for Highly Efficient Water Electrolysis. *Small Methods* **2018**, *2*, 1800001. [CrossRef]
218. Sun, Y.M.; Ren, X.; Sun, S.; Liu, Z.; Xi, S.; Xu, Z.J. Engineering high-spin state cobalt cations in spinel zinc cobalt oxide for spin channel propagation and active site enhancement in water oxidation. *Angew. Chem. Int. Ed.* **2021**, *60*, 14536–14544. [CrossRef]
219. Wu, C.; Sun, Y.; Yang, Z.; Hu, J.; Ding, T.Y.; Cheng, J.; Zhang, K.H.L. Tuning the Spin State of Co^{3+} by Crystal Facet Engineering for Enhancing the Oxygen Evolution Reaction Activity. *Chem. Mater.* **2022**, *34*, 10509–10516. [CrossRef]
220. Busca, G.; Lorenzelli, V.; Sanchez Escribano, V.; Guidetti, R. FT-IR Study of the Surface Properties of the Spinels $NiAl_2O_4$ and $CoAl_2O_4$ in Relation to those of Transitional Aluminas. *J. Catal.* **1991**, *131*, 167–177. [CrossRef]
221. Royer, S.; Duprez, D. Catalytic Oxidation of Carbon Monoxide over Transition Metal Oxides. *ChemCatChem* **2011**, *3*, 24–65. [CrossRef]
222. Gabrovska, M.; Edreva-Kardjieva, R.; Tenchev, K.; Tzvetkov, P.; Spojakina, A.; Petrov, L. Effect of Co-content on the structure and activity of Co-Al hydrotalcite- like materials as catalyst precursors for CO oxidation. *Appl. Catal. A Gen.* **2011**, *399*, 242–251. [CrossRef]
223. Cunningham, D.A.H.; Kobayashi, T.; Kamijo, N.; Haruta, M. Influence of dry operating conditions: Observation of oscillations and low temperature CO oxidation over Co_3O_4 and Au/Co_3O_4 catalysts. *Catal. Lett.* **1994**, *25*, 257–264. [CrossRef]
224. Wang, Y.Z.; Zhao, Y.X.; Gao, C.G.; Liu, D.S. Preparation and catalytic performance of Co_3O_4 catalysts for low-temperature CO oxidation. *Catal. Lett.* **2007**, *116*, 136–142. [CrossRef]
225. Mekhemer, G.A.H.; Rabee, A.I.M.; Gaid, C.B.A.; Zaki, M.I. Cobalt oxide-catalyzed CO oxidation under steady-state conditions: Influence of the metal oxidation state. *Coll. Surf. A Physicochem. Eng. Asp.* **2023**, *663*, 130992. [CrossRef]
226. Han, M.; Wang, Y.; She, X.; Zhang, Z.; Li, X.; Guo, Z. Recent Progress in CO Oxidation over Non-precious-metal Catalysts. *Ind. Eng. Chem. Res.* **2025**, *64*, 36–52. [CrossRef]
227. Yang, J.; Guo, J.; Wang, Y.; Wang, T.; Gu, J.; Peng, L.; Xue, N.; Zhu, Y.; Guo, X.; Ding, W. Reduction-oxidation pretreatment enhanced catalytic performance of Co_3O_4/Al_2O_3 over CO oxidation. *Appl. Surf. Sci.* **2018**, *453*, 330–335. [CrossRef]
228. Zhang, L.; Dong, L.; Yu, W.; Liu, L.; Deng, Y.; Liu, B.; Wan, H.; Gao, F.; Sun, K.; Dong, L. Effect of cobalt precursors on the dispersion, reduction, and CO oxidation of CoO_x/γ-Al_2O_3 catalysts calcined in N_2. *J. Colloid Interface Sci.* **2011**, *355*, 464–471. [CrossRef]
229. Zhang, R.; Li, P.; Liu, N.; Yang, W.; Wang, X.; Cui, R.; Chen, B. CO catalytic combustion over Co/Al_2O_3: Influence of diverse textural properties of alumina supports on the related oxidation activities. *Catal. Today* **2013**, *216*, 169–177. [CrossRef]
230. Thormählen, P.; Skoglundh, M.; Fridell, E.; Andersson, B. Low-Temperature CO Oxidation over Platinum and Cobalt Oxide Catalysts. *J. Catal.* **1999**, *188*, 300–310. [CrossRef]
231. Jansson, J. Low-temperature CO oxidation over Co_3O_4/Al_2O_3. *J. Catal.* **2000**, *194*, 55–60. [CrossRef]

232. Nguyen, L.; Zhang, S.; Yoon, S.J.; Tao, F. Preferential Oxidation of CO in H_2 on Pure Co_3O_{4-x} and Pt/Co_3O_{4-x}. *ChemCatChem* **2015**, *7*, 2346–2353. [CrossRef]
233. Zhong, L.; Kropp, T.; Baaziz, W.; Ersen, O.; Teschner, D.; Schlogl, R.; Mavrikakis, M.; Zafeiratos, S. Correlation Between Reactivity and Oxidation State of Cobalt Oxide Catalysts for CO Preferential Oxidation. *ACS Catal.* **2019**, *9*, 8325−8336. [CrossRef]
234. Fadlalla, M.I.; Nyathi, T.M.; Claeys, M. Magnesium as a Methanation Suppressor for Iron and Cobalt-Based Oxide Catalysts during the Preferential Oxidation of Carbon Monoxide. *Catalysts* **2022**, *12*, 118. [CrossRef]
235. Lukashuk, L.; Föttinger, K.; Kolar, E.; Rameshan, C.; Teschner, D.; Hävecker, M.; Knop-Gericke, A.; Yigit, N.; Li, H.; McDermott, E.; et al. Operando XAS and NAP-XPS studies of preferential CO oxidation on Co_3O_4 and CeO_2-Co_3O_4 catalysts. *J. Catal.* **2016**, *344*, 1–15. [CrossRef]
236. Nyathi, T.M.; Fischer, N.; York, A.P.E.; Claeys, M. Effect of crystallite size on the performance and phase transformation of Co_3O_4/Al_2O_3 catalysts during CO-PrOx—An in situ study. *Faraday Discuss.* **2017**, *197*, 269–285. [CrossRef] [PubMed]
237. Grzybek, G.; Ciura, K.; Grybos, J.; Indyka, P.; Davo-Quinonero, A.; Lozano-Castello, D.; Bueno-Lopez, A.; Kotarba, A.; Sojka, Z. CO-PROX Reaction over Co_3O_4/Al_2O_3 Catalysts Impact of the Spinel Active Phase Faceting on the Catalytic Performance. *J. Phys. Chem. C* **2019**, *123*, 20221−20232. [CrossRef]
238. Anderson, R.B.; Stein, K.C.; Feenan, J.J.; Hofer, L.J.E. Catalytic oxidation of methane. *Ind. Eng. Chem.* **1961**, *53*, 809–812. [CrossRef]
239. Arnone, S.; Bagnasco, G.; Busca, G.; Lisi, L.; Russo, G.; Turco, M. Catalytic combustion of methane over transition metal oxides. *Stud. Surf. Sci. Catal.* **1998**, *119*, 65–70.
240. Paredes, J.R.; Díaz, E.; Díez, F.V.; Ordóñez, S. Combustion of methane in lean mixtures over bulk transition-metal oxides: Evaluation of the activity and self-deactivation. *Energy Fuels* **2009**, *23*, 86–93. [CrossRef]
241. Trigueiro, F.E.; Ferreira, C.M.; Volta, J.-C.; Gonzalez, W.A.; Pries de Oliveria, P.G. Effect of niobium addition to Co/γ-Al2O3 catalyst on methane combustion. *Catal. Today* **2006**, *118*, 425–432. [CrossRef]
242. Eguchi, K.; Arai, H. Recent advances in high temperature catalytic combustion. *Catal. Today* **1996**, *29*, 379–386. [CrossRef]
243. Vatcha, S.R. Low-emission gas turbines using catalytic combustion. *Energy. Convers. Manag.* **1997**, *38*, 1327–1334. [CrossRef]
244. Milt, V.G.; Ulla, M.A.; Lombardo, E.A. Cobalt-containing catalysts for the high-temperature combustion of methane. *Catal. Lett.* **2000**, *65*, 67–73. [CrossRef]
245. Chen, J.; Arandiyan, H.; Gao, X.; Li, J. Recent Advances in Catalysts for Methane Combustion. *Catal. Surv. Asia* **2015**, *19*, 140–171. [CrossRef]
246. Hayes, R.E.; Profic-Paczkowska, J.; Jedrzejczyk, R.; Mmbaga, J.P. Catalytic Combustion of Fugitive Methane: Challenges and Current State of the Technology. *Appl. Sci.* **2025**, *15*, 10269. [CrossRef]
247. Hutter, R.; De Libero, L.; Elbert, P.; Onder, C.H. Catalytic methane oxidation in the exhaust gas aftertreatment of a lean-burn natural gas engine. *Chem. Eng. J.* **2018**, *349*, 156–167. [CrossRef]
248. Choya, A.; de Rivas, B.; González-Velasco, J.R.; Gutiérrez-Ortiz, J.I.; López-Fonseca, R. Oxidation of residual methane from VNG vehicles over Co3O4-based catalysts: Comparison among bulk, Al2O3-supported and Ce-doped catalysts. *Appl. Catal. B Environ.* **2018**, *237*, 844–854. [CrossRef]
249. Shao, C.; Li, W.; Lin, Q.; Huang, Q.; Pi, D. Low Temperature Complete Combustion of Lean Methane over Cobalt–Nickel Mixed-Oxide Catalysts. *Energy Technol.* **2017**, *5*, 604–610. [CrossRef]
250. Li, J.; Liang, X.; Xu, S.; Hao, J. Catalytic performance of manganese cobalt oxides on methane combustion at low temperature. *Appl. Catal. B Environ.* **2009**, *90*, 307–312. [CrossRef]
251. Yoo, S.; Lee, E.W.; Kim, D.H. Methane combustion over mesoporous cobalt oxide catalysts: Effects of acid treatment. *Mol. Catal.* **2021**, *511*, 111728. [CrossRef]
252. Chen, X.; Yu, S.; Liu, W.; Zhang, S.; Liu, S.; Feng, Y.; Zhang, X. Recent advance on cobalt-based oxide catalyst for the catalytic removal of volatile organic compounds: A review. *Res. Chem. Mater.* **2022**, *1*, 27–46. [CrossRef]
253. Yi, J.; Liu, J.; Gao, B.; Bo, L.; Cao, L.; Sillanpää, M. The comprehensive review of catalysts for catalytic oxidation of volatile organic compounds. *J. Environ. Chem. Eng.* **2025**, *13*, 115691. [CrossRef]
254. Bratan, V.; Vasile, A.; Chesler, P.; Hornoiu, C. Insights into the Redox and Structural Properties of CoO_x and MnO_x: Fundamental Factors Affecting the Catalytic Performance in the Oxidation Process of VOCs. *Catalysts* **2022**, *12*, 1134. [CrossRef]
255. Liotta, L.F.; Wu, H.; Pantaleo, G. Co_3O_4 nanocrystals and Co_3O_4–MO_x binary oxides for CO, CH_4 and VOC oxidation at low temperatures: A review. *Catal. Sci. Technol.* **2013**, *3*, 3085–3102. [CrossRef]
256. Solsona, B.; Davies, T.E.; Garcia, T.; Vázquez, I.; Dejoz, A.; Taylor, S.H. Total oxidation of propane using nanocrystalline cobalt oxide and supported cobalt oxide catalysts. *Appl. Catal. B Environ.* **2008**, *84*, 176–184. [CrossRef]
257. Finocchio, E.; Willey, R.J.; Busca, G.; Lorenzelli, V. FTIR studies on the selective oxidation and combustion of light hydrocarbons at metal oxide surfaces. Part 3. Comparison of the oxidation of C3 organic compounds over Co_3O_4, $MgCr_2O_4$ and CuO. *J. Chem. Soc. Faraday Trans.* **1997**, *93*, 175–180. [CrossRef]

258. Finocchio, E.; Busca, G.; Lorenzelli, V.; Sanchez Escribano, V. FTIR studies on the selective oxidation and combustion of light hydrocarbons at metal oxide surfaces Part 2.-Propane and propene oxidation on Co_3O_4. *J. Chem. Soc. Faraday Trans.* **1996**, *92*, 1587–1593. [CrossRef]
259. Busca, G.; Daturi, M.; Finocchio, E.; Lorenzelli, V.; Ramis, G.; Willey, R.J. Transition metal mixed oxides as combustion catalysts: Preparation, characterization and activity mechanisms. *Catal. Today* **1997**, *33*, 239–249. [CrossRef]
260. Deng, C.; Li, Q.; Huang, W.; Xia, D.; Huang, P.; Lu, R.; Tan, L.; Dong, L. Acid washing-assisted synthesis of porous Co3O4 nanosheet catalyst featuring efficient benzene oxidation performance. *Appl. Catal. A Gen.* **2025**, *690*, 120044. [CrossRef]
261. Shen, Y.; Deng, J.; Impeng, S.; Li, S.; Yan, T.; Zhang, J.; Shi, L.; Zhang, D. Boosting Toluene Combustion by Engineering Co−O Strength in Cobalt Oxide Catalysts. *Environ. Sci. Technol.* **2020**, *54*, 10342−10350. [CrossRef]
262. Zhang, W.; Descorme, C.; Valverde, J.L.; Giroir-Fendler, A. Effect of Calcination Conditions on Co_3O_4 Catalysts in the Total Oxidation of Toluene and Propane. *Catalysts* **2023**, *13*, 992. [CrossRef]
263. Garbowski, E.; Guenin, M.; Marion, M.C.; Primet, M. Catalytic properties and surface states of cobalt containing oxidation catalysts. *Appl. Catal. B* **1990**, *64*, 209–224. [CrossRef]
264. Xiao, T.; Ji, S.; Wang, H.; Coleman, K.S.; Green, M.L.H. Methane combustion over supported cobalt catalysts. *J. Mol. Catal. A Chem.* **2001**, *175*, 111–123. [CrossRef]
265. Choya, A.; de Rivas, B.; Gutiérrez-Ortiz, J.I.; López-Fonseca, R. Comparative Study of Strategies for Enhancing the Performance of Co_3O_4/Al_2O_3 Catalysts for Lean Methane Combustion. *Catalysts* **2020**, *10*, 757. [CrossRef]
266. Wang, Q.; Peng, Y.; Fu, J.; Kyzas, G.Z.; Billah, S.M.R.; An, S. Synthesis, characterization, and catalytic evaluation of Co_3O_4/γ-Al_2O_3 as methane combustion catalysts: Significance of Co species and the redox cycle. *Appl. Catal. B Environ.* **2015**, *168–169*, 42–50. [CrossRef]
267. Cai, T.; Deng, W.; Xu, P.; Yuan, J.; Liu, Z.; Zhao, K.; Tong, Q.; He, D. Great activity enhancement of Co_3O_4/γ-Al_2O_3 catalyst for propane combustion by structural modulation. *Chem. Eng. J.* **2020**, *395*, 125071. [CrossRef]
268. Ataloglou, T.; Vakros, J.; Bourikas, K.; Fountzoula, C.; Kordulis, C.; Lycourghiotis, A. Influence of the preparation method on the structure–activity of cobalt oxide catalysts supported on alumina for complete benzene oxidation. *Appl. Catal. B Environ.* **2005**, *57*, 299–312. [CrossRef]
269. Ding, Y.; Fan, Y.; Wei, X.; Li, D.; Xiao, Y.; Jiang, L. Total oxidation of benzene over cobalt-aluminum mixed oxides prepared from layered double hydroxides: Influence of preparation methods. *React. Kinet. Mech. Catal.* **2016**, *118*, 593–604. [CrossRef]
270. Tu, W.; Dong, X.; Du, R.; Wang, Q.; Yang, F.; Ou, R.; Wang, X.; Li, L.; Yuan, A. Hierarchical laminated Al_2O_3 in-situ integrated with high-dispersed Co_3O_4 for improved toluene catalytic combustion. *Adv. Powder Technol.* **2022**, *33*, 103377. [CrossRef]
271. Li, R.; Huang, Y.; Zhu, D.; Ho, W.; Lee, S.; Cao, J. A Review of Co_3O_4-based Catalysts for Formaldehyde Oxidation at Low Temperature: Effect Parameters and Reaction Mechanism. *Aerosol Sci. Eng.* **2020**, *4*, 147–168. [CrossRef]
272. Kupková, K.; Topka, P.; Balabánová, J.; Koštejn, M.; Jirátová, K.; Giraudon, J.-M.; Lamonier, J.-F.; Maixner, J.; Kovanda, F. Cobalt-Copper Oxide Catalysts for VOC Abatement: Effect of Co:Cu Ratio on Performance in Ethanol Oxidation. *Catalysts* **2023**, *13*, 107. [CrossRef]
273. Dissanayake, S.; Wasalathanthri, N.; Amin, A.S.; He, J.; Poges, S.; Rathnayake, D.; Suib, S.L. Mesoporous Co_3O_4 catalysts for VOC elimination: Oxidation of 2-propanol. *Appl. Catal. A Gen.* **2020**, *590*, 117366. [CrossRef]
274. Li, C.; Zhao, Y.; Song, H.; Li, H. A review on recent advances in catalytic combustion of chlorinated volatile organic compounds. *J. Chem. Technol. Biotechnol.* **2020**, *95*, 2069–2082. [CrossRef]
275. de Rivas, B.; López-Fonseca, R.; Jiménez-González, C.; Gutiérrez-Ortiz, J.I. Synthesis, characterisation and catalytic performance of nanocrystalline Co_3O_4 for gas-phase chlorinated VOC abatement. *J. Catal.* **2011**, *281*, 88–97. [CrossRef]
276. Yuan, C.; Liu, S.Y.; Wang, Z.Q.; Wang, G.-Y. Catalytic oxidation of low concentrations of vinyl chloride over spinel-type Co_3O_4 catalysts. *React. Kinet. Mech. Cat.* **2018**, *125*, 757–771. [CrossRef]
277. Gonzalez-Prior, J.; Gutierrez-Ortiz, J.I.; Lopez-Fonseca, R.; Busca, G.; Finocchio, E.; de Rivas, B. Oxidation of chlorinated alkanes over Co_3O_4/SBA-15 catalysts. Structural characterization and reaction mechanism. *Catal. Sci. Technol.* **2016**, *6*, 5618–5630. [CrossRef]
278. Finocchio, E.; Gonzalez-Prior, J.; Gutierrez-Ortiz, J.I.; Lopez-Fonseca, R.; Busca, G.; de Rivas, B. Surface Characterization of Mesoporous CoOx/SBA-15 Catalyst upon 1,2-Dichloropropane Oxidation. *Materials* **2018**, *11*, 912. [CrossRef] [PubMed]
279. Kozhukhova, A.E.; du Preez, S.P.; Bessarabov, D.G. Catalytic Hydrogen Combustion for Domestic and Safety Applications: A Critical Review of Catalyst Materials and Technologies. *Energies* **2021**, *14*, 4897. [CrossRef]
280. Yuan, L.J.; Zhao, Z.C.; Wang, W.Q.; Wang, Y.F.; Liu, Y.J. Review of Catalysts, Substrates, and Fabrication Methods in Catalytic Hydrogen Combustion with Further Challenges and Applications. *Energy Fuels* **2024**, *38*, 4881−4903. [CrossRef]
281. Haruta, M.; Sano, H. Catalytic combustion of hydrogen I—Its role in hydrogen utilization system and screening of catalyst materials. *Int. J. Hydrogen Energy* **1981**, *6*, 601–608. [CrossRef]
282. Kim, J.; Yu, J.; Lee, S.; Tahmasebi, A.; Jeon, C.H.; Lucas, J. Advances in catalytic hydrogen combustion research: Catalysts, mechanism, kinetics, and reactor designs. *Int. J. Hydrogen Energy* **2021**, *46*, 40073–40104. [CrossRef]

283. Zacharaki, I.; Kontoyannis, C.G.; Boghosian, S.; Lycourghiotis, A.; Kordulis, C. Cobalt oxide supported on alumina catalysts prepared by various methods for use in catalytic afterburner of PEM fuel cell. *Catal. Today* **2009**, *143*, 38–44. [CrossRef]
284. Christensen, J.M.; Grunwaldt, J.D.; Jense, A.D. Importance of the oxygen bond strength for catalytic activity in soot Oxidation. *Appl. Catal. B Environ.* **2016**, *188*, 235–244. [CrossRef]
285. Uner, D.; Demirkol, M.K.; Dernaika, B. A novel catalyst for diesel soot oxidation. *Appl. Catal. B Environ.* **2005**, *61*, 334–345. [CrossRef]
286. Zhao, T.; Song, Z.; Wu, C.; Li, Y.; Li, H.; Wei, Y.; Yao, S.; Xiao, M.; Zhao, M.; Cui, B. Advancements in cobalt-based oxide catalysts for soot oxidation: Enhancing catalytic performance through modification andmorphology control. *Smart Mol.* **2024**, *2*, e20240024. [CrossRef]
287. Álvarez-Docio, C.M.; Portela, R.; Reinosa, J.J.; Rubio-Marcos, F.; Granados-Miralles, C.; Pascual, L.; Fernández, J.F. Pt-free $CoAl_2O_4$ catalyst for soot combustion with NO_x/O_2. *Appl. Catal. A Gen.* **2020**, *591*, 117404. [CrossRef]
288. Dubkov, A.; Chigapov, A.; Carberry, B. Catalyst Composition for Diesel Particulate Filter. U.S. Patent US7797931B2, 21 September 2010.
289. Chigapov, A.; Dubkov, A.; Carberry, B. Soot Oxidation Catalyst and Method of Making. U.S. Patent US8052937B2, 20 March 2011.
290. Pope, D.; Walker, D.S.; Moss, R.L. Preparation of cobalt oxide catalysts and their activity for co oxidation at low concentration. *J. Catal.* **1977**, *47*, 33–47. [CrossRef]
291. Dakave, S.; Bhinge, G.; Kanamadi, C. Dual-capable spinel cobalt oxide nanoparticles for electrocatalytic oxygen evolution and water contaminant removal. *Environ. Sci. Pollut. Res.* **2025**, *32*, 22051–22063. [CrossRef]
292. McCarty, J.G.; Wise, H. Perovskite catalysts for methane combustion. *Catal. Today* **1990**, *8*, 231–248. [CrossRef]
293. Potoczna-Petru, D.; Kępiński, L. Reduction study of Co_3O_4 model catalyst by electron microscopy. *Catal. Lett.* **2001**, *73*, 41–46. [CrossRef]
294. Thiemann, M.; Scheibler, E.; Wiegand, K.W. *ULLMANN'S En-Cyclopedia of Industrial Chemistry—Nitric Acid. Nitrous Acid, and Nitrogen Oxides*; Wiley-VCH Verlag GmbH & Co. KGaA: Weinheim, Germany, 2012; Volume 24, pp. 177–225.
295. Sadykov, V.A.; Isupova, L.A.; Zolotarskii, I.A.; Bobrova, L.N.; Noskov, A.S.; Parmon, V.N.; Brushtein, E.A.; Telyatnikova, T.V.; Chernyshev, V.I.; Lunin, V.V. Oxide catalysts for ammonia oxidation in nitric acid production: Properties and perspectives. *Appl. Catal. A Gen.* **2000**, *204*, 59–87. [CrossRef]
296. Schmidt-Szałowski, K.; Krawczyk, K.; Petryk, J. The properties of cobalt oxide catalyst for ammonia oxidation. *Appl. Catal. A Gen.* **1998**, *175*, 147–157. [CrossRef]
297. Petryk, J.; Kołakowska, E. Cobalt oxide catalysts for ammonia oxidation activated with cerium and lanthanum. *Appl. Catal. B Environ.* **2000**, *24*, 121–128. [CrossRef]
298. Fung, W.-K.; Ledwaba, L.; Modiba, N.; Claeys, M.; van Steen, E. Choosing a suitable support for Co_3O_4 as an NH_3 oxidation catalyst. *Catal. Sci. Technol.* **2013**, *3*, 1905–1909. [CrossRef]
299. Campbell, L.E. Catalyst for the Production of Nitric Acid by Oxidation of Ammonia. U.S. Patent US5242882A, 7 September 1993.
300. Schwefer, M.; Siefert, R.; Ruthardt, K.; Cremona, A.; Vogna, E. Method for Oxidizing Ammonia and System Suitable Therefor. U.S. Patent CA2905560A1, 28 December 2021.
301. Wu, S.; Li, J.; Qiu, J.; Wang, C.; Wang, F.; Li, Z.; Ning, P.; Li, K. Regulating the valence and size of the active center of Co/Al_2O_3 catalyst improved the performance and selectivity of NH_3-SCO. *J. Environ. Sci.* **2025**, *150*, 188–201. [CrossRef] [PubMed]
302. Hong, Z.; Wang, Z.; Li, X. Catalytic oxidation of nitric oxide (NO) over different catalysts: An overview. *Catal. Sci. Technol.* **2017**, *7*, 3440. [CrossRef]
303. Gopakumar, J.; Myrstad, R.; Borresen Anda, R.; Øien, H.; Enger, B.C.; Waller, D.; Ronning, M. Ostwald Process Intensification by Catalytic Oxidation of Nitric Oxide. *ACS Omega* **2025**, *10*, 2197−2211. [CrossRef]
304. Irfan, M.F.; Goo, J.H.; Kim, S.D. Co_3O_4 based catalysts for NO oxidation and NO_x reduction in fast SCR process. *Appl. Catal. B Environ.* **2008**, *78*, 267–274. [CrossRef]
305. Ma, L.; Zhang, W.; Wang, Y.G.; Chen, X.; Yu, W.; Sun, K.; Sun, H.; Li, J.; Schwank, J.W. Catalytic performance and reaction mechanism of NO oxidation over Co_3O_4 Catalysts. *Appl. Catal. B Environ.* **2020**, *267*, 118371. [CrossRef]
306. Qi, Y.; Liu, W.; Liu, S.; Wang, W.; Peng, Y.; Wang, Z. A review on ammonia-hydrogen fueled internal combustion engines. *eTransportation* **2023**, *18*, 100288. [CrossRef]
307. Cano-Blanco, D.C.; Ma, E.; D'Alessandri, J.; Peitz, D.; Ferri, D.; Kröcher, O. Critical Aspects in the Catalytic Emission Control of ExhaustGases Containing NH_3, NO_x and N_2O. *J. Ammon. Energy* **2024**, *02*, 064–072.
308. Zhuang, Z.; Guan, B.; Chen, J.; Zheng, C.; Zhou, J.; Su, T.; Chen, Y.; Zhu, C.; Hu, X.; Zhao, S.; et al. Review of nitrous oxide direct catalytic decomposition and selective catalytic reduction catalysts. *Chem. Eng. J.* **2024**, *486*, 150374. [CrossRef]
309. Kapteijn, F.; Rodrigues-Mirasol, J.; Moulijn, J.A. Heterogeneous catalytic decomposition of nitrous oxide. *Appl. Catal. B* **1996**, *9*, 25–64. [CrossRef]
310. Russo, N.; Fino, D.; Saracco, G.; Specchia, V. N_2O catalytic decomposition over various spinel-type oxides. *Catal. Today* **2007**, *119*, 228–232. [CrossRef]

311. Ohnishi, C.; Asano, K.; Iwamoto, S.; Chikama, K.; Inoue, M. Alkali-doped Co_3O_4 catalysts for direct decomposition of N_2O in the presence of oxygen. *Catal. Today* **2007**, *120*, 145–150. [CrossRef]
312. Stelmachowski, P.; Maniak, G.; Kotarba, A.; Sojka, Z. Strong electronic promotion of Co_3O_4 towards N_2O decomposition by surface alkali dopants. *Catal. Commun.* **2009**, *10*, 1062–1065. [CrossRef]
313. Wójcik, S.; Gabriela Grzybek, G.; Stelmachowski, P.; Sojka, Z.; Kotarba, A. Bulk, Surface and Interface Promotion of Co_3O_4 for the Low-Temperature N_2O Decomposition Catalysis. *Catalysts* **2020**, *10*, 41. [CrossRef]
314. Armor, J.N.; Braymer, T.A.; Farris, T.S.; Li, Y.; Petrocelli, F.P.; Weist, E.L.; Kannan, S.; Swamy, C.S. Calcined hydrotalcites for the catalytic decomposition of N_2O in simulated process streams. *Appl. Catal. B Environ.* **1996**, *7*, 397–406. [CrossRef]
315. Kannan, S.; Swamy, C.S. Catalytic decomposition of nitrous oxide over calcined cobalt aluminum hydrotalcites. *Catal. Today* **1999**, *53*, 725–737. [CrossRef]
316. Chang, K.S.; Song, H.; Park, Y.; Woo, J. Analysis of N_2O decomposition over fixed bed mixed metal oxide catalysts made from hydrotalcite-type precursor. *Appl. Catal. A* **2004**, *273*, 223−231. [CrossRef]
317. Satsuma, A.; Maeshima, H.; Watanabe, K.; Suzuki, K.; Hattori, T. Effects of methane and oxygen on decomposition of nitrous oxide over metal oxide catalysts. *Catal. Today* **2000**, *63*, 347–353. [CrossRef]
318. Grzybek, G.; Gryboś, J.; Indyka, P.; Janas, J.; Ciura, K.; Leszczyński, B.; Zasada, F.; Kotarba, A.; Sojka, Z. Evaluation of the inhibiting effect of H_2O, O_2, and NO on the performance of laboratory and pilot K-$Zn_xCo_{3-x}O_4$ catalysts supported on α-Al_2O_3 for low-temperature N_2O decomposition. *Appl. Catal. B Environ.* **2021**, *297*, 120435. [CrossRef]
319. Nirisen, Ø.; Schöffel, K.; Waller, D.; Øvrebø, D. Catalyst for Decomposing Nitrous Oxide and Method for Performing Processes Comprising Formation of Nitrous Oxide. Patent WO/2002/002230, 4 July 2002.
320. Inger, M.; Moszowski, B.; Ruszak, M.; Rajewski, J.; Wilk, M. Two-Stage Catalytic Abatement of N_2O Emission in Nitric Acid Plants. *Catalysts* **2020**, *10*, 987. [CrossRef]
321. Tang, H.; He, Y.; Liu, P.; Shao, J.; Lin, F.; Wang, Z. Decomposition of N_2O on ZIF-67-Derived Co/CoO_x@Carbon Catalysts and SO_2 Interference. *Energy Fuels* **2021**, *35*, 18664−18679. [CrossRef]
322. Nova, I.; Tronconi, E. (Eds.) *Urea-SCR Technology for deNO$_x$ Aftertreatment of Diesel Exhausts*; Springer Publishing: New York, NY, USA, 2014.
323. Ye, B.; Jeong, B.; Lee, M.J.; Kim, T.H.; Park, S.S.; Jung, J.; Lee, S.; Kim, H.D. Recent trends in vanadium-based SCR catalysts for NO_x reduction in industrial applications: Stationary sources. *Nano Converg.* **2022**, *9*, 51–71. [CrossRef]
324. Iwasaki, M.; Shinjoh, H. A comparative study of "standard", "fast" and "NO_2" SCR reactions over Fe/zeolite catalyst. *Appl. Catal. A Gen.* **2010**, *390*, 71–77. [CrossRef]
325. Sunil Kumar, M.; Alphin, M.S.; Manigandan, S.; Vignesh, S.; Vigneshwaran, S.; Subash, T. A review of comparison between the traditional catalyst and zeolite catalyst for ammonia-selective catalytic reduction of NO_x. *Fuel* **2023**, *344*, 128125. [CrossRef]
326. Busca, G.; Lietti, L.; Ramis, G.; Berti, F. Chemical and mechanistic aspects of the selective catalytic reduction of NO_x by ammonia over oxide catalysts: A review. *Appl. Catal. B Environ.* **1998**, *18*, 1–36. [CrossRef]
327. Han, L.; Cai, S.; Gao, M.; Hasegawa, J.; Wang, P.; Zhang, J.; Shi, L.; Zhang, D. Selective Catalytic Reduction of NO_x with NH_3 by Using Novel Catalysts: State of the Art and Future Prospects. *Chem. Rev.* **2019**, *119*, 10916−10976. [CrossRef]
328. Pan, W.; Wei, Y.; Yang, W.; Fang, D. Recent advance of spinel-based catalysts for selective catalytic reduction of NO_x. *J. Energy Inst.* **2025**, *123*, 102301. [CrossRef]
329. Ke, R.; Li, J.; Liang, X.; Hao, J. Novel promoting effect of SO_2 on the selective catalytic reduction of NO_x by ammonia over Co_3O_4 catalyst. *Catal. Commun.* **2007**, *8*, 2096–2099. [CrossRef]
330. Meng, B.; Zhao, Z.; Wang, X.; Liang, J.; Qiu, J. Selective catalytic reduction of nitrogen oxides by ammonia over Co_3O_4 nanocrystals with different shapes. *Appl. Catal. B Environ.* **2013**, *129*, 491–500. [CrossRef]
331. Chen, L.; Horiuchi, T.; Mori, T. On the promotional effect of Sn in Co–Sn/Al_2O_3 catalyst for NO selective reduction. *Catal. Lett.* **2001**, *72*, 71–75. [CrossRef]
332. Zhang, F.; Zhang, S.; Guan, N.; Schreier, E.; Richter, M.; Eckelt, R.; Fricke, R. NO SCR with propane and propene on Co-based alumina catalysts prepared by co-precipitation. *Appl. Catal. B Environ.* **2007**, *73*, 209–219. [CrossRef]
333. Yan, J.Y.; Kung, M.C.; Sachtler, W.M.H.; Kung, H.H. Co/Al_2O_3 Lean NO_x Reduction Catalyst. *J. Catal.* **1997**, *172*, 178–186. [CrossRef]
334. Liotta, L.F.; Pantaleo, G.; Macaluso, A.; Di Carlo, G.; Deganello, G. CoO_x catalysts supported on alumina and alumina-baria: Influence of the support on the cobalt species and their activity in NO reduction by C_3H_6 in lean conditions. *Appl. Catal. A Gen.* **2003**, *245*, 167–177. [CrossRef]
335. Wang, Z.; Jiang, Z.; Shangguan, W. Simultaneous catalytic removal of NO_x and soot particulate over Co–Al mixed oxide catalysts derived from hydrotalcites. *Catal. Commun.* **2007**, *8*, 1659–1664. [CrossRef]
336. Carberry, B.; Chigapov, A.; Dubkov, A. Diesel Particulate Filter Catalyst with Low NO_2 Emissions. European Patent EP1837076B1, 9 August 2017.

337. Liu, S.; Wang, Y.; Liu, Y.; Chen, P.; Kong, T.; Duan, X.; Chen, C.; Sun, H.; Wang, S. Tailored ozone activation on geometrical site-dependent cobalt with selective coordination. *Nat. Commun.* **2025**, *16*, 5921. [CrossRef]
338. Konova, P.; Stoyanova, M.; Naydenov, A.; Christoskova, S.; Mehandjiev, D. Catalytic oxidation of VOCs and CO by ozone over alumina supported cobalt oxide. *Appl. Catal. A Gen.* **2006**, *298*, 109–114. [CrossRef]
339. Bilińska, M.; Bilińska, L.; Fronczak, M.; Kędzierska-Sar, A.; Kierzkowska-Pawlak, A.; Gmurek, M. Application of metal oxides thin film catalysts in structured catalytic ozonation reactor for dye and byproduct detoxification. *Sci. Rep.* **2025**, *15*, 18580. [CrossRef]
340. Jha, A.; Rode, C.V. Highly selective liquid-phase aerobic oxidation of vanillyl alcohol to vanillin on cobalt oxide (Co_3O_4) nanoparticles. *New J. Chem.* **2013**, *37*, 2669–2674. [CrossRef]
341. Albadi, J.; Alihosseinzadeh, A.; Jalali, M.; Shahrezaei, M.; Mansournezhad, A. Highly dispersed cobalt nanoparticles supported on a mesoporous Al_2O_3: An efficient and recyclable catalyst for aerobic oxidation of alcohols in aqueous media. *Mol. Catal.* **2017**, *440*, 133–139.
342. Pan, D.; Xu, Q.; Dong, Z.; Chen, S.; Yu, F.; Yan, X.; Fan, B.; Li, R. Facile synthesis of highly ordered mesoporous cobalt–alumina catalysts and their application in liquid phase selective oxidation of styrene. *RSC Adv.* **2015**, *5*, 98377. [CrossRef]
343. Bouzayani, B.; Elaoud, S.C.; Sanromán, M.Á. Current Progress in Advanced Oxidation Processes for the Removal of Contaminants of Emerging Concern Using Peracetic Acid as an Effective Oxidant. *Catalysts* **2025**, *15*, 469. [CrossRef]
344. Wu, W.; Tian, D.; Liu, T.; Chen, J.; Huang, T.; Zhou, X.; Zhang, Y. Degradation of Organic Compounds by Peracetic Acid Activated with Co_3O_4: A Novel Advanced Oxidation Process and Organic Radical Contribution. *Chem. Eng. J.* **2020**, *394*, 124938. [CrossRef]
345. Wu, J.; Zheng, X.; Wang, Y.; Liu, H.; Wu, Y.; Jin, X.; Chen, P.; Lv, W.; Liu, G. Activation of Peracetic Acid via Co_3O_4 with Double-Layered Hollow Structures for the Highly Efficient Removal of Sulfonamides: Kinetics Insights and Assessment of Practical Applications. *J. Hazard. Mater.* **2022**, *431*, 128579. [CrossRef]
346. Yun, W.C.; Lin, K.Y.A.; Tong, W.C.; Lin, Y.F.; Du, Y. Enhanced degradation of paracetamol in water using sulfate radical-based advanced oxidation processes catalyzed by 3-dimensional Co_3O_4 nanoflower. *Chem. Eng. J.* **2019**, *373*, 1329–1337. [CrossRef]
347. Ping Li, P.; Lin, Y.; Zhao, S.; Fu, Y.; Li, W.; Chen, R.; Tian, S. Defect-engineered Co_3O_4 with porous multishelled hollow architecture enables boosted advanced oxidation processes. *Appl. Catal. B Environ.* **2021**, *298*, 120596.
348. Yi, Q.; Li, X.; Li, Y.; Dai, R.; Wang, Z. Unraveling the Co(IV)-Mediated Oxidation Mechanism in a Co_3O_4/PMS-Based Hierarchical Reactor: Toward Efficient Catalytic Degradation of Aromatic Pollutants. *ACS EST Eng.* **2022**, *2*, 1836−1846. [CrossRef]
349. Silva, R.R.M.; Valenzuela, L.; Rosal, R.; Ruotolo, L.A.M.; Nogueira, F.G.E.; Bahamonde, A. Peroxymonosulfate activation by Co_3O_4 coatings for imidacloprid degradation in a continuous flow-cell reactor under simulated solar irradiation. *J. Environ. Chem. Eng.* **2023**, *11*, 109265. [CrossRef]
350. Tang, B.; Xiong, Z.; Tao, T.; Sun, Y.; Ding, D.; Li, X.; Wang, C.; Yan, J.; Chi, R.; Sun, L. Activation of peroxymonosulfate over recyclable Co_3O_4/rice straw lignin-based carbon fiber flexible membrane for the degradation of organic pollutants. *Int. J. Biol. Macromol.* **2024**, *283*, 137844. [CrossRef] [PubMed]
351. Zhang, S.; Dai, S.; Huang, Q.; Huang, J.; Hei, S.; Wang, P.; Liu, B. Insight into the Co_3O_4 nanoparticles confined in SiO_2 aerogel via peroxymonosulfate activation for enrofloxacin degradation: Performance and mechanism. *J. Environ. Chem. Eng.* **2025**, *13*, 119357. [CrossRef]
352. Sun, B.; Li, X.; Zheng, J. Hydrogen generation from $NaBH_4$ for portable proton exchange membrane fuel cell. *Mater. Rep. Energy* **2024**, *4*, 100248. [CrossRef]
353. Ji, J.; Deng, K.; Li, J.; Zhang, Z.; Duan, X.; Huang, H. In situ transformation of 3D Co_3O_4 nanoparticles to 2D nanosheets with rich surface oxygen vacancies to boost hydrogen generation from $NaBH_4$. *Chem. Eng. J.* **2021**, *424*, 130350. [CrossRef]
354. Ding, C.; Gao, Z.; Wang, J.; Ma, L.; Shangguan, J.; Yuan, Q.; Zhao, M.; Zhang, K. The coralline cobalt oxides compound of multiple valence states deriving from flower-like layered double hydroxide for efficient hydrogen generation from hydrolysis of $NaBH_4$. *Int. J. Hydrogen Energy* **2021**, *46*, 2390–2404. [CrossRef]
355. Abu-Zied, B.M.; Alamry, K.A. Green synthesis of 3D hierarchical nanostructured Co_3O_4/carbon catalysts for the application in sodium borohydride hydrolysis. *J. Alloys Compd.* **2019**, *798*, 820–831. [CrossRef]
356. Wu, X.; Zhang, X.; Han, G.; Liu, Y.; Liu, B.; Gao, J.; Fan, Y.; Li, B. Reaction of Co_3O_4 nanocrystals on graphene sheets to fabricate excellent catalysts for hydrogen generation. *ACS Sustain. Chem. Eng.* **2018**, *6*, 8427–8436. [CrossRef]
357. Mahpudz, A.; Lim, S.L.; Inokawa, H.; Kusakabe, K.; Tomoshige, R. Cobalt nanoparticle supported on layered double hydroxide: Effect of nanoparticle size on catalytic hydrogen production by $NaBH_4$ hydrolysis. *Environ. Pollut.* **2021**, *290*, 117990. [CrossRef] [PubMed]
358. Long, B.; Chen, J.; Sharshir, S.W.; Ibrahim, L.; Zhou, W.; Wang, C.; Wang, L.; Yuan, Z. The mechanism and challenges of cobalt-boron-based catalysts in the hydrolysis of sodium borohydride. *J. Mater. Chem. A* **2024**, *12*, 5606–5625. [CrossRef]
359. Butenko, V.R.; Komova, O.V.; Simagina, V.I.; Lipatnikova, I.L.; Ozerova, A.M.; Danilova, N.A.; Rogov, V.A.; Odegova, G.V.; Bulavchenko, O.A.; Chesalov, Y.A.; et al. Co and Co3O4 in the Hydrolysis of Boron-Containing Hydrides: H2O Activation on the Metal and Oxide Active Centers. *Materials* **2024**, *17*, 1794. [CrossRef]

360. Chauhan, A.; Kumar, R.; Devi, S.; Raizada, P.; Singh, P.; Kumar Ponnusamy, V.; Sudhaik, A.; Kumar Mishra, A.; Selvasembian, R. Recent advances on Co_3O_4-based nanostructure photocatalysis: Structure, synthesis, modification strategies, and applications. *Surf. Interf.* **2024**, *54*, 105152. [CrossRef]
361. Muscetta, M.; Ganguly, P.; Clarizia, L. Solar-powered photocatalysis in water purification: Applications and commercialization challenges. *J. Environ. Chem. Eng.* **2024**, *12*, 113073. [CrossRef]
362. Paiu, M.; Lutic, D.; Favier, L.; Gavrilescu, M. Heterogeneous Photocatalysis for Advanced Water Treatment: Materials, Mechanisms, Reactor Configurations, and Emerging Applications. *Appl. Sci.* **2025**, *15*, 5681. [CrossRef]
363. Yaghoubi, S.; Mousavi, S.M.; Babapoor, A.; Binazadeh, M.; Lai, C.W.; Althomali, R.H.; Rahman, M.M.; Chiang, W.H. Photocatalysts for solar energy conversion: Recent advances and environmental applications. *Renew. Sustain. Energy Rev.* **2024**, *200*, 114538. [CrossRef]
364. Dang, V.D.; Nhung, N.T.H.; Rabani, I.; Tran, N.T.; Thuy, B.T.P.; Truon, H.B. Advances in Co_3O_4 nanomaterial-based photocatalysts for water purification: Mechanisms, green synthesis, activation of oxidants, wastederived sources, and computational insights. *RSC Adv.* **2025**, *15*, 19088. [CrossRef]
365. Farhadi, S.; Javanmard, M.; Nadri, G. Characterization of Cobalt Oxide Nanoparticles Prepared by the Thermal Decomposition of $[Co(NH_3)_5(H_2O)](NO_3)_3$ Complex and Study of Their Photocatalytic Activity. *Acta Chim. Slov.* **2016**, *63*, 335–343. [CrossRef]
366. Chelliah, P.; Wabaidur, S.M.; Sharma, H.P.; Jweeg, M.J.; Majdi, H.S.; AL. Kubaisy, M.M.R.; Iqbal, A.; Lai, W.-C. Green Synthesis and Characterizations of Cobalt Oxide Nanoparticles and Their Coherent Photocatalytic and Antibacterial Investigations. *Water* **2023**, *15*, 910. [CrossRef]
367. Safdar, A.; Mohamed, H.E.A.; Hkiri, K.; Muhaymin, A.; Maaza, M. Green Synthesis of Cobalt Oxide Nanoparticles Using Hyphaene thebaica Fruit Extract and Their Photocatalytic Application. *Appl. Sci.* **2023**, *13*, 9082. [CrossRef]
368. Chowdhury, B.; Pradhan, S.S.; Das, H.S.; Biswas, B. Visible Light Induced Photocatalytic Dye Degradation by Cobalt Oxide Nanoparticles. *Fine Chem. Eng.* **2020**, *1*, 104–117. [CrossRef]
369. Pradhan, D.; Falletta, E.; Dash, S.K. Enhanced and rapid photocatalytic degradation of toxic dyes by cobalt oxide and modified cobalt oxide under solar light irradiation. *Opt. Mater.* **2023**, *135*, 113368. [CrossRef]
370. Roshni, C.P.; Jithes, K.; Anjana, P.M.; Govind Raj, K.; Rakhi, R.B. Synthesis and characterization of alpha and beta cobalt hydroxide nanostructures for photocatalytic dye degradation and supercapacitor applications. *Next Mater.* **2024**, *4*, 100199. [CrossRef]
371. Moridon, S.N.F.; Salehmin, M.I.; Mohamed, M.A.; Arifin, K.; Minggu, L.J.; Kassim, M.B. Cobalt oxide as photocatalyst for water splitting: Temperature-dependent phase structures. *Int. J. Hydrogen Energy* **2019**, *44*, 25495–25504. [CrossRef]
372. Hasan, I.; Alharthi, F.A. Synthesis of Cobalt Oxide (Co_3O_4) Nanoparticles for Efficient Photocatalytic Water Splitting and Hydrogen Production. *Chemistryselect* **2023**, *8*, e202302685. [CrossRef]
373. La, Y.; Wang, L.; Wang, S.; Yang, M.; Wang, T.; Yin, D.; Dong, X.; Yang, Y. Superhydrophilic/superaerophobic Co_3O_4 nanoneedle array electrocatalysts for efficient overall water splitting. *Int. J. Hydrogen Energy* **2025**, *178*, 151704. [CrossRef]
374. Huang, J.; Shang, Q.; Huang, Y.; Tang, F.; Zhang, Q.; Liu, Q.; Jiang, S.; Hu, F.; Liu, W.; Luo, Y.; et al. Oxyhydroxide Nanosheets with Highly Efficient Electron–Hole Pair Separation for Hydrogen Evolution. *Angew. Chem. Int. Ed.* **2016**, *55*, 2137–2141. [CrossRef]
375. Li, R.; Luan, J.; Zhang, Y.; Jiang, L.; Yan, H.; Chi, Q.; Yan, Z. A review of efficient photocatalytic water splitting for hydrogen production. *Renew. Sustain. Energy Rev.* **2024**, *206*, 114863. [CrossRef]
376. Sohail, M.; Rauf, S.; Irfan, M.; Hayat, A.; Alghamdi, M.M.; El-Zahhar, A.A.; Ghernaout, D.; Al-Hadeethihij, J.; Lv, W. Recent developments, advances and strategies in heterogeneous photocatalysts for water splitting. *Nanoscale Adv.* **2024**, *6*, 1286. [CrossRef] [PubMed]
377. Han, X.; Qian, A.; Ye, L.; Fan, M.; Yu, J.; Zhang, C.; Zheng, Y.; Yang, Q. Photocatalytic materials and reactors for hydrogen production: A review. *Mol. Chem. Eng.* **2025**, *1*, 100001. [CrossRef]
378. Chen, K.; Wang, Q.; Xie, H.; Yu, J.; Zhu, L.; Wu, B.; Xu, X. Oxygen Vacancy Drives CoO Atomic Layers Directional Photoreduction of CO_2 to CH_4. *Solar RRL* **2023**, *7*, 2300210. [CrossRef]
379. Wang, L.; Wan, J.; Zhao, Y.; Yang, N.; Wang, D. Hollow Multi-Shelled Structures of Co_3O_4 Dodecahedron with Unique Crystal Orientation for Enhanced Photocatalytic CO_2 Reduction. *J. Am. Chem. Soc.* **2019**, *141*, 2238–2241. [CrossRef]
380. Ni, M.; Zhu, Y.; Guo, C.; Chen, D.L.; Ning, J.; Zhong, Y.; Hu, Y. Efficient Visible-Light-Driven CO_2 Methanation with Self-Regenerated Oxygen Vacancies in $Co_3O_4/NiCo_2O_4$ Hetero-Nanocages: Vacancy-Mediated Selective Photocatalysis. *ACS Catal.* **2023**, *13*, 2502−2512. [CrossRef]
381. Qian, G.; Lyu, W.; Zhao, X.; Zhou, J.; Fang, R.; Wang, F.; Li, Y. Efficient Photoreduction of Diluted CO_2 to Tunable Syngas by Ni-Co Dual Sites through d-band Center Manipulation. *Angew. Chem. Int. Ed. Engl.* **2022**, *61*, e202210576. [CrossRef]
382. Choi, J.Y.; Lim, C.K.; Park, B.; Kim, M.; Jamal, A.; Song, H. Surface activation of cobalt oxide nanoparticles for photocatalytic carbon dioxide reduction to methane. *J. Mater. Chem. A* **2019**, *7*, 15068–15072. [CrossRef]
383. Gayer, K.H.; Garrett, A.B. The Solubility of Cobalt Hydroxide, $Co(OH)_2$, in Solutions of Hydrochloric Acid and Sodium Hydroxide at 25 °C. *J. Am. Chem. Soc.* **1950**, *72*, 3921–3923. [CrossRef]

384. Ziemniak, S.E.; Goyette, M.A.; Combs, K.E.S. Cobalt(II) Oxide Solubility and Phase Stability in Alkaline Media at Elevated Temperatures. *J. Sol. Chem.* **1999**, *28*, 809–836. [CrossRef]
385. Gupta, S.; Fernandes, R.; Patel, R.; Spreitzer, M.; Patel, N. A review of cobalt-based catalysts for sustainable energy and environmental applications. *Appl. Catal. A Gen.* **2023**, *661*, 119254. [CrossRef]
386. Liu, L.; Jiang, Z.; Fang, L.; Xu, H.; Zhang, H.; Gu, X.; Wang, Y. Probing the Crystal Plane Effect of Co_3O_4 for Enhanced Electrocatalytic Performance toward Efficient Overall Water Splitting. *ACS Appl. Mater. Interfaces* **2017**, *9*, 27736–27744. [CrossRef]
387. Nguyen, K.N.; Nguyen, L.B.H.; Bui, T.K.; Nguyen, K.Q.; Pham, V.V. Review of Water Splitting Electrolysis over Cobalt Oxide Nanomaterials. *ACS Appl. Nano Mater.* **2025**, *8*, 3254−3271. [CrossRef]
388. Chen, M.; Guan, J. Achievements and challenges in cobalt-based catalysts for water electrolysis. *Chem. Eng. J.* **2024**, *500*, 157080. [CrossRef]
389. Wang, H.; Zhai, T.; Wu, Y.; Zhou, T.; Zhou, B.; Shang, C.; Guo, Z. High-Valence Oxides for High Performance Oxygen Evolution Electrocatalysis. *Adv. Sci.* **2023**, *10*, 2301706. [CrossRef] [PubMed]
390. Huang, J.; Borca, C.N.; Huthwelker, T.; Nur Sena Yüzbasi, N.S.; Baster, D.; El Kazzi, M.; Schneider, C.W.; Schmidt, T.J.; Fabbri, E. Surface oxidation/spin state determines oxygen evolution reaction activity of cobalt based catalysts in acidic environment. *Nat. Commun.* **2024**, *15*, 3067. [CrossRef] [PubMed]
391. Mei, J.; Liao, T.; Ayoko, G.A.; Bell, J.; Sun, Z. Cobalt oxide-based nanoarchitectures for electrochemical energy applications. *Prog. Mater. Sci.* **2019**, *103*, 596–677. [CrossRef]
392. Pattayil, A.J.; Pillai, V.K.; Rani, R.M.; Debgupta, J. Electrochemical Process for Water Splitting Using Porous Co_3O_4 Nanorods. U.S. Patent US9879354B2, 30 January 2018.
393. Ehsen, M.A.; Hakeem, A.S.; Rehman, A. Thin Film Electrode Containing Nanostructured Cobalt Oxide for Water Splitting. U.S. Patent US11408084B2, 9 August 2022.
394. Mondschein, J.S.; Callejas, J.F.; Read, C.G.; Chen, J.Y.C.; Holder, C.F.; Badding, C.K.; Schaak, R.E. Crystalline cobalt oxide films for sustained electrocatalytic oxygen evolution under strongly acidic conditions. *Chem. Mater.* **2017**, *29*, 950–957. [CrossRef]
395. Bergmann, A.; Martinez-Moreno, E.; Teschner, D.; Chernev, P.; Gliech, M.; de Araújo, J.F.; Reier, T.; Dau, H.; Strasser, P. Reversible amorphization and the catalytically active state of crystalline Co3O4 during oxygen evolution. *Nat. Commun.* **2015**, *6*, 8625. [CrossRef]
396. Harada, M.; Saito, A.; Nakahira, H.; Mori, Y.; Kawaguchi, S. In Situ Observations of Catalytically Active Sites of Cobalt−Manganese Spinel Oxides as Efficient Bifunctional Electrocatalysts for Oxygen Evolution and Reduction Reactions. *ACS Appl. Energy Mater.* **2025**, *8*, 13390−13406. [CrossRef]
397. Zhang, S.; Yu, T.; Wen, H.; Ni, Z.; He, Y.; Guo, R.; You, J.; Liu, X. The latest development of CoOOH two-dimensional materials used as OER catalysts. *Chem. Commun.* **2020**, *56*, 15387. [CrossRef] [PubMed]
398. Li, F.; Ai, H.; Liu, D.; Lob, K.H.; Pan, H. An enhanced oxygen evolution reaction on 2D CoOOH via strain engineering: An insightful view from spin state transition. *J. Mater. Chem. A* **2021**, *9*, 17749–17759. [CrossRef]
399. Zhou, J.; Wang, Y.; Su, X.; Gu, S.; Liu, R.; Huang, Y.; Yan, S.; Li, J.; Zhang, S. Electrochemically accessing ultrathin Co (oxy)hydroxide nanosheets and operando identifying their active phase for the oxygen evolution reaction. *Energy Environ. Sci.* **2019**, *12*, 739. [CrossRef]
400. Kormányos, A.; Priamushko, T.; Samu, G.F.; Samu, A.; Endrődi, B.; Cherevko, S.; Janáky, C. Application of Co_3O_4 as anode catalyst in CO_2 electrolyzer cells. *NPG Asia Mater.* **2025**, *17*, 18. [CrossRef]
401. Zhang, C.; Lu, B.; Xiong, H.; Lin, C.; Fang, L.; Fu, J.; Deng, D.; Fan, X.; Li, Y.; Wu, Q.-H. Cobalt-Based Perovskite Electrodes for Solid Oxide Electrolysis Cells. *Inorganics* **2022**, *10*, 187. [CrossRef]
402. Ma, J.; Wei, H.; Liu, Y.; Ren, X.; Li, Y.; Wang, F.; Han, X.; Xu, E.; Cao, X.; Wang, G.; et al. Application of Co_3O_4-based materials in electrocatalytic hydrogen evolution reaction: A review. *Int. J. Hydrogen Energy* **2020**, *45*, 21205–21220. [CrossRef]
403. Yan, X.; Tian, L.; He, M.; Chen, X. Three-Dimensional Crystalline/Amorphous Co/Co_3O_4 Core/Shell Nanosheets as Efficient Electrocatalysts for the Hydrogen Evolution Reaction. *Nano Lett.* **2015**, *15*, 6015–6021. [CrossRef]
404. Risplendi, F.; Garino, N.; Zeng, J.; Sacco, A.; Mehta, S.; Deriu, C.; Fabris, L.; Fontana, M.; Chiodoni, A.; Cicero, G.; et al. Single-atom cobalt on N-doped reduced graphene oxide pushes the oxygen reduction reaction toward 4-electron pathway. *NPJ 2D Mater. Appl.* **2025**, *9*, 83. [CrossRef]
405. Liang, Y.; Li, Y.; Wang, H.; Zhou, J.; Wang, J.; Regier, T.; Dai, H. Co_3O_4 nanocrystals on graphene as a synergistic catalyst for oxygen reduction reaction. *Nat. Mater.* **2011**, *10*, 780–786. [CrossRef]
406. Chen, Y.; Hinerman, A.; Liang, L.; Gerdes, K.; Navia, S.; Prucz, J.; Song, X. Conformal coating of cobalt oxide on solid oxide fuel cell cathode and resultant continuously increased oxygen reduction reaction kinetics upon operation. *J. Power Sources* **2018**, *405*, 45–50. [CrossRef]
407. Vinoth Kumar, R.; Khandale, A.P. A review on recent progress and selection of cobalt-based cathode materials for low temperature-solid oxide fuel cells. *Renew. Sustain. Energy Rev.* **2022**, *156*, 111985. [CrossRef]

408. Mehdi, A.M.; Hussain, A.; Song, R.H.; Lim, T.H.; Kazmi, W.W.; Ishfaq, H.A.; Khan, M.Z.; Qamar, S.U.; Syeda, M.W.; Mehra, M.T. Improving the durability of cobaltite cathode of solid oxide fuel cells—A review. *RSC Adv.* **2023**, *13*, 25029. [CrossRef] [PubMed]
409. Shabeer, Y.; Madani, S.S.; Panchal, S.; Mousavi, M.; Fowler, M. Different Metal–Air Batteries as Range Extenders for the Electric Vehicle Market: A Comparative Study. *Batteries* **2025**, *11*, 35. [CrossRef]
410. Wu, X.; Zhang, Z.; He, C.; Shen, Y.; Wu, X.; Wang, H.; Ma, Z.; Li, Q. Mixed-valence cobalt oxides bifunctional electrocatalyst with rich oxygen vacancies for aqueous metal-air batteries. *Chem. Eng. J.* **2023**, *453*, 139831. [CrossRef]
411. Saha, P.; Shah, S.S.; Ali, M.; Shaikh, N.; Aziz, A.; Ahammad, A.J.S. Cobalt Oxide-Based Electrocatalysts with Bifunctionality for High-Performing Rechargeable Zinc-Air Batteries. *Chem. Rec.* **2024**, *24*, e202300216. [CrossRef] [PubMed]
412. Meng, N.; Feng, Y.; Zhao, Z.R.; Lian, F. Boosting the ORR/OER Activity of Cobalt-Based Nano-Catalysts by Co 3d Orbital Regulation. *Chem. Rec.* **2024**, *24*, e202300216. [CrossRef]
413. Choudhary, D.; Kumar, V.; Bala, R.; Kumar, P.; Bag, M.; Sarkar, D.; Dhima, R. Cobalt Oxide Nanorods Supported on rGO as anElectrocatalyst Material for Gel Polymer Electrolyte BasedHybrid Zn-Metal/Air Batteries. *Adv. Mater. Technol.* **2025**, *10*, e01009. [CrossRef]
414. Tao, A.N.; Ge, X.; Liu, Z.L.; Zong, Y. Bi-Functional Electrode for Metal-Air Batteries and Method for Producing Same. U.S. Patent US10964982B2, 30 March 2021.
415. Sprague-Klein, E.A.; He, X.; Mara, M.W.; Reinhart, B.J.; Lee, S.; Utschig, L.M.; Mulfort, K.L.; Chen, L.X.; Tiede, D.M. Photoelectrochemical Effect in the Amorphous Cobalt Oxide Water Oxidation Catalyst Cobalt–Phosphate (CoPi). *ACS Energy Lett.* **2022**, *7*, 3129–3138. [CrossRef]
416. Hidayatullah, K.; Manopo, J.; Supu, I.; Hadju, A.; Ofiyen, C.; Mahardhika, M.K.; Darma, Y. Enhancing hydrogen evolution reaction via photoelectrochemical water splitting: A review on recent strategies of metal oxide-based photoanode materials. *Inorg. Chem. Commun.* **2025**, *179*, 114885. [CrossRef]
417. Hou, C.; Wang, B.; Murugadoss, V.; Vupputuri, S.; Chao, Y.; Guo, Z.; Wang, C.; Du, W. Recent advances in Co_3O_4 as anode materials for high-performance lithium-ion batteries. *Eng. Sci.* **2020**, *11*, 19–30. [CrossRef]
418. Konkena, B.; Kalapu, C.; Kaur, H.; Holzinger, A.; Geaney, H.; Nicolosi, V.; Scanlon, M.D.; Coleman, J.N. Cobalt Oxide 2D Nanosheets Formed at a Polarized Liquid | Liquid Interface toward High-Performance Li-Ion and Na-Ion Battery Anodes. *ACS Appl. Mater. Interfaces* **2023**, *15*, 58320−58332. [CrossRef]
419. Fu, Y.; Guo, X.; Xu, Z.; Zhao, G.; Xu, C.; Zhu, Y.; Zhou, L. Nanostructure-Mediated Phase Evolution in Lithiation/Delithiation of Co_3O_4. *ACS Appl. Mater. Interfaces* **2021**, *13*, 28171−28180. [CrossRef] [PubMed]
420. Mokhlesur Rahman, M.M.; Glushenkov, A.M.; Ramireddy, T.; Chen, Y. Electrochemical investigation of sodium reactivity with nanostructured Co_3O_4 for sodium-ion batteries. *Chem. Commun.* **2014**, *50*, 5057—5060.
421. Zhang, Y.; Wang, N.; Bai, Z. The Progress of Cobalt-Based Anode Materials for Lithium Ion Batteries and Sodium Ion Batteries. *Appl. Sci.* **2020**, *10*, 3098. [CrossRef]
422. Li, R.; Rao, D.; Zhou, J.; Wu, G.; Wang, G.; Zhu, Z.; Han, X.; Sun, R.; Li, H.; Wang, C.; et al. Amorphization-induced surface electronic states modulation of cobaltous oxide nanosheets for lithium-sulfur batteries. *Nat. Commun.* **2021**, *12*, 3102. [CrossRef] [PubMed]
423. Mussa, Y.; Arsalan, M.; Alsharaeh, E. Cobalt Oxide/Graphene Nanosheets/Hexagonal Boron Nitride (Co_3O_4/CoO/GNS/h-BN) Catalyst for High Sulfur Utilization in Li−S Batteries at Elevated Temperatures. *Energy Fuels* **2021**, *35*, 8365−8377. [CrossRef]
424. Pahalagedara, L.R.; Poyraz, A.S.; Song, W.; Kuo, C.-H.; Pahalagedara, M.N.; Meng, Y.-T.; Suib, S.L. Low Temperature Desulfurization of H_2S: High Sorption Capacities by Mesoporous Cobalt Oxide via Increased H_2S Diffusion. *Chem. Mater.* **2014**, *26*, 6613. [CrossRef]
425. Wang, J.; Yang, C.; Zhao, Y.R.; Fan, H.L.; Wang, Z.D.; Shangguan, J.; Mi, J. Synthesis of Porous Cobalt Oxide and Its Performance for H2S Removal at Room Temperature. *Ind. Eng. Chem. Res.* **2017**, *56*, 12621−12629. [CrossRef]
426. Florent, M.; Bandosz, T.J. Effects of Surface Heterogeneity of Cobalt Oxyhydroxide/graphite Oxide Composites on Reactive Adsorption of Hydrogen Sulfide. *Microp. Mesop. Mater.* **2015**, *204*, 8–14. [CrossRef]
427. Chung, J.B.; Chung, J.S. Desulfurization of H_2S using cobalt-containing sorbents at low temperatures. *Chem. Eng. Sci.* **2005**, *60*, 1515–1523. [CrossRef]
428. Štrbac, N.; Mihajlović, I.; Živković, D.; Boyanov, B.; Živković, Ž; Cocić, M. Kinetics and mechanism of synthetic cos oxidation process. *J. Min. Met. B* **2006**, *42*, 81–91. [CrossRef]
429. Kim, H.-J.; Lee, J.-H. Highly sensitive and selective gas sensors using p-type oxide semiconductors: Overview. *Sens. Actuators B Chem.* **2014**, *192*, 607–627. [CrossRef]
430. Xu, J.M.; Cheng, J.P. The advances of Co_3O_4 as gas sensing materials: A review. *J. Alloys Compd.* **2016**, *686*, 753–768. [CrossRef]
431. Wöllenstein, J.; M Burgmair, M.; Plescher, G.; Sulima, T.; Hildenbrand, J.; Böttner, H.; Eisele, I. Cobalt oxide based gas sensors on silicon substrate for operation at low temperatures. *Sens. Actuators B* **2003**, *93*, 442–448. [CrossRef]
432. Wu, R.J.; Wu, J.G.; Tsai, T.K.; Yeh, C.T. Use of Cobalt Oxide CoOOH in a Carbon Monoxide Sensor Operating at Low Temperatures. *Sens. Actuators B Chem.* **2006**, *120*, 104–109. [CrossRef]

433. Venkatraman, M.; Kadian, A.; Choudhary, S.; Subramanian, A.; Singh, A.; Sikarwar, S. Ultra-Fast Benzene Gas (C_6H_6) Detection Characteristics ofCobalt-Doped Aluminum Oxide Sensors. *ChemistrySelect* **2023**, *8*, e202204531. [CrossRef]
434. Nam, H.J.; Sasaki, T.; Koshizaki, N. Optical CO Gas Sensor Using a Cobalt Oxide Thin Film Prepared by Pulsed Laser Deposition under Various Argon Pressures. *J. Phys. Chem. B* **2006**, *110*, 23081–23084. [CrossRef] [PubMed]
435. Mondal, S.; Madhuri, R.; Sharma, P.K. Probing the shape-specific electrochemical properties of cobalt oxide nanostructures for their application as selective and sensitive non-enzymatic glucose sensors. *J. Mater. Chem. C* **2017**, *5*, 6497–6505. [CrossRef]
436. Zhao, J.; Zheng, C.; Gao, J.; Gui, J.; Deng, L.; Wang, Y.; Xu, R. Co_3O_4 nanoparticles embedded in laser-induced graphene for a flexible and highly sensitive enzyme-free glucose biosensor. *Sens. Actuators B* **2021**, *347*, 130653. [CrossRef]
437. Yin, Z.; He, S.; Li, Y.; Dai, W.; Wang, H.; He, R.; Tang, K.; Xiao, Y.; Wang, S.; Gao, J.; et al. Self-supported carbon electrodes with a carbon membrane and Co_3O_4 nanosheets for high-performance enzymeless glucose detection and supercapacitors. *ACS Appl. Nano Mater.* **2023**, *6*, 6208–6220. [CrossRef]
438. Hilal, M.; Xie, W.; Yang, W. Straw-sheaf-like Co_3O_4 for preparation of an electrochemical non-enzymatic glucose sensor. *Microchim. Acta* **2022**, *189*, 364. [CrossRef]
439. You, T.; Xiao, S.; Huang, P.; Wang, C.; Deng, Q.; Jiang, P.; He, D. Localized photothermal effect of Co_3O_4 nanowires boosts catalytic performance in glucose electrochemical detection. *Inorg. Chem. Front.* **2024**, *11*, 6527–6535. [CrossRef]
440. Alsaiari, M.; Younus, A.R.; Rahim, A.; Alsaiari, R.; Muhammad, N. An electrochemical sensing platform of cobalt oxide@SiO_2/C mesoporous composite for the selective determination of hydrazine in environmental samples. *Microchem. J.* **2021**, *165*, 106171. [CrossRef]
441. Masrat, S.; Nagal, V.; Khan, M.; Moid, I.; Alam, S.; Bhat, K.S.; Khosla, A.; Ahmad, R. Electrochemical Ultrasensitive Sensing of Uric Acid on Non-Enzymatic Porous Cobalt Oxide Nanosheets-Based Sensor. *Biosensors* **2022**, *12*, 1140. [CrossRef]
442. Wang, J.; Wu, C.; Wu, K.; Cheng, Q.; Zhou, Y. Electrochemical sensing chemical oxygen demand based on the catalytic activity of cobalt oxide film. *Anal. Chim. Acta* **2012**, *736*, 55–61. [CrossRef]
443. Dissanayake, K.; Kularatna-Abeywardana, D. A review of supercapacitors: Materials, technology, challenges, and renewable energy applications. *J. Energy Storage* **2024**, *96*, 112563. [CrossRef]
444. Yang, L.; Zhu, Q.; Yang, K.; Xu, X.; Huang, J.; Chen, H.; Wang, H. A Review on the Application of Cobalt-Based Nanomaterials in Supercapacitors. *Nanomaterials* **2022**, *12*, 4065. [CrossRef]
445. Shinde, S.; Kumar, A.R. Advances in Cobalt Oxide-Based Supercapacitors: Recent Strategies and Performance Enhancement. *ChemistrySelect* **2025**, *10*, e01497. [CrossRef]
446. Tao, K.; Bi, Q.; Han, L. Porous Co3O4@ Ni-MOF Core-Shell Structure Nanosheet Array Material and Preparation Method and Application Thereof. Chinese Patent CN112670093A, 31 May 2022.
447. Wang, J.; Wang, D.; Chen, Y.; Wang, W.; Mitsuzaki, N.; Chen, Z. Activity engineering of cobalt-based oxide materials for high performance supercapacitors: From morphology regulation to structural optimization. *Sustain. Energy Fuels* **2022**, *6*, 5243. [CrossRef]
448. Beknalkar, S.A.; Teli, A.M.; Shin, J.C. Current innovations and future prospects of metal oxide electrospun materials for supercapacitor technology: A review. *J. Mater. Sci. Technol.* **2023**, *166*, 208–233. [CrossRef]
449. Garcia, M.F.L.; Arzuza, L.C.C.; Neves, G.A.; Loureiro, F.J.A.; Morales, M.A.; Macedo, D.A.; Lira, H.L.; Menezes, R.R. Structure and Morphological Properties of Cobalt-Oxide-Based (Co_3O_4) Materials as Electrodes for Supercapacitors: A Brief Review. *Materials* **2025**, *18*, 413. [CrossRef] [PubMed]
450. Rajeshkhanna, G.; Umeshbabu, E.; Rao, G.R. In Situ Grown Nano-Architectures of Co_3O_4 on Ni-Foam for Charge Storage Application. *J. Chem. Sci.* **2017**, *129*, 157–166. [CrossRef]
451. Nayak, P.K.; Munichandraiah, N. Cobalt Hydroxide as a Capacitor Material: Tuning Its Potential Window. *J. Electrochem. Soc.* **2008**, *155*, A855–A861. [CrossRef]
452. Aghazadeh, M.; Malek Barmi, A.A.; Yousefi, T. Synthesis, characterization, and supercapacitive properties of β-$Co(OH)_2$ leaf-like nanostructures. *J. Iran. Chem. Soc.* **2012**, *9*, 225–229. [CrossRef]
453. Naeem, S.; Patil, A.V.; Shaikh, A.V.; Shinde, U.P.; Husain, D.; Alam, M.T.; Sharma, M.; Tewari, K.; Ahmad, S.; Shah, A.A.; et al. A Review of Cobalt-Based Metal Hydroxide Electrode for Applications in Supercapacitors. *Adv. Mater. Sci. Eng.* **2023**, 1133559. [CrossRef]
454. Glaubitz, F.; Lindemann, E.; Mirceski, V.; Schröder, U. Kinetic and Mechanistic Investigation of Cobalt Oxide Hydroxide Thin Films by Square-Wave Voltammetry and Multi-Frequency Electrochemical Faradaic Spectroscopy. *ChemElectroChem* **2025**, *12*, e202400694. [CrossRef]
455. Seijas-Da Silva, A.; Sanchis-Gual, R.; Carrasco, J.A.; Oestreicher, V.; Abellán, G.; Coronado, E. Boosting the Supercapacitive Behavior of CoAl Layered Double Hydroxides via Tuning the Metal Composition and Interlayer Space. *Batt. Supercaps* **2020**, *3*, 499–509. [CrossRef]
456. Mars, P.; van Krevelen, D.W. Oxidations carried out by means of vanadium oxide catalysts. *Chem. Eng. Sci.* **1954**, *3*, 41–59. [CrossRef]

457. Bielański, A.; Haber, J. Oxygen in Catalysis on Transition Metal Oxides. *Catal. Rev. Sci. Eng.* **1979**, *19*, 1–41. [CrossRef]
458. Jansson, J.; Palmqvist, A.E.; Fridell, E.; Skoglundh, M.; Osterlund, L.; Thromahlen, P.; Langer, V. On the Catalytic Activity of Co_3O_4 in Low-Temperature CO Oxidation. *J. Catal.* **2002**, *211*, 387–397. [CrossRef]
459. Pollard, M.J.; Weinstock, A.; Bitterwolf, T.E.; Griffiths, P.R.; Newbery, A.P.; Paine, J.B. A mechanistic study of the low-temperature conversion of carbon monoxide to carbon dioxide over a cobalt oxide catalyst. *J. Catal.* **2008**, *254*, 218–225. [CrossRef]
460. Xie, Y.; Dong, F.; Heinbuch, S.; Rocca, J.J.; Bernstein, E.R. Oxidation reactions on neutral cobalt oxide clusters: Experimental and theoretical studies. *Phys. Chem. Chem. Phys.* **2010**, *12*, 947–959. [CrossRef]
461. Bahlawane, N. Kinetics of methane combustion over CVD-made cobalt oxide catalysts. *Appl. Catal. B Environ.* **2006**, *67*, 168–176. [CrossRef]
462. Zasada, F.; Janas, J.; Piskorz, W.; Gorczyńska, M.; Sojka, Z. Total Oxidation of Lean Methane over Cobalt Spinel Nanocubes Controlled by the Self-Adjusted Redox State of the Catalyst: Experimental and Theoretical Account for Interplay between the Langmuir–Hinshelwood and Mars–Van Krevelen Mechanisms. *ACS Catal.* **2017**, *7*, 2853–2867. [CrossRef]
463. Zhong, J.; Zeng, Y.; Zhang, M.; Feng, W.; Xiao, D.; Wu, J.; Chen, P.; Fu, M.; Ye, D. Toluene oxidation process and proper mechanism over Co_3O_4 nanotubes: Investigation through in-situ DRIFTS combined with PTR-TOF-MS and quasi in-situ XPS. *Chem. Eng. J.* **2020**, *397*, 125375. [CrossRef]
464. Shojaee, K.; Haynes, B.S.; Montoya, A. The catalytic oxidation of NH_3 on Co_3O_4 (110): A theoretical study. *Proc. Comb. Inst.* **2017**, *36*, 4365–4373. [CrossRef]
465. Pérez-Ramírez, J.; Kondratenko, E.V. Mechanism of ammonia oxidation over oxides studied by temporal analysis of products. *J. Catal.* **2007**, *250*, 240–246. [CrossRef]
466. Weiss, B.M.; Artioli, N.; Iglesia, E. Catalytic NO Oxidation Pathways and Redox Cycles on Dispersed Oxides of Rhodium and Cobalt. *ChemCatChem* **2012**, *4*, 1397–1404. [CrossRef]
467. Wang, T.; Chen, H.C.; Yu, F.; Zhao, X.S.; Wang, H. Boosting the cycling stability of transition metal compounds-based supercapacitors. *Energy Storage Mater.* **2019**, *16*, 545–573. [CrossRef]
468. Raveau, B.; Seikh, M. (Eds.) *Cobalt Oxides: From Crystal Chemistry to Physics*; Wiley: Hoboken, NJ, USA, 2012.